International Ocean Discovery Program Expedition 353 Preliminary Report

Indian Monsoon Rainfall

29 November 2014–29 January 2015

Steven C. Clemens, Wolfgang Kuhnt, Leah J. LeVay, and the
Expedition 353 Scientists

IODP
INTERNATIONAL OCEAN DISCOVERY PROGRAM

Publisher's notes

Core samples and the wider set of data from the science program covered in this report are under moratorium and accessible only to Science Party members until 29 January 2016.

This publication was prepared by the International Ocean Discovery Program *JOIDES Resolution* Science Operator (IODP JRSO) as an account of work performed under the International Ocean Discovery Program. Funding for the program is provided by the following implementing organizations and international partners:

National Science Foundation (NSF), United States
Ministry of Education, Culture, Sports, Science and Technology (MEXT), Japan
European Consortium for Ocean Research Drilling (ECORD)
Ministry of Science and Technology (MOST), People's Republic of China
Korea Institute of Geoscience and Mineral Resources (KIGAM)
Australian-New Zealand IODP Consortium (ANZIC)
Ministry of Earth Sciences (MoES), India
Coordination for Improvement of Higher Education Personnel, Brazil (CAPES)

Portions of this work may have been published in whole or in part in other International Ocean Discovery Program documents or publications.

Disclaimer

Copyright

Citation

Clemens, S.C., Kuhnt, W., LeVay, L.J., and the Expedition 353 Scientists, 2015. Indian monsoon rainfall. *International Ocean Discovery Program Preliminary Report,* 353. http://dx.doi.org/10.14379/iodp.pr.353.2015

ISSN
World Wide Web: 2372-9562

April 2015

Expedition 353 participants

Expedition 353 scientists

Steven C. Clemens
Co-Chief Scientist
Department of Geological Sciences
Brown University
324 Brooks Street
Providence RI 02912-1846
USA
steven_clemens@brown.edu

Wolfgang Kuhnt
Co-Chief Scientist
Institut für Geowissenschaften
Christian-Albrechts-Universität zu Kiel
Olshausenstrasse 40
24118 Kiel
Germany
wk@gpi.uni-kiel.de

Leah J. LeVay
Expedition Project Manager/Staff Scientist
International Ocean Discovery Program
1000 Discovery Drive
College Station TX 77845
USA
levay@iodp.tamu.edu

Pallavi Anand
Physical Properties Specialist
Department of Earth Sciences
The Open University
Milton Keyes
MK7 6AA
United Kingdom
pallavi.anand@open.ac.uk

Takuto Ando
Sedimentologist
Hokkaido University
Department of Natural History Sciences
N10W8 Kita-ku
Sapporo 060-0810
Japan
tact@mail.sci.hokudai.ac.jp

Milos Bartol
Paleontologist (nannofossils)
Institute of Earth Sciences
Uppsala University
Villavagen 16
752036 Uppsala
Sweden
Milos.Bartol@geo.uu.se

Clara T. Bolton
Paleontologist (nannofossils)
Bioindicators and Paleoenvironmental Tracers Research Group
CEREGE, Europole de l'Arbois
Europole Mediterranaen de l'Arbois Avenue
BP 80 13545
Aix en Provence Cedex 4
France
bolton@cerege.fr

Xuan Ding
Paleontologist (foraminifers)
Department of Marine Science and Engineering
China University of Geosciences
29 Xue Yuan Road
Haidian District
Beijing
China
dingx@cugb.edu.cn

Karen Gariboldi
Paleontologist (diatoms)
Dipartimento di Scienze della Terra
Università degli Studi di Pisa
Via Santa Maria 53
56126 Pisa
Italy
karen.gariboldi@for.unipi.it

Liviu Giosan
Stratigraphic Correlator
Department of Geology and Geophysics
Woods Hole Oceanographic Institution
266 Woods Hole Road, MS 22
Woods Hole MA 02543
USA
lgiosan@whoi.edu

Edmund C. Hathorne
Inorganic Geochemist
GEOMAR, Research Center for Marine Geosciences
Wischhofstrasse 1-3
24148 Kiel
Germany
ehathorne@geomar.de

Yongsong Huang
Organic Geochemist
Department of Geological Sciences
Brown University
324 Brook Street
Providence RI 02806
USA
yongsong_huang@brown.edu

Priyank Jaiswal
Downhole Tools Specialist/Physical Properties Specialist
Boone Pickens School of Geology
Oklahoma State University
105 Noble Research Center
Stillwater OK 74075
USA
priyank.jaiswal@okstate.edu

Sunghan Kim
Sedimentologist
Busan National University
Department of Oceanography
Busan 609-735
Republic of Korea
delongksh@pusan.ac.kr

John B. Kirkpatrick
Inorganic Geochemist
Graduate School of Oceanography
University of Rhode Island
215 South Ferry Road
Narragansett RI 02882
USA
jbk@gso.uri.edu

Kate Littler
Sedimentologist
Camborne School of Mines
University of Exeter
Penryn Campus
Cornwall TR10 9FE
United Kingdom
k.littler@exeter.ac.uk

Gianluca Marino
Stratigraphic Correlator
Research School of Earth Sciences
The Australian National University
Building 124 Mills Road
Canberra ACT 2601
Australia
gianluca.marino@anu.edu.au

Philippe Martinez
Sedimentologist
University of Bordeaux
UMR CNRS 5805 EPOC
Allee Geoffroy de Saint Hilaire
33615 Pessac
France
philippe.martinez@u-bordeaux.fr

Dinesh Naik (boarded 30 December 2014)
Sedimentologist
Geological Oceanography Division
National Institute of Oceanography
Dona Paula
Goa 403 004
India
dnaik@nio.org

Aditya Peketi (boarded 30 December 2014)
Inorganic Geochemist
Geological Oceanography Division
National Institute of Oceanography
Dona Paula
Goa 403 004
India
aditya@nio.org

Stephen C. Phillips
Sedimentologist
Department of Earth Sciences
University of New Hampshire
214 James Hall
56 College Road
Durham NH 03824
USA
phillips.stephen.c@gmail.com

Marci M. Robinson
Paleontologist (foraminifers)
Eastern Earth Surface Processes
United States Geological Survey
926A National Center
12201 Sunrise Valley Drive
Reston VA 20192
USA
mmrobinson@usgs.gov

Oscar E. Romero
Paleontologist (diatoms)
MARUM
University of Bremen
Leobenerstrasse
28359 Bremen
Germany
oromero@uni-bremen.de

Netramani Sagar (boarded 30 December 2014)
Inorganic Geochemist
Geochemistry Division
National Geophysical Research Institute (NGRI)
Uppal Road
Hyderabad Andhra
Pradesh 500 007
India
n.sagar@ngri.res.in

Katie B. Taladay
Downhole Tools Specialist/Physical Properties Specialist
Department of Geology and Geophysics SOEST
University of Hawaii at Manoa
POST Building, Room 813
1680 East-West Road
Honolulu HI 96822
USA
taladay@hawaii.edu

Samuel N. Taylor
Paleomagnetist
Laboratoire de Paleomagnetisme
Institut de Physique du Globe de Paris
1 Rue Jussieu
75005 Paris
France
taylor@ipgp.fr

Kaustubh Thirumalai
Sedimentologist
Institute for Geophysics
University of Texas at Austin
J.J. Pickle Research Campus
Building 196
10100 Burnet Road
Austin TX 78758-4445
USA
kau@ig.utexas.edu

Goichiro Uramoto
Sedimentologist
Kochi Institute for Core Sample Research
Japan Agency for Marine-Earth Science and Technology
B200 Monobe, Nankoku City
Kochi 783-8502
Japan
uramotog@jamstec.go.jp

Yoichi Usui
Paleomagnetist
Institute for Research on Earth Evolution
Japan Agency for Marine-Earth Science and Technology
2-15 Natsushima-cho
Yokosuka 237-0061
Japan
yoichi@jamstec.go.jp

Jiasheng Wang
Physical Properties Specialist
Faculty of Earth Sciences
China University of Geosciences
Lumo Rodd 388
Wuhan Hubei Province
China
js-wang@cug.edu.cn

Masanobu Yamamoto
Organic Geochemist
Hokkaido University
Faculty of Environmental Earth Science
Kita-10, Nishi-5, Kita-ku
Sapporo 060-0810
Japan
myama@ees.hokudai.ac.jp

Liping Zhou
Sedimentologist
Centre for Ocean Research
Peking University
Yiheyuan Road Number 5
Beijing 100871
China
lpzhou@pku.edu.cn

Education and outreach

Juliet Crowell
Education Officer
Smithsonian Science Education Center
901 D Street, SW, Suite 704-B
Washington DC 20024
USA
belize67@aol.com

Markus Fingerle
Education Officer
Peutinger Gymnasium (High School)
Peutinger Strasse 16
73479 Ellwangen/Jagst
Germany
markus.fingerle@gmx.de

Siem Offshore AS officials

Terry Skinner
Master of the Drilling Vessel

Sam McLelland
Offshore Installation Manager

Technical support

Heather Barnes
Assistant Laboratory Officer

Susan Boehm
X-Ray Laboratory

Adam Bogus
Marine Laboratory Specialist (temporary)

Chad Broyles
Curatorial Specialist

Michael Cannon
Marine Computer Specialist

Colin Carney
Marine Laboratory Specialist (temporary)

Etienne Claassen
Marine Instrumentation Specialist

William Crawford
Senior Imaging Specialist

Aaron de Loach
Marine Laboratory Specialist (temporary)

Edwin Garrett
Petrophysics Laboratory

Kevin Grigar
Operations Superintendent

Margaret Hastedt
Core Laboratory

Jon Howell
Applications Developer

Brad Julson
Laboratory Officer

Jan Jurie Kotze
Marine Instrumentation Specialist

Aaron Mechler
Marine Laboratory Specialist (temporary)

Erik Moortgat
Chemistry Laboratory

Algie Morgan
Applications Developer

Chieh Peng
Assistant Laboratory Officer

Vincent Percuoco
Chemistry Laboratory

Alyssa Stephens
Publications Specialist

Kerry Swain
Schlumberger Engineer

Steven Thomas
Marine Computer Specialist

Kevin Werts
Underway Geophysics Laboratory

Abstract

International Ocean Discovery Program (IODP) Expedition 353 (29 November 2014–29 January 2015) drilled six sites in the Bay of Bengal, recovering 4280 m of sediments during 32.9 days of on-site drilling. Recovery averaged 97%, including coring with the advanced piston corer, half-length advanced piston corer, and extended core barrel systems. The primary objective of Expedition 353 is to reconstruct changes in Indian monsoon circulation since the Miocene at tectonic to centennial timescales. Analysis of the sediment sections recovered will improve our understanding of how monsoonal climates respond to changes in forcing external to the Earth's climate system (i.e., insolation) and changes in forcing internal to the Earth's climate system, including changes in continental ice volume, greenhouse gases, sea level, and the ocean-atmosphere exchange of energy and moisture. All of these mechanisms play critical roles in current and future climate change in monsoonal regions.

The primary signal targeted is the exceptionally low salinity surface waters that result, in roughly equal measure, from both direct summer monsoon precipitation to the Bay of Bengal and runoff from the numerous large river basins that drain into the Bay of Bengal. Changes in rainfall and surface ocean salinity are captured and preserved in a number of chemical, physical, isotopic, and biological components of sediments deposited in the Bay of Bengal. Expedition 353 sites are strategically located in key regions where these signals are the strongest and best preserved. Salinity changes at IODP Sites U1445 and U1446 (northeast Indian margin) result from direct precipitation as well as runoff from the Ganges-Brahmaputra river complex and the many river basins of peninsular India. Salinity changes at IODP Sites U1447 and U1448 (Andaman Sea) result from direct precipitation and runoff from the Irrawaddy and Salween river basins. IODP Site U1443 (Ninetyeast Ridge) is an open-ocean site with a modern surface water salinity very near the global mean but is documented to have recorded changes in monsoonal circulation over orbital to tectonic timescales. This site serves as an anchor for establishing the extent to which the north to south (19°N to 5°N) salinity gradient changes over time.

Introduction

The R/V *JOIDES Resolution* has conducted scientific ocean drilling in many of the marginal basins surrounding monsoon-influenced regions of India and Asia including the Arabian Sea (Ocean Drilling Program [ODP] Leg 117), the South China Sea (ODP Leg 184), the East China Sea (Integrated Ocean Drilling Program Expedition 346), and the marginal sea bordered by the Eurasian continent, the Korean Peninsula, and the Japanese Islands (Expedition 346). Sediments recovered have been used to reconstruct changes in summer monsoon upwelling and eolian transport (Leg 117), summer and winter monsoon surface and intermediate water dynamics in the northern and southern regions of the South China Sea (Leg 184), the influence of the westerlies on monsoonal circulation in the marginal sea bordered by the Eurasian continent, the Korean Peninsula, and the Japanese Islands (Expedition 346), and the influence of Yangtze River runoff on the surface waters of the East China Sea (Expedition 346). These records will be complemented by future drilling during scheduled International Ocean Discovery Program (IODP) expeditions in the Eastern Arabian Sea (Expedition 355), the Maldives (Expedition 359), and the Timor Sea (Expedition 363) (Figure **F1**). Prior to Expedition 353, however, no scientific drilling has occurred in the core convective region of the Indo-Asian monsoon system, the northern Bay of Bengal. Scientific drilling last occurred in the Bay of Bengal in 1972 (Deep Sea Drilling Project Leg 22) when the D/V *Glomar Challenger* drilled Sites 217 and 218 in the southernmost Bay of Bengal (8°N to 9°N). However, scientific studies performed on India's National Gas Hydrate Program Expedition 1 cores collected aboard the *JOIDES Resolution* in 2006 (Collett et al., 2008; Ramana et al., 2014), which provided the foundation for selecting most of the sites for Expedition 353, indicate the excellent potential for paleoclimatic and paleoceanographic reconstructions in the region (i.e., Ponton et al., 2012; Cawthern et al., 2014; Flores et al., 2014; Johnson et al., 2014; Phillips et al., 2014a, 2014b; Ali et al., in press). Expedition 353 fills this scientific/geographic gap by drilling targets in the Bay of Bengal that span 5°N to 20°N (Figure **F2**). Analysis of these sediments will help to address the scientific objectives outlined below.

Objectives

Pliocene–Pleistocene objectives

- Establish the sensitivity and timing of changes in monsoon circulation relative to insolation forcing, latent heat export from the Southern Hemisphere, global ice volume extent, and greenhouse gas concentrations;
- Determine the extent to which Indian and East Asian monsoon winds and precipitation are coupled and at what temporal and geographic scales;
- Better separate the effects of climate change and tectonics on erosion and runoff; and
- Provide verification targets for climate models, including the rapidly evolving water isotope–enabled, time-dependent models.

Campanian–Miocene objectives

- Understand the timing and conditions under which monsoonal circulation initiated and reconstruct the variability of the Indian monsoon at orbital timescales;
- Understand the relationship between Indian monsoon variability and major past global climatic events such as the Oligocene/Miocene cooling (Zachos et al., 1997), the onset of the mid-Miocene climatic optimum (Holbourn et al., 2007, 2014; Zachos et al., 2001), mid-Miocene cooling and Antarctic cryosphere expansion (Holbourn et al., 2013), and the Pliocene–Pleistocene enhancement of Northern Hemisphere glaciation (Lisiecki and Raymo, 2005, 2007);
- Establish a complete Oligocene–present astronomically tuned timescale based on high-resolution benthic and planktonic isotope reference curves for the Indian Ocean; and
- Integrate high-resolution distribution studies of well-preserved Oligocene–recent calcareous and siliceous microfossils from the Indian Ocean into global compilation studies of paleoclimatic and biotic evolution.

Background

Motivation for drilling in the Bay of Bengal

Pliocene–Pleistocene

The three regions chosen for drilling during Expedition 353 (Mahanadi Basin, Andaman Islands, and northern Ninetyeast Ridge) delineate a north–south transect designed to capture past

changes in the exceptionally strong salinity gradient observed in the modern Bay of Bengal (19°N to 5°N). A threefold motivation exists for targeting this precipitation/salinity signal. First, the Bay of Bengal/Andaman Sea and surrounding catchments are within the Earth's strongest hydrological regime (Figure **F3**), impacting billions of people; a solid understanding of the physics behind monsoonal climate change is of significant societal relevance (Nicholls et al., 2007). The net annual surface water exchange (precipitation plus runoff minus evaporation) within the Bay of Bengal and Andaman Sea during the summer monsoon is 184×10^{10} m^3, dominating the winter signal of -32×10^{10} m^3 for an annual average of 152×10^{10} m^3 (Varkey et al., 1996). The effects of this budget are clearly evident in the surface salinity climatology (Figure **F4**) (Antonov et al., 2010), indicating a well-defined, strong signal that can be used to monitor changes in monsoonal precipitation via chemical, physical, and isotopic indicators for changes in precipitation, salinity, and terrestrial erosion/runoff. The extent of the low-salinity surface waters is sufficient to mute (via stratification) what would otherwise yield strong summer season productivity in response to wind-driven upwelling along the eastern Indian margin, similar to that seen in the Arabian Sea (Guptha et al., 1997; Kumar et al., 2002; Phillips et al., 2014b). Hence, the Bay of Bengal is optimal for isolating and recording the summer monsoon precipitation signal in that the vast majority of precipitation, sourced from the Southern Hemisphere Indian Ocean, occurs during boreal summer (Figure **F5**).

Second, recent studies have called into question the extent to which basin-scale monsoon winds and continental precipitation are coupled over a range of timescales and space scales (Clemens et al., 2010; Clemens and Prell, 2007; Liu et al., 2006; Molnar, 2005; Ruddiman, 2006; Wang et al., 2008; Ziegler et al., 2010). Nearly all proxy records indicate strong coupling between summer monsoon winds and precipitation across the Indo-Asian monsoon subsystems at the millennial scale (Altabet et al., 2002; Cai et al., 2006; Clemens, 2005; Schulz et al., 1998; Sun et al., 2011; Wang et al., 2001); this tight coupling is likely attributed to the strong role of the winter westerlies in coupling high- and low-latitude climate change. However, the physical mechanisms behind these links are not fully understood; this was a primary goal of recent Expedition 346. Progress is also being made in understanding winter monsoon and summer monsoon linkages at the millennial timescale. For example, recent work offshore Goa, western India, shows synchronous breakdown in summer and winter monsoon airflow over the Arabian Sea during Heinrich events (Singh et al., 2011), which is in contrast to the East Asian Monsoon system that shows an asynchronous relationship between summer and winter monsoon strength at the millennial scale (Yancheva et al., 2007).

Consensus does not yet exist on the extent of the coupling or the ultimate forcing of monsoon winds and precipitation at the orbital and longer timescales (An et al., 2011; Caley et al., 2011a, 2011b, 2011c; Cheng et al., 2009; Clemens and Prell, 2007; Clemens et al., 1996, 1991, 2008; Clift et al., 2008; Ruddiman, 2006; Wang et al., 2008; Ziegler et al., 2010). Some argue for a close coupling between changes in Indian and East Asian summer monsoon winds and precipitation across the entire region spanning the Arabian Sea (Leg 117), the South China Sea (Leg 184), and terrestrial records from the Loess Plateau. In this case, changes in the strength of summer monsoon circulation across these regions are thought to be sensitive to Northern Hemisphere sensible heating (insolation), the timing of energy release from the Southern Hemisphere Indian Ocean, and the timing of global ice volume minima (An et al., 2011; Caley et al., 2011b, 2011c; Clemens and Prell, 2003, 2007; Clemens et al., 1996, 2008). In contrast, others interpret the timing of summer monsoon circulation, on the basis of speleothem records from southeast China, as forced directly by external insolation with little or no influence from internal boundary conditions such as ice volume or Southern Hemisphere ocean–atmosphere latent heat exchange (Cheng et al., 2009; Ruddiman, 2006; Wang et al., 2008). Caballero-Gill et al. (2012) demonstrate that these contrasting interpretations are not attributable to differences in terrestrial and marine chronologies. Therefore, this lack of consensus points either to a strong deficit in our understanding of monsoon sensitivity to changes in the fundamental boundary conditions including insolation, ocean/atmosphere energy exchange, ice volume, and atmospheric greenhouse gas concentrations or to the confounding influence of seasonality on interpretation of proxy records (Figure **F5**).

Lack of consensus also extends to the tectonic scale, where the timing of monsoon intensification to modern strength is debated. Some proxy records suggest initial intensification occurred at ~7–8 Ma (e.g., Kroon et al., 1991; Prell et al., 1992), whereas others suggest a considerably earlier intensification, perhaps as early as early Miocene (~22 Ma) (Clift et al., 2008; Guo et al., 2002; Sun and Wang, 2005) or even late Eocene (~45 Ma) (Licht et al., 2014). Emergence and expansion of arid-adapted C_4 flora in South Asia argues for reduced precipitation since ~8 Ma (e.g., Cerling et al., 1997; Huang et al., 2007; Quade and Cerling, 1995), whereas proxies dedicated to reconstructing seasonality suggest, instead, little variability in the monsoon over the last 10 My (Dettman et al., 2001). Clift and Plumb (2008), Molnar et al. (2010), and the report from the Detailed Planning Group "Asian Monsoon and Cenozoic Tectonic History" (**www.iodp.org/doc_download/2336-mmdp-greport**) provide comprehensive overviews of these issues. More recently, Rodriguez et al. (2014) suggested that the ~8 Ma intensification inferred on the basis of increased *Globigerina bulloides* concentrations is an artifact of increased preservation related to uplift of the Owen Ridge at this time, resulting in enhanced preservation.

Third, recent work suggests that interpretation of the oxygen minimum zone (OMZ) signal in the northern Arabian Sea (Leg 117) may be complicated by changing oxygen content of southern-source intermediate waters (Anand et al., 2008; Caley et al., 2011c; Schmittner et al., 2007; Ziegler et al., 2010). This presents a potential complication in the interpretation of the OMZ signal as a direct response to atmospheric circulation in the core region of summer monsoon winds (i.e., oxygen drawdown in response to decay of upwelling-produced organic carbon). Precipitation, salinity, and runoff indicators are not influenced by the chemistry of externally sourced intermediate and deep water masses, offering the potential to disentangle the influences of these factors in interpreting monsoon proxy records.

The Expedition 353 drilling effort, targeting the core geographic region of summer monsoon precipitation, directly addressed these outstanding issues. Resolving these questions using the geological archive is important to providing verification targets for climate models, especially given that the majority of current Atmosphere-Ocean General Circulation Models (AOGCMs) used in the Intergovernmental Panel on Climate Change (IPCC) reports do not accurately simulate the spatial or intraseasonal variability of monsoon precipitation (Randall et al., 2007; Sharmila et al., 2015).

Deep time

Benthic foraminiferal diversity and assemblage composition, in conjunction with geochemical proxies of carbon flux, indicate a

stepwise increase in primary production and carbon flux and an expansion of the intermediate water OMZ in the northeastern Indian Ocean since the late Oligocene (Gupta et al., 2013). The main increases in productivity started at 14 Ma (Gupta et al., 2013) or 10 Ma (Gupta et al., 2004) and reached levels associated with present Indian monsoon conditions around 2.3 Ma. This late Miocene to Pliocene "biogenic bloom" (Farrell et al., 1995) implies important changes in nutrient cycling in the Indian Ocean and probably on a global scale, which in particular affected the silica and phosphate cycles (Dickens and Owen, 1999). The productivity increase between 10 and 8 Ma in the eastern equatorial Indian Ocean (onset of the biogenic bloom) may have been linked either to global cooling and the expansion of Antarctic ice sheets leading to a major change in deep ocean circulation and nutrient cycling, to the initiation of the Indian monsoons, or to a combination of both (Gupta et al., 2004).

Deep-sea benthic foraminiferal diversity in the Indian Ocean further decreased between 8 and 6 Ma and is associated with a negative $\delta^{13}C$ shift at 3.2–2.3 and 1.6–0.9 Ma, coinciding with an increased abundance of species indicative of increased organic carbon flux (Singh and Gupta, 2005). Since ~2.8 Ma, roughly coeval with the onset of Northern Hemisphere glaciation, benthic foraminiferal species that are well adapted to seasonally strong fluctuating carbon flux dominate the assemblages. This has been related to increased duration and strength of the northeast (winter) monsoon, which is accompanied by relatively low primary production in the eastern equatorial Indian Ocean (Gupta and Thomas, 2003). Expedition 353 will provide new Neogene intermediate water benthic foraminiferal $\delta^{18}O$ and $\delta^{13}C$ records along a meridional transect to better understand the relative contribution of monsoon-induced changes in carbon flux and changes in intermediate water circulation linked to high-latitude climatic events such as fluctuations in the extension of the East Antarctic ice sheet. Analysis of Bay of Bengal surface sediments indicates that the foraminiferal lysocline, the depth delimiting well preserved from noticeably dissolved assemblages, shoals significantly from south to north. The foraminiferal lysocline rises from 3800 to 3300 m between 0°N and 7°N (about Site U1443) then systematically shoals to ~2000 m at ~20°N (Indian margin sites) (Cullen and Prell, 1984), indicating enhanced carbon flux to the deep sea in the northern part of the Bay of Bengal.

The Expedition 353 meridional transect provides a unique opportunity to investigate the nature and timing of variations in deepwater radiogenic isotope composition in response to restriction of the deepwater connection between the Pacific and Indian Oceans through the Indonesian Gateway since the mid-Miocene, to disentangle climatic variability from direct tectonic influences using non-Himalayan sedimentary sequences on the Indian continental margin, and to evaluate the influence of enhanced Himalayan erosion since the late Oligocene at sites affected by a Himalayan signal in the Andaman Sea and Ninetyeast Ridge. The broad Oligocene passage between the Indian and Pacific Oceans must have enabled significant surface and intermediate water exchange and the possibility of deepwater flow from the Indian Ocean to the Pacific Ocean (Thomas et al., 2003). The progressive closure of the Indonesian Gateway caused by the northward movement of Australia (Hall, 2002; Hall et al., 2011; Kuhnt et al., 2004) induced changes in deepwater and intermediate water circulation through the Indonesian Gateway, which may have resulted in a significant change in the Eastern Indian Ocean Nd isotope composition during the middle Miocene (Frank et al., 2006; Gourlan et al., 2008). A second shift in Eastern Indian Ocean Nd isotopes may have been related to a shift in the source area of the Indonesian Throughflow toward the North Pacific around 3.5 Ma (Cane and Molnar, 2001; Gourlan et al., 2008).

Geological setting

The eastern continental margin of India is the result of the separation of India and the Australia/Antarctica portion of Gondwanaland during the Early Cretaceous at ~130 Ma (Powell et al., 1988; Scotese et al., 1988). The 2000 m isobaths of the northeast Indian continental margin and Lambert Graben of East Antarctica (Prydz Bay) are closely matched, supporting the inferred alignment of India and Antarctica prior to rifting (Subrahmanyam et al., 2008). The major Indian peninsular rivers draining into the Bay of Bengal (Figure **F6**) are thought to be associated with graben features resulting from the rifting of India from Antarctica as well as subsequent Indian plate motion. The Mahanadi Graben, for example, appears to have a continuation in Prydz Bay, Antarctica, known as Lambert Graben (Federov et al., 1982). Combined, the major river systems draining into the Bay of Bengal (Figure **F6**) discharge ~1630 km^3/y (Achyuthan et al., 2013), accounting for ~50% of the total freshwater input, the remaining being from direct precipitation (Akhil et al., 2014).

Ninetyeast Ridge (NER) is an aseismic volcanic ridge spanning ~31°S to ~10°N, where it is buried beneath Bengal Fan sediments. The NER is thought to have formed by age-progressive hotspot volcanism from plume sources currently beneath the Kerguelen Plateau (Royer et al., 1991; Sager et al., 2010). The ridge top rises to a height of ~3.5 km above the surrounding abyssal plain with depths as shallow as ~2000 meters below sea level (mbsl). Site U1443 is located at ~5°N at 2925 mbsl. This location provides good preservation of carbonate microfossils given that the foraminiferal lysocline in this region is close to 3300 m (Cullen and Prell, 1984).

The Andaman Sea is situated between the Andaman Islands and the Malaya Peninsula (Figure **F2**). The Andaman-Sumatra island arc system results from oblique subduction of the Indo-Australian plate beneath the Eurasian plate (Singh et al., 2013). Stretching and rifting of the overriding plate in the early Miocene (~25 Ma) has resulted in two distinct plates (Sunda and Burma) separated by an active spreading center (Curray, 1991) located in the deepest portion of the Andaman Sea. An accretionary wedge complex, which scraped off the subducting slab, lies west of the spreading center, forming a series of shallower basins associated with backthrust faulting within the accreted sediments (Figure **F7**). The Andaman Sea drilling sites are within the Nicobar-Andaman Basin, bounded on either side by the Diligent and Eastern margin faults. Terrigenous sediment supply to the Andaman Sea originates dominantly from the Irrawaddy and Salween Rivers (Colin et al., 1998). Analysis of Andaman Sea surface sediments indicates that foraminifers are abundant and well preserved shallower than ~1800 mbsl (>100,000 individuals/gram) and decrease to <100 individuals/gram deeper than 3000 mbsl (Frerichs, 1971).

Modern atmospheric and oceanographic circulation

The Indian summer monsoon is characterized by low atmospheric pressure over the Indo-Asian continent (Indo-Asian Low) relative to high atmospheric pressure over the southern subtropical Indian Ocean (Mascarene High). The resulting pressure gradient leads to large-scale displacement of the Intertropical Convergence Zone and cross-equatorial flow of low-level winds carrying mois-

ture that is ultimately released over South Asia, the Bay of Bengal, and southeast China (Hastenrath and Greischar, 1993; Liu et al., 1994; Loschnigg and Webster, 2000; Webster, 1987a, 1987b, 1994; Webster et al., 1998). Modern meteorological observations and moisture transport budgets (Figure **F8**) quantitatively show that the Southern Hemisphere Indian Ocean is the dominant source of moisture (latent heat) to the Indian and East Asian summer monsoons during June, July, and August (JJA) (Bosilovich and Schubert, 2002; Ding and Chan, 2005; Ding et al., 2004; Emile-Geay et al., 2003; Liu and Tang, 2004, 2005; Park et al., 2007; Simmonds et al., 1999; Wajsowicz and Schopf, 2001; Xie and Arkin, 1997; Zhu and Newell, 1998). The Arabian Sea is a very minor moisture source (evaporation > precipitation), whereas the Bay of Bengal/Andaman Sea, India, the South China Sea, and southeast China are all moisture sinks (precipitation > evaporation) (Figure **F8**).

A total of 12 major rivers feed the Bay of Bengal/Andaman Sea (Ganges, Brahmaputra, Meghna, Damodar, Mahanadi, Godavari, Krishna, Irrawaddy, Salween, Penner, Kavery, and Mahaweli Rivers), discharging in total 943×10^9 m^3 of water during the summer monsoon months (JJA) (Varkey et al., 1996). Annual rainfall within and surrounding the Bay of Bengal is dominated by precipitation during JJA with the exception of the Madras Basin in southernmost peninsular India, where rainfall peaks in November (Figure **F9**). The dominance of the JJA precipitation signal is reflected in the Bay of Bengal surface salinity patterns (Figure **F4**), spanning salinities of 20–34 over both seasonal (summer–winter) and spatial (north–south) scales, with lowest values in August and September.

Primary surface ocean currents (Schott and McCreary, 2001; Schott et al., 2009) reflect the seasonal wind forcing in both the eastern Arabian Sea and the Bay of Bengal (Figure **F10**). The West Indian Coastal Current (WICC) flows south during the summer monsoon, connecting with the Southwest Monsoon Current (SMC) that carries high-salinity waters eastward around the tip of India and Sri Lanka into the southern Bay of Bengal at a rate of 8.4 Sverdrup (Sv =10^6 m^3/s). This influx of high-salinity water is reflected in the southern Bay of Bengal July, August, and September salinity patterns (Figure **F4**) and is successfully modeled as a passive tracer in mixed-layer ocean models (Jensen, 2001, 2003). Southwest summer monsoon winds in the Bay of Bengal also drive the northward-flowing East Indian Coastal Current (EICC). During the winter monsoon, northeast winds drive all these surface currents in the opposite directions, transporting 11 Sv of water toward the eastern Arabian Sea.

Salinity on the Indian margin, northwest Bay of Bengal, reaches a minimum of ~22 in September (Figure **F4**); this is a lagged response to JJA rainfall over the Bay of Bengal and the surrounding drainage basins. Salinity at this location reaches a maximum of 34 during the spring months. The Andaman Sea sites, situated between the modern 32 and 33 annual average isohalines, monitor drainage from the Irrawaddy and Salween Rivers. Salinity in the southern Bay of Bengal (Site U1443) is closely pinned to the 34 isohaline year round, anchoring the southern end of the modern salinity gradient at near open-ocean values. Although this site does not currently experience significant seasonal salinity variability, it does record large-scale changes in precipitation and runoff at the millennial, orbital, glacial–interglacial, and tectonic scales as discussed below. The full meridional transect (spanning the Indian margin, Andaman Sea, and northern NER) has a modern salinity range of 12.

Estimates for expected $\delta^{18}O_{G.ruber}$ values can be calculated by combining climatologies for monthly temperature and salinity with regional $\delta^{18}O_{seawater}$-salinity equations (Figure **F11**). Northern (20°N) values range between –1.9‰ for January and –3.3‰ for October with strong sensitivity to the salinity seasonality. Estimates for 5°N range from –2.5‰ (August–December) to –2.9‰ (April) with strong sensitivity to the temperature seasonality.

Terrestrial runoff products are also of significant utility in assessing linkages between monsoon circulation, chemical weathering, and transport at timescales from millennial to tectonic (Clift and Plumb, 2008; Wang et al., 2005). Changes in monsoon strength are well documented at ~23, 15, 8–7, and 2.75 Ma (Clift and Plumb, 2008). The Expedition 353 targets will allow measurement of the consequent impact on weathering rates and transport of particulate materials to the ocean basins in a variety of settings both proximal and distal relative to river inputs.

Water masses and deep circulation

Comprehensive descriptions of eastern Indian Ocean regional oceanography are provided in Wyrtki (1971), Mantyla and Reid (1995), Tomczak and Godfrey (2003), and Schott et al. (2009), from which we briefly summarize descriptions of water masses and circulation patterns relevant for Bay of Bengal drilling in the depth range between 1100 and 3000 m targeted for Expedition 353.

Indian Deep Water (IDW) occupies the depth range from 3800 to ~1500 m within the equatorial and northern Indian Ocean (Figure **F12**). IDW in the eastern Indian Ocean is characterized by high salinities, reaching maxima of 34.8 in the southwestern Indian Ocean and 34.75 in the southeastern Indian Ocean, where the IDW upper limit rises to 500 m (Tomczak and Godfrey, 2003). IDW temperature, salinity, and oxygen properties in the high-salinity core are virtually identical with those of North Atlantic Deep Water (NADW) in the Atlantic sector of the Southern Ocean, indicating that IDW is mainly of NADW origin and not originally formed in the Southern Ocean, as is the Antarctic Bottom Water (AABW) that occupies the Indian Ocean deeper than 3800 m (Tomczak and Godfrey, 2003). The flow of IDW is northward and concentrated along the African margin and the NER as indicated by the World Ocean Circulation Experiment (WOCE) 95°E oxygen, silicate, and temperature profiles (Figure **F13**). IDW further penetrates northward into the Northern Hemisphere, is modified by mixing with thermocline water from above and upwelling of AABW from below, and spreads into the Arabian Sea and the Bay of Bengal.

Two water masses occupy the thermocline of the Indian Ocean, Indian Central Water (ICW) and Indonesian Throughflow Water (ITW) or Australasian Mediterranean Water (Figure **F14**). ICW originates from downwelling in the subtropical convergence south of 30°S, and ITW is derived from North Pacific Intermediate Water, strongly modified during its passage through the Indonesian archipelago. There is no formation of thermocline water in the Bay of Bengal, and its thermocline water masses to 1500 m water depth are derived from ICW and ITW. Transfer of ICW to the northern Indian Ocean is accompanied by a rapid decrease in oxygen content, indicating aging along the path. The lowest oxygen values occur in the Bay of Bengal, which contains the oldest ICW. The strong oxygen decrease in the northern Indian Ocean can be explained by reduction of the transfer of ICW during the southwest monsoon season, resulting in a small annual net transfer rate. ITW also contributes to the renewal of thermocline water in the northern Indian Ocean, resulting in significant freshening of the ICW along its path into the Bay of Bengal. Further freshening is observed in the Bay of Bengal near 90°E, resulting from ITW advection directly from its outflow area into the tropical eastern Indian Ocean. Variability and

evolution of thermocline circulation in the Bay of Bengal are strongly dependent on monsoonal forcing; however, the present extremely low oxygen levels indicate a very low renewal rate for the thermocline waters of the Bay of Bengal.

The uppermost 100 m of the eastern Indian Ocean in the Bay of Bengal consists of a low-salinity water mass derived from river runoff from India and Indochina, the Bay of Bengal Water (BBW), with surface salinity strongly fluctuating with seasons but remaining below 33 throughout the year. The lower boundary to the ICW is characterized by a strong halocline. The southward extension of the BBW surface water mass is highest during October–December when it reaches the area along the western Indian coast and is lowest during April–June before the summer monsoon leads to a new expansion of the BBW.

Site summaries

Site U1443

Background and objectives

The NER represents the trace of the Kerguelen/Ninetyeast hotspot prior to middle Eocene rifting (Peirce, Weissel, et al., 1989). As a result of northward movement, Site U1443 moved from temperate southern latitudes during the Campanian to ~5°S near the Oligocene/Miocene boundary and to its present 5°N present location in the southernmost Bay of Bengal. The site has been within 10° of the Equator for the past 35 My (Shipboard Scientific Party, 1989). The ridge-top location (2935 mbsl) has prevented the deposition of sedimentary sequences typically associated with fan transport processes and is thus a useful location for recovery of open-ocean pelagic sediments.

Site U1443 is located ~100 m southeast of ODP Site 758 on the crest of the NER and is a redrill of Site 758 (Figure **F2**). Previous drilling at this site included overlapping holes (758A and 758B) only for the uppermost 92 m of the total 527 m of sediments drilled. This limited the resulting composite record to the past 7.3 My (Farrell and Janecek, 1991).

In spite of these limitations, the IODP sample database shows that more than 16,000 sediment samples have been taken from Site 758 cores in the last 10 y. Parts of the uppermost sections are almost entirely depleted, and sampling has moved to the archive half. Recent research using Site 758 sediments include high-resolution (suborbital) late Pleistocene reconstruction of changes in upper water column structure based on multispecies planktonic foraminifer records (Bolton et al., 2013), reconstruction of the Li isotope composition of seawater over the past 70 My (Misra and Froelich, 2012), Late Cretaceous to early Eocene reconstruction of seawater neodymium (Le Houedec et al., 2012), and glacial–interglacial scale reconstruction of Os isotopic composition of seawater (Burton et al., 2010). Drilling Site U1443 had the following main objectives:

- Establish a composite section for the entire Miocene–Oligocene sedimentary succession at the NER, which would be the base for establishing a first orbitally tuned Indian Ocean isotope stratigraphy for this time interval.
- Recover a more complete record of the Cretaceous/Paleogene boundary interval, which was only incompletely retrieved at the base of the core catcher of Core 121-758A-31X.
- Correlate the onset of increased terrigenous clay component and sedimentation rates in the late Miocene to orbitally tuned isotope and magnetic reversal stratigraphy.
- Precisely determine the timing of intensifications of the Indian monsoon, as evident from increased freshwater input to the Bay of Bengal and northern end of the NER using salinity proxies based on Mg/Ca-temperature estimates and $\delta^{18}O$ of surface-dwelling planktonic foraminifers.
- Investigate variability and possible influence of orbital forcing on fluxes of terrigenous material to the northern NER since the middle Miocene. In particular, relate terrigenous pulses at ~7.0–5.6 and ~3.9–2.0 Ma, which were interpreted to represent variations in the fluvial flux resulting from the uplift and erosion of the Himalaya (Hovan and Rea, 1992), to the variability of the Indian monsoon.
- Extend the Pliocene–Pleistocene stable isotope record for Site 758, which is the only "high-resolution" record across the initiation of Northern Hemisphere glaciation in the Indian Ocean (Hoogakker et al., 2006; Mudelsee and Raymo, 2005), into the Miocene and Oligocene.
- Use the Nd isotope composition of NER sediments to extend reconstructions of the relative contribution of discharge from the Ganges-Brahmaputra, Irrawaddy, Arakan, and Indian peninsular rivers as indicators of glacial–interglacial variability in monsoon strength into the Miocene (Burton and Vance, 2000; Stoll et al., 2007; Gourlan et al., 2008, 2010). A complete Neogene sediment archive at Site U1443 opens the possibility to obtaining proxy records for river discharge in sufficient time resolution to document the relation between global climate and the Indian monsoon throughout the Neogene.

Lithostratigraphy

Sediments recovered from Site U1443 reveal a range of pelagic and hemipelagic sediments of Late Pleistocene to Campanian age, comprising four distinct lithologic units (I–IV):

- Unit I (0–107.8 m core depth below seafloor [CSF-A]) is composed of Late Pleistocene–late Miocene light–dark gray nannofossil oozes with varying proportions of foraminifers, clay, and volcanic ash.
- Unit II (107.8–242.36 m CSF-A) is composed of pale yellow to white nannofossil oozes and chalks with varying amounts of authigenic carbonate and foraminifers that are late Miocene to early Oligocene in age.
- Unit III (242.36–308.68 m CSF-A) is late Paleocene to late Campanian in age and comprises a 66 m thick package of pale yellow and brown nannofossil chalks with varying proportions of authigenic carbonate and occasional chert and porcellanite nodules and thin beds.
- In Unit IV, a total of 31 m (308.68–341.35 m CSF-A), comprising a succession of greenish gray marlstones with glauconite of late Campanian age, was recovered before Hole U1443A was terminated at 344 m drilling depth below seafloor (DSF).

Lithostratigraphic units are defined by changes in lithology (as identified by visual core description and smear slide observations), physical properties, and color reflectance (L*, a*, and b*). The observed lithologic differences between the units are primarily the result of varying abundances of nannofossils, clay, and authigenic carbonate, with glauconite influencing the color and magnetic susceptibility (MS) properties in Unit IV. Lithologic descriptions are based primarily on sediments recovered from Hole U1443A, supplemented with observations from Holes U1443B–U1443D.

Biostratigraphy

Calcareous nannofossils are abundant throughout the section in Hole U1443A, which is Late Pleistocene (<0.29 Ma) to Campanian (>72.1 Ma) in age, with a large unconformity that spans most of the

Eocene and the latest Paleocene. Nannofossil assemblages are typically tropical to subtropical and are well preserved in the Pleistocene to the upper Miocene sections (~110 m CSF-A, lithologic Unit I). Below this interval, evidence of diagenetic overgrowth becomes apparent. Scanning electron microscope (SEM) analyses revealed that *Emiliania huxleyi* (<0.29 Ma) is present in intervals 353-U1443A-1H-1, 0–50 cm, and 353-U1443B-1H-1, 0–10 cm. Cretaceous sediments contain abundant moderately to poorly preserved calcareous nannofossils. The Cretaceous/Paleogene (K/Pg) boundary was identified in Core 353-U1443A-39X but is highly bioturbated and appears to be incomplete.

Planktonic foraminifers are dominant to abundant in Samples 353-U1443A-1H-CC through 43X-CC, which are Pleistocene to Late Cretaceous in age. Abundance decreases from common to few in Samples 44X-CC through 48X-CC. Preservation is good to moderate throughout the Cenozoic with a few exceptions in the late Miocene (Sample 13H-CC) and the Oligocene to Paleocene (Samples 33X-CC and 34X-CC), where preservation is poor. Preservation in the Cretaceous (Samples 39X-CC to 48X-CC) is moderate to poor.

At Site U1443, diatoms are most abundant from 0 to 28 m CSFA, whereas their occurrence becomes sporadic downsection until 192 m CSFA. The diatom community in the uppermost 28 m of Site U1443 is diverse and mainly consists of Pleistocene to Holocene species, mostly typical of warm to temperate low-latitude ocean waters, and includes species indicating transport of coastal waters to Site U1443.

The age-depth relationship for Hole U1443A is based on the biostratigraphy of the three fossil groups studied (diatoms, planktonic foraminifers, and calcareous nannofossils) and paleomagnetic stratigraphy. Age datums of the fossil groups and paleomagnetism show good agreement for the Pleistocene. Calcareous nannofossils and planktonic foraminifers show consistent age-depth relationships throughout the Cenozoic and Late Cretaceous, with no major outliers. The combined biostratigraphic and paleomagnetic age model indicates a mean sedimentation rate of 1.20 cm/ky in the upper part of lithologic Unit I (0–80 m CSF-A, Pleistocene to late Miocene). The mean sedimentation rate decreases to 0.41 cm/ky between 100 and 130 m CSF-A (the upper part of lithologic Subunit IIa, late Miocene to middle Miocene). Sedimentation rates between 135 and 200 m CSF-A (the lower half of lithologic Subunit IIa) average 0.81 cm/ky (early Miocene to Oligocene). Finally, following a hiatus that spans the late Oligocene to late Paleocene, the mean sedimentation rate in the late Paleocene and Late Cretaceous (lithologic Units III and IV) is 0.36 cm/ky. These sedimentation rate and age estimates broadly agree with those published for Site 758.

Geochemistry

The composition of the interstitial water (IW) and bulk sediment samples reflects the variation in sediment composition and reactions that occurred since deposition. Overall, the sediments have high carbonate content (>80 wt% throughout most of the section) and low total organic carbon (<0.3 wt%). IW major and minor element concentrations vary downhole. The depositional environment changed as the site migrated from the Southern Hemisphere to the current location, as the collision of India with Asia delivered more and more terrigenous material to the location. In the upper sediments, ash deposition from the nearby Indonesian arc plays an important role. In general, the data from Site U1443 agree well with data from Site 758, but the new data provide a better resolution in the sections recovered by advanced piston corer (APC)/half-length advanced piston corer (HLAPC) coring compared to the extended core barrel (XCB) coring at Site 758.

Paleomagnetism

Paleomagnetic measurements were conducted on all of the archive half sections and 127 discrete samples taken from Holes U1443A–U1443C. Some of the discrete samples were also subjected to rock magnetic analyses. Magnetic polarity patterns were recovered for most of the APC and HLAPC cores but not for the XCB cores. The resulting magnetostratigraphy was produced for two time periods: 0–6 Ma (Holes U1443A and U1443C) and 18–25 Ma (Hole U1443A). The age-depth model from paleomagnetic measurements agrees well with the biostratigraphic ages. Between these age intervals, patterns based on pass-through magnetic measurements were inconclusive because of a decrease in natural remanent magnetization (NRM) intensity. A lithologic change to higher carbonate content and a decrease in the concentration of fine-grained ferrimagnetic minerals explains the poor signal. Preliminary rock magnetic experiments suggest changes in bulk magnetic properties are primarily controlled by variations in the concentration of fine-grained magnetite/maghemite.

Physical properties

Downhole variations in physical property measurements at Site U1443 reflect changes in lithology, condensed sections associated with depositional hiatuses, and diagenetic processes. The overall suite of physical property data is divided into three broad units with two subunits occurring within Unit II. These subunits mark important anomalous events in the depositional history of this site. The general porosity trend decreases with depth with a few excursions correlating with the three subunits. In Unit I, high variability in MS, natural gamma radiation (NGR), *P*-wave velocity, and color reflectance reflect numerous ash layers intercalated within clayey nannofossil ooze. MS peaks are likely the result of higher iron content in the ash layers, and the color reflectance data display changes between darker ash and lighter nannofossil ooze as well as changes in the clay content of the nannofossil ooze. Unit II is defined by a jump to an overall lighter color, with relatively uniform low NGR and low *P*-wave velocity trends. The sedimentologists identified this unit to be composed of chalk. From the physical property data, two anomalous intervals were identified within Unit II. These intervals show a marked change to increased density, *P*-wave velocity, and NGR with no corresponding change in color reflectance. Thus, these changes in physical properties were undetectable by visual analysis of the core. The physical property anomalies were used to assist in directing sampling for smear slide and SEM analysis, which together provided evidence that the anomalous intervals reflected high authentic overgrowth and carbonate cementation correlating with strong, positive seismic reflections and biostratigraphically defined depositional hiatuses. Unit III data display an abrupt change to a darker color with higher NGR, MS, and *P*-wave values, suggesting a transition to a stronger, more lithified material with an increase in magnetic minerals and clays that are likely the result of an increase in terrigenous sediments. Overall, our physical properties results were generally found to be in good agreement with the lithostratigraphy at this site.

Stratigraphic correlation

A composite section and splice to establish a continuous sediment sequence was created using Holes U1443A–U1443D. Correlation and splicing was based on MS, NGR, and reflectance spectroscopy b* data. The MS data proved particularly useful for

correlation in the upper ~63 m core composite depth below seafloor (CCSF-A) because several tephra layers coincided with positive MS peaks. NGR and reflectance spectroscopy b* data were used throughout the rest of the records. A continuous splice was created spanning the upper 180 m, approximately tripling the length of time over which a continuous record was achieved for Site 758. This is mostly due to the use of the HLAPC, which greatly extended the length of piston-cored section.

Highlights

Pliocene–Pleistocene tephrochronology

The Pliocene to Holocene tephra layers of the northern NER provide a unique record of explosive volcanism derived from the Indonesian island of Sumatra, the northernmost part of the Sunda arc, and the nearest volcanically active region (Dehn et al., 1991). Recovery of a complete succession of tephra layers within a complete splice with a high-resolution orbitally tuned isotope stratigraphy and the possibility of correlation of individual tephra layers between three holes make Site U1443 a unique observatory of volcanic activity in this region over the last 5 My (Figure **F15**, **F16**, **F17**). The volcanic tephra layers form excellent tools for lithostratigraphic correlation of the marine sediment successions within the five different holes on the northern NER. Detailed studies of the tephra layers will contribute to the understanding of the magmatic evolution in the source region and allow determination and precise dating of eruptive cycles. In particular, the eruption history of the Toba Caldera in northern Sumatra is well documented on the northern NER (Ninkovich, 1979; Ninkovich et al., 1978; Dehn et al., 1991), and individual tephra layers at Site U1443 can be tentatively correlated to the main eruptions of the Toba Caldera complex at 75, ~450, ~840, and ~1200 ka (Chesner and Rose, 1991; Dehn et al., 1991; Farrell and Janecek, 1991). The possibility of $^{40}Ar/^{39}Ar$ dating of these ash layers and correlation to a robust paleomagnetic reversal scheme at Site U1443 in combination with high-resolution stable isotope records will further contribute to intercalibrating Pliocene–Pleistocene geomagnetic reversal and $\delta^{18}O$ chronostratigraphy (Hall and Farrell, 1993, 1995).

Transitional Cretaceous/Paleogene boundary

The sedimentary record of the Cretaceous/Paleogene (K/Pg) boundary transition was difficult to assess at Site 758 because this interval was only recovered in Hole 758A. The transition occurs at the base of the core catcher of Core 121-758A-31X (295.6 meters below seafloor [mbsf]) and is potentially incomplete because of the nearby coring gap between Cores 121-758A-31X and 32X. The Site U1443 K/Pg boundary (66.04 Ma) was identified between Samples 353-U1443A-39X-4W, 40 cm, and 39X-5W, 60 cm (Figure **F18**). Sediments in this interval are heavily bioturbated (containing burrows, blebs, patches, color banding, and mottles), and most samples studied within this interval contain a mixture of Cretaceous and Paleocene nannoplankton species. In particular, *Zoophycos* spreite burrows are common in the K/Pg boundary succession and are a prominent feature in upper Maastrichtian sediments of Holes U1443A and U1443B. The interval below Section 353-U1443A-39X-5W contains moderately to poorly preserved Cretaceous nannofossil assemblages. No latest Maastrichtian marker events were found, possibly a result of a minor hiatus.

First complete spliced record of Neogene deepwater sediments in the Indian Ocean

The continuous pelagic sediment record of Site U1443 with well-preserved benthic and planktonic foraminifers will allow extension of existing Pliocene–Pleistocene isotope records from Site 758 to the base of the Neogene and tracking of deepwater and surface water isotopic signals in the eastern equatorial Indian Ocean over the last 25 My. Sedimentation rates >0.41 cm/ky will still allow analyses of stable isotopes and geochemical records in a resolution sufficient to resolve orbital-scale climate variability and to correlate these records to existing Atlantic and Pacific orbitally tuned isotope curves.

Late Oligocene to middle Miocene paleomagnetic record

The high-quality paleomagnetic record of Site 758 was limited to the uppermost 100 m, which was retrieved by APC coring. Below this level, biscuiting of the cored sediment by XCB coring prohibited high-quality magnetic measurements. At Site U1443, it was possible to use the APC and HLAPC core barrels to deeper than 200 m CSF-A, which opened up a new window for obtaining paleomagnetic records for the lower part of the Miocene and upper Oligocene. In particular, the record between 130 and 200 m CSF-A is characterized by high-quality paleomagnetic data that allow establishment of a complete paleomagnetic reversal scale that covers the entire lower Miocene and upper Oligocene, including the Oligocene/Miocene stage boundary.

Recovery of expanded Campanian–Maastrichtian sediment succession

The Campanian to Maastrichtian part of the succession at Site U1443 is characterized by moderate to high recovery of indurated yellowish brown nannoplankton chalk, which grades downcore into greenish glauconite-rich chalk with intervals of abundant *Inoceramus* shell fragments (Figure **F19**). The lower part of this interval includes several centimeter-thick indurated chert nodules and nodular layers, which caused a significant decrease in drilling progress and recovery in the lowermost two cores of Hole U1443A (Cores 353-U1443A-47X and 48X). The recovery of Upper Cretaceous sediments above these Campanian siliceous layers was good in both Holes U1443A and U1443B, resulting in a complete stratigraphic record of this interval, which was characterized by only fragments recovered at Site 758. The low degree of diagenesis and the complete recovery may allow construction of a spliced bulk carbonate carbon isotope record that covers the entire Maastrichtian to the middle/late Campanian including the Campanian/Maastrichtian boundary.

A note on the Hole U1443A CSF-A depth scale

Stratigraphic and visual correlation indicates that ~5.4 m of sediment was lost from the bottom of Core 353-U1443A-1H (Figure **F20**). This is not surprising in light of the fact that four APC core barrels were bent or broke during attempts to establish the various holes at Site U1443. In this case, it is useful to know that one should add ~5.4 m to the CSF-A depth of all cores below Core 1H to make the CSF-A depths more consistent with those in Holes U1443B–U1443D.

Site U1444

Background and objectives

The main scientific objective of Expedition 353 is to analyze the variability of the salinity gradient in the Bay of Bengal on suborbital to orbital timescales. To achieve this objective, site locations were selected according to the likelihood of continuous sedimentation and proximity to the main sources of freshwater feeding the Northern Bay of Bengal, including the Mahanadi River and the Ganges-Brahmaputra river complex, and the Andaman Sea, including the Irrawaddy and Salween river systems.

Within one month prior to the start of the expedition, an alternate drilling plan was requested, one that included only sites in international waters. To accommodate this, we utilized existing site survey data acquired by the University of Bremen in 1997 and 2006 to locate drilling targets in the central Bengal Fan, following a latitudinal transect approach. This alternate plan included sets of sites at three different latitudes in international waters at 11°N, 14°N, and 17°/18°N.

Sediments at these alternative sites do not meet the paleoclimatic time-series oriented scientific objectives of Expedition 353 because the sedimentary archive of the Bengal Fan includes abundant coarse-grained turbidite sequences that do not have the stratigraphic integrity required for high-resolution reconstruction of climate change. However, the alternate sites on the Bengal Fan are complementary to the objectives of IODP Expedition 354 (France-Lanord et al., 2014). One of the crucial issues for Expedition 354 is the continuity of the terrigenous flux from the Himalayan source to the ~8°N drilling targets. Channel migration may, at times, decouple the middle fan from the supply. The addition of sites north of the 8°N Expedition 354 transect sites may help to evaluate these processes and provide additional material for the understanding of terrigenous flux into the Bengal Fan, one of the main objectives of the Expedition 354 drilling proposal.

Site U1444 (14°N, 84°49.74′E; 3143 mbsl) is located at common midpoint (CMP) 1302 on seismic Line GeoB97-041 (Schwenk and Spieß, 2009) (Figure **F21A**). The site is located in the western part of the lower Bengal Fan, close to the westernmost abandoned channel that fed the western part of the lower fan (Emmel and Curray, 1984). Seismics (Figure **F21B–F21C**) suggest that these sediments are composed of a series of buried channel-levee sequences incised into hemipelagic sediments atop the underlying 85°E ridge. Schwenk and Spieß (2009) identified two prominent unconformities (Uc and Ud) bounding a more transparent hemipelagic unit between 4.32 and 4.20 s two-way traveltime (TWT), corresponding to ~105 to 185 mbsf. These unconformities can be traced for several hundred kilometers to the east along Line GeoB97-041 (Schwenk and Spieß, 2009). Similar regional-scale unconformities in the lower fan have been correlated to Site 218 and dated as earliest Pliocene (~4.8 Ma) and middle Pleistocene (~0.65 Ma) in age (von der Borch, Sclater, et al., 1974; Schwenk and Spieß, 2009). Unconformities Uc and Ud were inferred to be Pleistocene and Pliocene in age as well, but prior to drilling Site U1444, they had not been dated. A primary objective of this site was to determine the lithologic changes associated with seismic Reflectors (Unconformities) Uc and Ud and to date these reflectors in an effort to assess the degree to which turbidite and intercalated hemipelagic sequences are continuous from the upper to lower fan regions.

Coring summary

At Site U1444, Holes U1444A and U1444B were drilled to total depths of 330.6 and 128.6 m DSF, respectively. In Holes U1444A and U1444B, the full-length (9.7 m long) APC system and the XCB system were primarily used. The HLAPC (4.7 m long) was used only for Core 353-U1444A-24F. For Holes U1444A and U1444B, the APC system was used to refusal followed by the XCB. A total of 46 cores were recovered at Site U1444. The APC cored interval was 160.0 m with a recovery of 156.21 m (98% recovery). The HLAPC cored interval was 4.8 m with a recovery of 3.94 m of core (82%). The XCB cored interval was 246.9 m with a recovery of 140.06 m of core (57%). Hole U1444B contained a drilled interval from 47.5 to 95.0 m DSF. The overall recovery for Site U1444 was 73%.

Lithostratigraphy

Sediments recovered from Holes U1444A and U1444B can be divided into four lithostratigraphic units based on visual description, smear slide analysis, and physical property measurements. The recovered lithologies are siliciclastic and are composed of turbidites with intercalated hemipelagic intervals.

- Unit I (0–95.01 m CSF-A) is composed of silty sand and silty clay with numerous turbidites.
- Unit II (95.01–168.91 m CSF-A) is primarily nannofossil-rich clay with silt and foraminifers. Turbidites in Unit II are less abundant, thinner, and finer than in Unit I.
- Unit III (176.1–255.6 m CSF-A) is characterized by very poor recovery and is dominated by silty fine to medium sand.
- Unit IV (255.6–323.3 m CSF-A) is composed primarily of nannofossil-rich clay and clayey silt interbedded with sand and silt turbidites.

Turbidites at this site show typical erosional bases and normal (fining-upward) grading but rarely show structures typical of classic Bouma or Stow sequences (e.g., parallel, wavy, or lenticular laminae). Structureless turbidites suggest very rapid sedimentation and/or disturbance of the water-saturated sands during drilling and recovery. Turbidites were classified visually by their maximum grain size as either silt or sand. At Site U1444, turbidites can be classified compositionally from visual and smear slide descriptions as mica rich, well sorted quartz dominant, organic debris rich, or glauconite rich. The overall lithologic differences between units and variation in turbidite grain size and thickness are consistent with fluctuations in the proximity of active turbidity current channels on the Bengal Fan.

Biostratigraphy

The biostratigraphic age model for Site U1444 was established by combining nannofossil and planktonic foraminifer datums from Hole U1444A. Age-depth relationships for the two fossil groups show good agreement. All samples were nearly or completely barren of diatoms. Calcareous microfossils (nannofossils, planktonic foraminifers, and benthic foraminifers) at Site U1444 were rare or absent in turbidite-rich sequences and common to abundant in hemipelagic sediment sequences. Where calcareous microfossils were present, preservation was good to moderate and rarely poor. Foraminifers ranged in preservation from poor to good in the samples in which they occur.

Nannofossil assemblages were of Pleistocene to late Miocene age and tropical/subtropical in character. Most Pleistocene, Pliocene, and late Miocene calcareous nannofossil bioevents used to define the biostratigraphic zones were present. This enabled us to assign all samples from hemipelagic sediment sequences and many samples from turbidite-rich sequences to a single biozone. *Emiliania huxleyi* is present in Sample 353-U1444A-9H-CC near the

bottom of lithologic Unit I, suggesting that this entire unit (95 m) was deposited during the Late Pleistocene and Holocene. The top of lithologic Unit II (95–177 m CSF-A) was placed within nannofossil Zone NN20. Sample 353-U1444A-20X-CC (168.89 m CSF-A), near the base of Unit II, falls within nannofossil Zone NN16 (late Pliocene). The lithologic Unit IV sequence spans Zone NN13 (middle Pliocene) to Zone NN11 (late Miocene). Sample 353-U1444A-37X-CC, 18 cm, collected 12 cm above the bottom of Hole U1444A, contained common *Discoaster loeblichii*, which suggests that the oldest sediments in Hole U1444A are younger than 7.53 Ma (late Miocene).

Planktonic foraminifer assemblages in Hole U1444A are tropical to subtropical throughout the Neogene and include species indicative of upwelling. The last occurrence (LO) of *Globigerinoides ruber* (pink) in Sample 353-U1444A-4H-CC and the first occurrence (FO) of *Globorotalia flexuosa* in Sample 14X-CC indicate that sediments between 35.80 and 119.42 m CSF-A are of Pleistocene age. Pliocene datums were found in Samples 16X-CC through 19X-CC (137.41–166.53 m CSF-A) and in Cores 32X and 33X (282.00–290.50 m CSF-A). Eleven core catcher samples from 168.89 to 270.34 m CSF-A were either barren or contained no index species. Miocene sediments are identified in Samples 35X-CC and 36X-CC. The occurrence of *Candeina nitida* in Sample 36X-CC indicates that it can be no older than 8.43 Ma.

Site U1444 is characterized by large variations in sedimentation rate that occur because of high-frequency large-scale episodes of terrigenous deposition. Mean sedimentation rates reach >20 cm/ky in lithologic Unit I (0–95 m CSF-A) and >30 cm/ky in Unit III (264–323.5 m CSF-A). Lithologic Units II and IV are mostly hemipelagic with sedimentation rates an order of magnitude lower than Units I and III, around 1.39 cm/ky for Unit II and 1.60 cm/ky for Unit IV.

Geochemistry

Site U1444 varies geochemically, as it reflects the depositional history of this section of the Bengal Fan. Significant changes in bulk and IW chemistry reflect the major changes in lithology; lithologic Unit I features a complete drawdown of sulfate and increases in methane, alkalinity, and nutrients. Deeper units are less reducing with opposing trends in many elements, including pronounced secondary peaks in sulfate, silicate, B, Li, Mn, and K. Organic C is low but variable, ranging between 0 and 2 wt%, whereas carbonate content tracks lithologic units: Units I and III are low, whereas Units II and IV are variable but generally higher (10–30 wt%).

Paleomagnetism

Paleomagnetic measurements were conducted on archive-half sections for both Holes U1444A and U1444B. Sections dominated by sand were not measured because of their unstable texture and the risk of contamination to the magnetometer. All sections from XCB cores were severely affected by drilling-related overprint and were difficult to interpret. A selection of discrete samples (N = 119) taken from working-half sections was also analyzed. Based on APC section measurements and discrete data, we propose tentative magnetozones throughout Hole U1444A. Magnetostratigraphic ages are given as 0.781 Ma at ~112–118 m CSF-A and 2.581 Ma at ~148–151 m CSF-A. Other magnetozones were difficult to correlate with the geomagnetic polarity timescale because of poor recovery in some intervals and drilling-related overprint remanence. Most of the discrete data to ~100 m CSF-A are influenced by gyroremanent magnetization, likely due to the presence of greigite (a ferrimagnetic iron sulfide). Rock magnetic evaluation of greigite abundance revealed depth distribution in broad agreement with some interstitial water geochemistry.

Physical properties

The physical property data collected at Site U1444 were found to be in good agreement with the lithostratigraphic data. Four physical property units were identified in Hole U1444A that are identical to the lithostratigraphic units, and three physical property units were identified in Hole U1444B that are different and are not directly related to the units defined for Hole U1444A. MS values were higher in coarse-grained sediments than in the clay-rich sections. Core-length MS trends, with high values at the bottom of cores to low values at the top, indicate mechanical sorting at core-length scales. These trends are present in APC cores that are entirely composed of coarse watery sands, indicating mechanical sorting because of severe disturbance during coring and recovery.

Stratigraphic correlation

No composite depth scale or splice was constructed for Site U1444. Coring disturbance and mechanical sorting of turbidite sands leading to a restructuring of the physical properties on a core-by-core basis in the upper part of the site (see **Physical properties**) and a lack of signal in the XCB cores in the lower part of the site prevented establishment of reliable tie points between Holes U1443A and U1444B.

Highlights: dating the Schwenk and Spieß (2009) seismic Unconformities Uc and Ud in Hole U1444A

The middle Bengal Fan is characterized by channel-levee systems that are erosionally incised into underlying hemipelagic sediments (Schwenk and Spieß, 2009). Seismic profiles indicate two major regional unconformities, which were dated at Site 218 as earliest Pliocene (~4.8 Ma) and Middle Pleistocene (0.65 Ma) (von der Borch, Sclater, et al., 1974; Schwenk and Spieß, 2009). The extent of the regional unconformities, the onset of levee systems, and faults terminating within Pleistocene sediments suggest that tectonic events, in addition to changes in sediment supply and transport, exerted major controls on the sedimentation patterns of the Bengal Fan (Schwenk and Spieß, 2009).

Regional Unconformity Uc (Schwenk and Spieß, 2009), is clearly recognizable in the sedimentary succession of Site U1444. It is defined by a lithologic change from hemipelagic clays and silty clays (with foraminifer and nannofossil ages of ~200 ka) to a turbidite-dominated sequence composed of silty sands and silty clays that are largely barren of microfossils. This 95 m long sequence represents the last 200 ky of sedimentary deposition at Site U1444. The deeper regional unconformity (Ud in Schwenk and Spieß, 2009) comprises a change from very poorly recovered turbiditic silty sands and clayey silts to hemipelagic clays and silty clays in the middle Pliocene (between ~3.6 and 3.8 Ma). Within the error of the dating, which includes sedimentation rate–based extrapolations over tens of meters at Site 218, the Late Pleistocene regional Unconformity Uc could be the same age as the unconformity at Site 218. The deeper Pliocene Unconformity Ud at Site U1444 appears to be on the order of 1 My younger relative to the unconformity at Site 218.

The onset of channel-levee systems in the latest Miocene is indicated by downhole data from ODP Leg 116 and seismic data along an east–west transect at 8°N (Schwenk and Spieß, 2009). These changes were possibly related to changes in the erosion and weathering regime in the drainage area of the Ganges River (Schwenk and Spieß, 2009). At Site U1444, a strong increase in coarse-grained

silty–sandy levee and turbidite sediments representing a fan lobe occurred later in the middle Pliocene around 3.8 Ma, whereas the oldest sediments of Hole U1444A (3.8 to ~6 Ma) consist of fine-grained mudstones with intercalated thin-bedded levee sediments.

Site U1445

Background and objectives

Site U1445 (2513 mbsl) is located near the southern end of the Mahanadi basin, on the eastern margin of India. This location, ~94 km offshore, offers the opportunity to drill sediments underlying the low-salinity waters of the Indian margin, a result of summer monsoon rainfall and runoff from the peninsular rivers of India, including the Ganges-Brahmaputra river complex and the Mahanadi River. The location of this site, seaward of the base of the slope, offers the potential to reach Miocene sediments but is not protected from turbidite deposition. Objectives at this site were to recover late Miocene to Holocene sediment sections in order to reconstruct changes in the Indian summer monsoon at orbital to suborbital timescales.

Coring summary

At Site U1445, Holes U1445A, U1445B, and U1445C were drilled to total depths of 672.6, 33.0, and 305.6 m DSF, respectively. In Holes U1445A and U1445C, the APC and XCB systems were primarily used; only the APC system was used in Hole U1445B. For Holes U1445A and U1445C, the APC system was used to refusal. Following refusal of the APC, the XCB was deployed to total depth. Overall, 117 cores were recorded for the site. A total of 487.34 m of core over a 476.3 m cored interval was recovered using the APC (102% recovery). The cored interval with the XCB was 534.5 m with a core recovery of 518.02 m (97%). The overall recovery percentage for Site U1445 was 99%. The total time spent on Site U1445 was 9.3 days.

Lithostratigraphy

Sediments recovered from Holes U1445A–U1445C are principally composed of hemipelagic clays with a significant biogenic component and occasional thin turbidites of Holocene to late Miocene age. Because of the homogeneous nature of the sediments, only one stratigraphic unit is recognized and divided into two subunits (Ia and Ib), primarily based on nannofossil and biosilica content.

- Subunit Ia (0–165.28 m CSF-A) is a sequence of Holocene to Middle Pleistocene olive-gray to dark greenish gray clay with biosilica and clay with nannofossils with occasional beds of biosilica-rich clay.
- Subunit Ib (165.28–667.56 m CSF-A) comprises the interval between the first downcore occurrence of biosilica-rich clays to the bottom of Hole U1445A.

Foraminifers are a persistent but variable component of the Subunit Ia clays. Subunit Ib is dominated by very dark greenish gray biosilica-rich clay with glauconite, with significant periods of increased diatom content between ~160 and 330 m CSF-A. Foraminifers and nannofossils are both much less common in Subunit Ib than in Subunit Ia but are present in small numbers throughout, particularly between ~570 and 670 m CSF-A where an increase in calcareous nannofossils is observed. Thin (~2–20 cm) turbidites are present in sediments from both Subunits Ia and Ib, varying in composition from silt-sized quartz-rich silt/sands to foraminifer-rich sands with occasional bioclastic-rich sands. Soupy and mousselike intervals, characteristic of gas hydrate dissociation, were identified in sediments recovered using the APC system in Holes U1445A–U1445C from both Subunits Ia and Ib. Overall, cores from Hole U1445C were considerably less disturbed (drilling disturbance and gas expansion) than those recovered from Hole U1445A at equivalent depths, possibly due to reduced heave during Hole U1445C operations.

Biostratigraphy

Calcareous and siliceous microfossils are present in Hole U1445A with variable downcore abundance trends. Calcareous nannofossil preservation is good to moderate, and their abundances vary between rare and abundant. Pleistocene to late Miocene nannofossil assemblages are typical of tropical/subtropical paleoenvironments. Foraminifers are dominant to abundant in the uppermost 188 m in Hole U1445A. Abundance decreases rapidly deeper than 188 m CSF-A and falls to few or rare deeper than 290 m CSF-A. Foraminifer preservation is good to moderate, with the exception of three samples that show poor preservation. Diatom preservation ranges from good to poor and tends to be better whenever diatom abundance is higher.

All Pleistocene nannofossil marker species are found, with the exception of *Reticulofenestra asanoi*. The Pliocene/Pleistocene boundary (2.59 Ma), located between Cores 353-U1445A-31X and 38X, is bracketed by a number of *Discoaster* LOs that are dated between 2.39 and 2.8 Ma. The Miocene/Pliocene boundary (5.33 Ma) is well constrained between 603.22 and 606.19 m CSF-A and is based on the LO of *Triquetrorhabdulus rugosus* (5.28 Ma) and the FO of *Ceratolithus acutus* (5.35 Ma) in this interval. The oldest calcareous nannofossil sample studied (353-U1445-A-77X-CC; 667.46 m CSF-A) contained *Discoaster quinqueramus* and *Discoaster berggrenii*, suggesting an age between 5.59 and 7.53 Ma. Beyond the age model, nannofossil biostratigraphy was of great use to date some rip-up clasts found in several horizons in Holes U1445A and U1445C. The matrix surrounding the clasts was of the same age as the sediment above and below the horizons containing the clasts, whereas the rip-up clasts themselves were of different ages, ranging from Late Pleistocene to late Eocene.

Planktonic foraminifer biostratigraphy is based on the shipboard study of core catcher samples from Hole U1445A. The percent of planktonic foraminifers is high (mean = 86.4%) in the uppermost 158.97 m but lower (mean = 59.9%) throughout the remaining Hole U1445A core catchers. The total number of foraminifers per 10 cm^3 raw sediment is highly variable, ranging from 0 to >24,000, with a marked decrease deeper than 180 m CSF-A. The number of benthic foraminifers per 10 cm^3 raw sediment follows the same pattern, averaging 1667 between 0 and 180 m CSF-A and 129 deeper. Reworking is apparent in many late Miocene through Pleistocene samples. Pleistocene planktonic foraminifer assemblages were recovered from 6.9 to 261.51 m CSF-A. Planktonic assemblages are dominated by tropical to warm subtropical species and by some temperate species. Species commonly associated with upwelling zones are common to abundant throughout Samples 353-U1445A-1H-CC to 20H-CC, indicating coastal upwelling or vertical mixing. Species of markedly different last appearance ages are found in samples within a zone between Samples 9H-CC and 18H-CC, which implies reworking. Pliocene planktonic foraminifer assemblages are recovered from Samples 29X-CC to 68X-CC. Miocene sediments span Samples 69X-CC to 77X-CC. The occurrence

of *Globigerinoides conglobatus* in Sample 76X-CC suggests a maximum age of 6.20 Ma.

Diatoms are useful for age estimation throughout the entire sedimentary column of Hole U1445A. Several diatom events are recognized between the LO of *Nitzschia reinholdii* (0.90–1.0 Ma) and the LO of *Nitzschia miocenica* (5.7 Ma). Valve preservation is mostly good to moderate. Strong variations in abundance and shifts in the species composition of the diatom assemblage will help to reconstruct paleoceanographic changes in the eastern Indian Ocean between the late Miocene and the Late Pleistocene. The highly diverse diatom community mainly consists of species typical of warm to temperate low-latitude ocean waters. High-productivity species, including *Thalassionema nitzschioides* var. *nitzschioides* and resting spores of *Chaetoceros*, tend to dominate whenever total diatom abundance is higher than "few." A certain degree of freshwater/land input, through winds or river runoff, is revealed by the recurrent presence of numerous phytoliths and freshwater diatoms.

The age model for Site U1445 was established by combining nannofossil, planktonic foraminifer, and diatom datums with paleomagnetic reversal datums. Age-depth relationships for Hole U1445A of the three fossil groups studied (diatoms, planktonic foraminifers, and calcareous nannofossils) show good agreement and match the magnetochron boundary datums very well. The combined biostratigraphy/magnetostratigraphy age model suggests a mean sedimentation rate of 11.4 cm/ky, assuming a linear fit of all data.

Geochemistry

The geochemistry of Site U1445 strongly reflects the processes of sulfate reduction and methanogenesis associated with microbial degradation of organic matter. High methane concentrations are found in headspace and void space gas samples. A high methane/ethane ratio suggests that the methane is mostly of biogenic origin. The organic carbon content is as high as 4 wt%, and carbonate is associated with intervals of more abundant calcite microfossils. The IW chemistry of Site U1445 reflects reducing conditions with pore water sulfate depleted at around 18 m CSF-A. Other examples are alkalinity peaking at around 30 mM near 50 m CSF-A and dissolved barium and silicate increasing downhole. The influence of seawater contamination and oxygen during processing associated with XCB coring is noticeable in the profiles of some elements, most notably sulfate, phosphate, and iron.

Paleomagnetism

Paleomagnetic measurements were conducted on the archive-half sections for all three holes at Site U1445, with alternating field (AF) demagnetization typically up to 10 mT. Discrete samples (N = 219) taken from the working-half sections were also analyzed, with AF demagnetization typically up to 30 mT. Characteristic remanent magnetizations (ChRMs) of discrete samples were calculated using the principal component analysis (PCA) technique. Additionally, the bulk magnetic properties of the discrete samples were assessed.

Remanence intensities drop significantly in the uppermost 10–20 m because of diagenetic reduction. Nonetheless, a magnetic polarity stratigraphy was produced, except for the lower part of Hole U1445A (deeper than ~470 m CSF-A). Rock magnetic measurements on the discrete samples provide promising variations in the bulk magnetic properties for the last 6 My. The significance of these trends has yet to be evaluated; however, a periodicity, possibly on the order of 40–60 ky, could be underlying astronomical-scale cycles.

Physical properties

The physical property data collected at Site U1445 were found to be in good agreement with the lithostratigraphic data; however, the physical property unit division boundaries differ. Three physical property units are identified in Hole U1445A and two units in Hole U1445C. The data between Holes U1445A and U1445C correlate well. The distinct change in physical property characteristics of Hole U1445A between Units I and II is likely related to a lithologic change to biosilica-rich clay at the top of Unit II, based on smear slide analysis. MS, density, and NGR values are lower, whereas porosity values are high in the more diatom-rich clays of Unit II. Changes observed in color reflectance could be a result of a change from APC to XCB coring. A zone containing high NGR peaks in Unit III could be related to drilling disturbance or coarse-grained fractions in a few turbidites.

Stratigraphic correlation

A composite scale (CCSF-A) and a splice were constructed for Site U1445 using Holes U1445A and U1445C using MS, NGR, and red, green, and blue (RGB) data. Splicing among these holes enabled us to construct a continuous stratigraphic sequence to ~252 m CCSF-D. Because of data quality issues, correlation should be viewed with caution deeper than ~50 m CCSF-A and especially deeper than ~236 m CCSF-A.

Downhole logging

Wireline logging in Hole U1445A was initiated following coring operations. The hole was swept with a heavy-weight water-based mud that included barite as a weighing additive to improve hole stability. The presence of barite in the mud must be taken into consideration when interpreting logging results; incoming gamma rays will be blocked, attenuating the NGR measurement, and the photoelectric factor should be used cautiously. Two passes were made with both the triple combo and Formation MicroScanner (FMS)-sonic tool strings for better data comparison of repeatability. The first logging run was made with the triple combo, which encountered a bridge at ~440.0 mbsf, and all subsequent passes and runs were limited to this depth. The upper 80 m of the hole was not logged because it was occupied by the drill string. For the purpose of discussion, the wireline logging suites are divided into three units based on hole conditions inferred from the caliper data. The caliper data for Units I (100–237 m CSF-A) and III (380–440 m CSF-A) show highly irregular hole conditions with large washout zones, and thus we are not confident in the quality of logging data in these units. The caliper data for Unit II (237–380 m CSF-A) shows that the hole is close to bit size, NGR counts were found to agree in magnitude with shipboard Natural Gamma Radiation Logger logs, and the wireline density data are in excellent agreement with moisture and density measurements, suggesting that the data in this unit are reliable. However, the density logs from the Whole-Round Multisensor Logger and Special Task Multisensor Logger appear to consistently underestimate the true density of the formation. The wireline porosity curves show high apparent porosity as a result of water bound in the structure of the clays that dominate the downhole lithology. There are no resistivity spikes suggestive of concentrated gas hydrate occurrence, and thus the gas hydrate morphology at this site is dispersed and occurrence is likely reflected in the FMS high-resistivity bands.

Highlights

Sediments at this site were remarkably conducive to XCB coring. The deepest hole at Site U1445 was cored to 673 mbsf, 447 m of which was cored using the XCB, with an overall recovery of 99%. Within intervals where core expansion was strong because of microbial gas, an 8 m advance of the XCB was employed to provide expansion room within the liner, thereby significantly reducing the loss of sediment out of the top of the corer.

Discrete intervals in the late Miocene, middle Pliocene, and Middle Pleistocene are characterized by abundant diatoms, including species characteristic of high-productivity environments and those found in coastal and freshwaters. Similarly, species of planktonic foraminifers characteristic of higher productivity environments increase in abundance in the middle Pliocene and Pleistocene, possibly suggesting nutrient input because of changes in surface water stratification or runoff.

All cores were infrared scanned on the catwalk prior to sectioning. A number of centimeter-scale cold spots were detected, having up to 7°C difference relative to background core temperatures. Rhizon pore water sampling confirmed these as hydrates, based on chloride values well below that of seawater.

Splicing among overlapping holes (0 to ~305 m) at Site U1445 will yield the first continuous section recovered from the Indian margin that spans the Pleistocene. Over this interval, fine-scale turbidites averaged ~1 per core (<5 cm thick). Excellent XCB recovery (99%) over the remaining ~360 m will allow for high-resolution monsoon reconstruction into the late Miocene.

Site U1446

Background and objectives

Site U1446 (1440 mbsl) is located within the Mahanadi basin on the eastern margin of India. This location, ~70 km offshore, offers the opportunity to drill sediments underlying the low-salinity waters of the Indian margin, a result of summer monsoon rainfall and runoff from the peninsular rivers of India, including the Ganges-Brahmaputra river complex and the Mahanadi River. Located atop a small rise near the base of the slope, this site should be protected from turbidite deposition. Objectives at this site were to recover Late Pleistocene to Holocene sediment sections in order to reconstruct changes in the Indian summer monsoon at orbital to suborbital timescales.

Coring summary

At Site U1446, Holes U1446A, U1446B, and U1446C were drilled to total depths of 180.0, 27.1, and 182.0 m DSF, respectively. In Holes U1446A and U1446C, the APC and HLAPC systems were deployed. In Hole U1446B, only the APC system was used. Overall, 47 cores were recorded for the site. A total of 344.95 m of core over a 342.3 m cored interval was recovered using the APC system (101% recovery). The HLAPC cored interval was 46.8 m with a recovery of 49.43 m of core (106%). The overall recovery percentage for Site U1446 was 101%. The total time spent on Site U1446 was 2.3 days.

Lithostratigraphy

Sediments recovered from Holes U1446A–U1446C are Holocene to Middle Pleistocene in age and are typical of continental margin settings, falling within the hemipelagic classification as a mixture of a dominant lithogenic fraction diluting a minor biogenic fraction. They are primarily composed of dark gray to gray clay with nannofossils, nannofossil-rich clay, clay with foraminifers, clay, clay with biosilica, and biosilica-rich clay. Because of the homogeneous clayey nature of the sediments, only one lithostratigraphic unit (Unit I) is recognized at this site (0–180.11 m CSF-A) with no subunit divisions. Visual core description and smear slide observations were used with supporting information from physical properties (primarily NGR) and geochemical parameters (weight percent $CaCO_3$) to evaluate the varying abundances of the siliciclastic fraction (clays, silts, and occasionally sands) versus the biogenic fraction (calcareous and siliceous). Turbidites are rare at Site U1446, with only occasional thin quartz-rich or shallow-water carbonate-rich intervals indicative of transported sediments. Overall, drilling disturbance is generally slight to moderate because all cores were retrieved using the APC system and is characterized by voids and gas expansion cracks.

Biostratigraphy

Calcareous microfossils are continuously present in the sediments of Hole U1446A, whereas siliceous microfossils are sporadically present. Calcareous nannofossils show abundances ranging from few to abundant in the smear slides studied, and their preservation is generally very good to good and occasionally moderate. Foraminifers are dominant to abundant in Hole U1446A in 19 of 21 core catcher samples. Preservation is good to moderate in all foraminifer samples. Diatoms are present in the lower and upper part of the Hole U1446A record. Valve preservation ranges from good to poor and tends to be better whenever abundance is higher.

All Late Pleistocene calcareous nannofossil events are identified. Late to Middle Pleistocene assemblages are typical of tropical/subtropical paleoenvironments. All core catcher samples from Hole U1446A contain Pleistocene planktonic foraminifer assemblages. Planktonic assemblages are dominated by tropical to warm subtropical species. The diatom community is highly diverse and resembles that of Site U1445. The diatom assemblage consists of species typical of warm to temperate, low- to mid-latitude ocean waters.

The age model for Site U1446 was established by combining nannofossil, planktonic foraminifer, and diatom datums with paleomagnetic reversal datums. The combined biostratigraphy/magnetostratigraphy age model indicates a mean sedimentation rate of ~16 cm/ky from 0 Ma to just over 1 Ma. The oldest planktonic foraminifer datum encountered is the LO of *Globorotalia tosaensis* (0.61 Ma) in Sample 353-U1446A-12H-CC, whereas the combination of nannofossils and diatoms datums constrains the basal age of Hole U1446A to between 0.90–1.0 and 1.26 Ma

Geochemistry

The organic carbon content of Site U1446 ranges from 0.8 to 1.6 wt% (average = 1.2 wt%), and the geochemistry of the site mainly reflects the anaerobic processes of sulfate reduction and methanogenesis associated with microbial degradation of organic matter. Sulfate declines rapidly from 28 mM at sediment/water interface to nearly zero values at approximately 20 m CSF-A. Alkalinity peaks at 20 m depth, consistent with the production of bicarbonate during the sulfate reduction. Sulfate reduction appears to continue throughout the core, as suggested by the gradual increase in dissolved Ba concentration with depth, as this Ba is likely derived from barite. Changes in the concentration of other cations and anions (Fe, Mg, Ca, ammonium, and Sr) in IW can be readily explained by the microbial-induced chemical reactions and their effects on pH, alkalinity, and mineral dissolution and precipitation. Methane concentrations in sediment are generally low shallower than 30 m CSF-A but rise between 30 and 70 m CSF-A, peaking at ~50 m CSF-A, with a moderate concentration of 1000 ppm. High meth-

ane/ethane ratios suggest that the methane is mostly of biogenic origin (methanogenesis). Carbonate content varies significantly between 2 and 20 wt% within the scale of a few meters, with the low content intervals corresponding to high NGR (terrestrial clay-rich materials).

Paleomagnetism

Paleomagnetic measurements were conducted on archive-half sections for all three holes at Site U1446, with AF demagnetization up to 10 mT. Discrete samples taken from the working-half sections of Holes U1446A (N = 53) and U1446C (N = 9) were also analyzed, with AF demagnetization up to 40–80 mT. ChRMs of these discrete samples were calculated using the PCA technique. The paleomagnetic signal was generally good to ~120 m CSF-A but poor deeper. A magnetostratigraphy is constructed from 0 to 1.173 Ma (~170 m CSF-A) in Hole U1446A with a certain degree of ambiguity for some of the chrons. In addition, anhysteretic remanent magnetization (ARM) was acquired and measured on a selection of Hole U1446A discrete samples. A significant decrease in ARM because of diagenetic reduction at 30 m CSF-A was observed for Hole U1446A. Deeper than 30 m CSF-A, ARM intensity increases slightly from 40 to 60 m CSF-A and decreases from 100 to 130 m CSF-A.

Physical properties

The physical property data collected at Site U1446 were found to be in good agreement with the lithostratigraphic data. However, based on density and porosity changes with depth, Hole U1446A is divided into three physical property subunits (Ia, Ib, and Ic). The changes in bulk density and porosity are possibly due to changes in sediment composition. We observe similar trends in all physical property data between Holes U1446A and U1446C. Cyclic variability in NGR values could be reflecting changes in lithogenic input.

Stratigraphic correlation

A composite scale (CCSF-A) and a splice were constructed for Site U1446 using Holes U1446A and U1446C using MS, NGR, and RGB data. Splicing among these holes enabled us to construct a continuous stratigraphic sequence to ~108 m CCSF-D. Because of data quality and time availability issues, correlation should be viewed with caution deeper than ~78 m CCSF-A.

Highlights

Site U1446 recovered ~180 m of section from two holes, ranging from the Late Pleistocene to the Holocene, with a mean sedimentation rate of ~16 cm/ky. Hole U1446C recovered an excellent mudline, with common fragile epifaunal tubular agglutinated foraminifers. The entire interval was APC cored with excellent recovery. Toba ash was recovered at ~15 m CSF-A. Although the site is within the hydrate stability zone and in the same general vicinity as Site U1445, no indications of hydrates were found, possibly due to the finer grained nature of the sediments. The spliced section at this site will yield an excellent continuous Late Pleistocene section. The high sedimentation rate offers excellent opportunities to reconstruct monsoon climates at suborbital to orbital timescales over the entire interval.

Site U1447

Background and objectives

Site U1447 is located in the Andaman Sea, ~45 km offshore Little Andaman Island at 1392 mbsl. The site lies within a basin on the eastern flank of a rise that separates two north-south–oriented basins structurally related to the Eastern margin and Diligent faults penetrating upward from the underlying accretionary wedge complex. The location yields access to older sediments but is not protected from potential turbidite deposition. The objectives at this site were to recover Miocene to recent sediments in order to reconstruct changes in summer monsoon rainfall and runoff from the Irrawaddy and Salween Rivers at tectonic to suborbital timescales.

Coring summary

At Site U1447, Holes U1447A, U1447B, and U1447C were drilled to total depths of 738.0, 24.4, and 158.9 m DSF, respectively. In Hole U1447A the APC, HLAPC, and XCB systems were deployed. In Holes U1447B and U1447C only the APC system was used. Overall, 108 cores were recorded for the site. A total of 451.27 m of core over a 444.3 m cored interval was recovered using the APC system (102% recovery). The HLAPC cored interval was 67.8 m with a core recovery of 69.12 m (102%). The XCB cored interval was 409.2 m with a core recovery of 395.15 m (97%). The overall recovery percentage for Site U1447 was 99%. The total time spent on Site U1446 was 6.13 days.

Lithostratigraphy

Sediments recovered from Holes U1447A, U1447B, and U1447C are principally composed of Late Pleistocene to late Miocene hemipelagic clays with a significant biogenic component and occasional thin turbidites, composing four distinct lithologic units (I–IV):

- Unit I (0–126.66 m CSF-A) is composed of Late Pleistocene greenish gray clayey nannofossil oozes with foraminifers and foraminifer-rich nannofossil oozes with clay.
- Unit II (126.6–319.67 m CSF-A) is composed of Late Pleistocene–late Pliocene greenish gray clayey nannofossil oozes with foraminifers, foraminifer-rich nannofossil oozes with clay, and clayey calcareous oozes with varying proportions of foraminifers. This unit is also characterized by the presence of numerous thin to thick light gray turbidites, described as foraminifer-rich sand or silt and bioclastic-rich layers with authigenic carbonate and foraminifers.
- Unit III (325.63–507.74 m CSF-A) is composed of early Pliocene to late Miocene greenish gray clayey nannofossil oozes to calcareous oozes with varying amounts of glauconite.
- Unit IV (507.70–585.33 m CSF-A) is composed of late Miocene greenish gray–gray clayey nannofossil ooze with glauconite or biosilica, biosilica-rich clay with varying proportions of glauconite and nannofossils, and nannofossil-rich clay with biosilica.

The observed lithologic differences between the units are primarily the result of varying abundances of biosilica (principally diatoms and sponge spicules), turbidites, and nannofossils.

Biostratigraphy

Calcareous nannofossils are abundant or common throughout Hole U1447A. Their preservation is generally very good to moderate, except in two samples that contain poorly preserved, overgrown nannofossils. Foraminifers are dominant to abundant and very well preserved throughout the Pliocene–Pleistocene, with a few exceptions in the turbiditic interval of lithostratigraphic Unit II where preservation decreases to moderate or poor and/or abundance decreases to common. Foraminifers are dominant to abundant in most Miocene sediments as well, though abundance decreases to common or few in samples where diatom abundance is high. Preserva-

tion in the Miocene continues to be good with only two exceptions where moderate preservation accompanies low foraminifer abundances. Diatoms are sporadically present in the uppermost 566 m of Hole U1447A. Their abundance varies between abundant and few downcore. Valve preservation ranges from good to poor, and valves are better preserved whenever abundance is higher than common.

The frequency and distribution of nannofossil and foraminifer bioevents meant that we were able to construct a high-resolution age model for Site U1447. Diatoms were also useful for age estimation deeper than 556.11 m CSF-A. A few paleomagnetic reversal datums fit well into the general age model. The base of the Late Pleistocene was delineated by the LO of *Globigerinoides ruber* (pink) at 32.25 m CSF-A. The Pliocene/Pleistocene boundary (2.59 Ma) is placed just below the LO of *Discoaster pentaradiatus* (2.39 Ma), which occurs between 299.78 and 301.89 m CSF-A. The Miocene/Pliocene boundary (5.33 Ma) occurs between 468.89 and 470.19 m CSF-A based on the LO of *Triquetrorhabdulus rugosus* (5.28 Ma) and the FO of *Ceratolithus acutus* (5.35 Ma) in this interval.

The oldest calcareous nannofossil sample studied contained *Discoaster hamatus*, suggesting an age older than 9.53 Ma The oldest planktonic foraminifer datum encountered is the FO of *Neogloboquadrina acostaensis* (9.83 Ma). *Globorotalia limbata* is found, suggesting that the basal age of Hole U1447A is between 9.83 and 10.66 Ma. The oldest diatom datum is the FO of *T. burckliana* (between 719.87 and 721.31 m CSF-A), suggesting that the bottom of Hole U1447A is slightly older than 9.1 Ma. Based on linear fits, including all biostratigraphy and magnetostratigraphy data, sedimentation rates in Hole U1447A are highest in the Pleistocene (average = 12 cm/ky linear sedimentation rate [LSR]), moderate in the Pliocene and most of the Miocene (average = 6.5 cm/ky LSR), and possibly lowest in the Miocene deeper than 700 m CSF-A.

Geochemistry

The geochemistry of Site U1447 mainly reflects the anaerobic processes of sulfate reduction and methanogenesis associated with microbial degradation of organic matter. The organic carbon content ranges from 0.1 to 2.0 wt% (average = 0.8 wt%). Sulfate declines rapidly from 28 mM at the sediment/water interface to nearly zero values at approximately 20 m CSF-A. A convex-up shaped sulfate profile shows sulfate reduction by means of organic matter degradation, whereas the role of anaerobic methane oxidation appears low. Alkalinity peaks at 20 m depth, consistent with the production of bicarbonate during sulfate reduction. A gradual increase in dissolved Ba concentration with depth suggests ongoing barite dissolution and potential deep sulfate reduction. Changes in the concentration of other elements and ions (Fe, Mn, Ca, B, ammonium, and Sr) in IW can be readily explained by microbially mediated chemical reactions and their effects on pH, alkalinity, and mineral dissolution and precipitation. Headspace methane concentrations in sediment peak at 125 m, abruptly decrease below the peak, and are consistently low to the bottom. High methane/ethane ratios suggest that the methane is mostly of biogenic origin (methanogenesis). Carbonate content varies significantly between 9 and 55 wt%.

Paleomagnetism

Paleomagnetic measurements were conducted on archive-half sections for all three holes at Site U1447, with AF demagnetization up to 10 mT. Discrete samples taken from the working-half sections of Holes U1447A were also analyzed, with stepwise AF demagnetization up to 40–80 mT. ChRMs of these discrete samples were calculated using the PCA technique. Both types of data became noisy deeper than ~90 m CSF-A, with predominant drilling-related overprint. Tentative magnetostratigraphy was proposed on the basis of these data to 1.778 Ma at ~220 m CSF-A for Hole U1447A. In addition, ARM was acquired and measured on a selection of Hole U1447A discrete samples for preliminary insight into depth variations in Site U1447 sediment bulk magnetic properties.

Physical properties

The physical property data collected at Site U1447 were found to be in good agreement with the lithostratigraphic data. However, based on overall physical property data we have divided Hole U1447A into four physical property units. The shifts in bulk density and porosity reflect changes in sediment composition. We observe similar trends in all physical property data between Holes U1447A and U1447C. Long-term cyclic variability in NGR values may reflect periodic changes in lithogenic input.

Stratigraphic correlation

A composite scale (CCSF-A) and a splice were constructed for Site U1447 using Holes U1447A and U1447C using MS, NGR, and RGB data. Splicing among these holes enabled us to construct a continuous stratigraphic sequence to ~147 m CCSF-D. Because of data quality and time availability issues, correlation should be viewed with caution deeper than ~112 m CCSF-A.

Highlights

Site U1447 exhibits a nearly complete hemipelagic succession from the recent (mudline with common fragile epifaunal tubular agglutinated foraminifers of the genera *Rhabdammina* and *Saccorhiza*) to middle Miocene (~9.8 Ma), with all nannofossil biostratigraphic markers present.

Unconformities with possible short-term stratigraphic hiatuses in the upper part of the sedimentary succession include the following:

- A massive carbonate turbidite bed in the uppermost (Holocene) part of the succession at ~1.40–2.4 m CSF-A.
- A hiatus at ~290 m CSF-A (~2.17 s TWT on Line AN-01-25A) is indicated by the co-occurrence of several biostratigraphic events within the same stratigraphic interval. This unconformity may be associated with a prominent turbidite bed at Section 353-U1447A-36F-1, 40 cm, close to the Pliocene–Pleistocene transition.
- A similar possible hiatus is indicated by a cluster of biostratigraphic events at 340 m CSF-A (~2.23 s TWT on Line AN-01-25A) within the early–late Pliocene transition. The unconformity would be located within Core 46X, which had no recovery, whereas drilling progress indicated a noticeable change in lithology.
- A third possible hiatus is located at 470 m CSF-A (~2.38 s TWT on Line AN-01-25A), within the Miocene–Pliocene transition (several nannoplankton events clustering around 5.35 Ma datum) with the LO of *Globoquadrina dehiscens* (5.92 Ma) in Core 61X-CC close below this interval. The sedimentary succession in this interval shows a distinct unconformity at the base of a distinct black layer at Sample 60X-4, 70–73 cm.

These unconformities may be related to distinct regional tectonic events, and further investigation of their stratigraphic and re-

gional extent will provide new insight into the Miocene–recent tectonic evolution of the Andaman accretionary wedge complex.

The expanded stratigraphic section in Hole U1447A provides a first high-resolution record of late Miocene Indian monsoon variability in the Bay of Bengal. Shipboard investigations provided the first evidence for a link between monsoonal intensity and biosiliceous paleoproductivity patterns in the Andaman Sea over the last 9.8 My. All Pleistocene and most of the Pliocene sediments of Site U1447 are virtually barren of diatoms, which exhibit last common occurrences below the Miocene/Pliocene boundary. This temporal distribution pattern is distinctly different from the late Miocene–early Pliocene "biogenic bloom" observed throughout the open tropical Indo-Pacific and Atlantic Oceans (e.g., Farrell et al., 1995; Dickens and Owen, 1999; Hermoyian and Owen, 2001). The maximum in diatom abundance in the Andaman area (roughly between 9.8 and 6.5 Ma at Site U1447) together with an increase in authigenic pyrite and carbonate started earlier and lasted shorter than the open-ocean biogenic bloom. These peculiar productivity changes within the Bay of Bengal could either reflect the availability of nutrients brought into the Bay of Bengal by rivers under a variable monsoonal intensity since the middle Miocene (Clift, 2006) or be related to the presence or absence of a seasonal freshwater lid, which would prevent upwelling of nutrient-rich intermediate waters during the monsoon season.

Site U1448

Background and objectives

Site U1448 (1097 mbsl) is located in the Andaman Sea, ~44 km offshore Little Andaman Island, 17.7 km south of Site U1447. The site lies atop a rise separating north-south–oriented basins associated with the Eastern margin and Diligent faults, both related to the underlying accretionary wedge complex. The ridge-top location should have a lower sedimentation rate and be better protected from turbidite deposition. The objectives at this site are to recover Pliocene to recent sediments in order to reconstruct changes in summer monsoon rainfall and runoff from the Irrawaddy and Salween Rivers at tectonic to suborbital timescales.

Coring summary

At Site U1448, Holes U1448A, U1448B, and U1448C were drilled to total depths of 421.0, 358.6, and 34.3 m DSF, respectively. In Hole U1448A the APC, HLAPC, and XCB systems were deployed. In Hole U1448B the APC and HLAPC systems were used, and only the APC system was deployed for Hole U1448C. Overall, 121 cores were recorded for the site. A total of 427.52 m of core over a 416.2 m cored interval was recovered using the APC system (103% recovery). The HLAPC cored interval was 318.6 m with a core recovery of 333.24 m (105%). The XCB cored interval was 77.6 m with a core recovery of 78.21 m (101%). The overall recovery percentage for Site U1448 was 103%. The total time spent on Site U1448 was 3.9 days.

Lithostratigraphy

Sediments recovered from Site U1448 are principally composed of hemipelagic clays with a significant biogenic component composing four distinct lithologic units (I–IV) and are Late Pleistocene to middle–early Miocene age.

- Unit I (0–183.11 m CSF-A) is composed of Late to early Pleistocene greenish gray clay with varying proportions of nannofossils and foraminifers, and clayey nannofossil ooze.
- Unit II (183.11–338.6 m CSF-A) is composed of early Pleistocene to late Miocene greenish clay with varying proportions of nannofossils and foraminifers, and characterized by the low proportions (≤1%) of biosilica.
- Unit III (338.6–379.11 m CSF-A) is composed of late Miocene greenish dark to light gray nannofossil-rich clay and clay with nannofossils, and characterized by the increased abundances of glauconite (up to 7%) and siliceous sponge spicules (up to 4%). A hiatus representing ~7 My occurs at the base of Unit III at 379.11 m CSF-A, where there is an abrupt change to lithologic Unit IV.
- Unit IV (379.11–420.60 m CSF-A) is composed of middle–early Miocene greenish gray–light greenish gray biosiliceous ooze with varying proportions of clay and nannofossils.

The observed lithologic differences between the units are primarily the result of varying abundances of biogenic components (nannofossils, foraminifers, diatoms, and sponge spicules), clay, and glauconite.

Biostratigraphy

Calcareous nannofossils are abundant throughout Hole U1448A, and their preservation is very good in the Pleistocene, Pliocene, and uppermost Miocene sediments (0–379.1 m CSF-A), with few reworked species. Below the hiatus, at 379.11 m CSF-A (separating late Miocene and middle Miocene sediments), nannofossils are abundant as well but moderately preserved. Nannofossil assemblages are typical of tropical/subtropical paleoenvironments. Foraminifers are well-preserved in all core catcher samples from Hole U1448A; they are dominant in the upper 340 m, whereas their abundance decreases to common just above the hiatus and drops to few to common below the hiatus. Diatoms are rarely present in the uppermost 379.04 m of Hole U1448A. Their abundance abruptly increases just below the hiatus and their preservation varies from moderate to good.

The age model for Site U1448 was established by combining nannofossil, planktonic foraminifer, and diatom datums (the latter below the hiatus only). The oldest calcareous nannofossil sample studied above the hiatus suggests an age between 6.91 and 7.42 Ma, whereas planktonic foraminifer datums suggest that the age of the oldest core catcher sample above the hiatus is between 5.92 and 8.58 Ma. Slightly different ages are suggested for the sediments below the hiatus by the three different microfossil groups. The interval between the hiatus and the bottom of Hole U1448A was constrained between 14.91 and 17.71 Ma based on nannofossils. The foraminifer assemblage in the youngest core catcher sample below the hiatus is older than 14.53 Ma, whereas the oldest planktonic foraminifer datum encountered is the LO of *Praeorbulina glomerosa* (14.78 Ma). The foraminifer *P. glomerosa* is found in the deepest sample (353-U1448A-60X-CC), defining the basal age of Hole U1448A as 14.78–16.27 Ma. Combining the ages of biostratigraphic events of nannofossil and planktonic foraminifers provides the basis for estimating the duration of the Miocene hiatus to approximately 8 My between 6.91–7.47 and 14.91–16.38 Ma. The co-occurrence of the diatom species *Rhaphidodiscus marylandicus* and *Annellus californicus* in the lowermost part of Hole U1448A suggests the bottom of this hole is older than 16.7 Ma (LO of *R. marylandicus*) and younger than 17.3 Ma (FO of *A. californicus*).

Age-depth relationships for Hole U1448A based on biostratigraphy for the three fossil groups studied show good agreement. Sedimentation rates above the hiatus are between 5 and 6 cm/ky.

Sedimentation rates below the hiatus are difficult to quantify given the wide range of estimated ages.

Geochemistry

The geochemistry of Site U1448 mainly reflects the anaerobic processes of sulfate reduction and methanogenesis associated with microbial degradation of organic matter. The organic carbon content ranges from 0.2 to 1.4 wt% (average = 0.6 wt%). Sulfate declines from 28 mM at the sediment/water interface to nearly zero values at approximately 40 m CSF-A. Alkalinity has a broad peak, significantly lower than Site U1447, starting from 40 m to 150 m CSF-A before gradually decreasing, consistent with the production of bicarbonate during sulfate reduction. Headspace methane concentrations increase immediately below the sulfate interface and continue downcore with the highest values between 200 and 250 m CSF-A. The overall concentrations (20–30 ppmv), however, are quite low compared to Site U1447. High methane/ethane ratios suggest that the methane is mostly of biogenic origin (methanogenesis). A gradual increase in dissolved Ba concentration with depth suggests ongoing barite dissolution. Changes in the concentration of other elements and ions (Fe, Mn, Ca, B, ammonium, and Sr) in IW can be readily explained by microbially mediated chemical reactions and their effects on pH, alkalinity, and mineral dissolution and precipitation. Carbonate content varies significantly between 12 and 37 wt%.

Paleomagnetism

Paleomagnetic measurements were conducted on archive-half sections for all three holes at Site U1448. To accommodate the core flow, only APC and HLAPC cores from Hole U1448A were demagnetized by AF demagnetization up to 10 mT. XCB cores from Hole U1448A and APC cores from Holes U1448B and U1448C were measured only for NRM, with a few exceptions. HLAPC cores from Site U1448B have not been measured. Declination values from section measurements suggest the uppermost 200 m is largely divided into three magnetozones, corresponding to the Brunhes (C1n), Matuyama (C1r), and Gauss (C2An) Chrons. Discrete samples taken from the working-half sections of Hole U1448A (N = 90) were also analyzed, with stepwise AF demagnetization typically up to 80 mT, but generally the determination of ChRM was difficult. Stability of NRM appears to be high just below the hiatus (379.11 m CSF-A), with higher resolution measurements possibly inferring polarity transitions. ARM was acquired and measured on a selection of Hole U1448A discrete samples for preliminary insight into depth variations in Site U1448 sediment bulk magnetic properties.

Physical properties

The physical property data collected at Site U1448 were generally found to be in good agreement with the lithostratigraphy at this site; however, our unit division boundaries are different for the upper 182.9 m. We identified six physical property units in Hole U1448A. The data between Holes U1448A and U1448B correlate well. Many of the changes in physical property characteristics of Hole U1448A were gradual shifts to increasing or decreasing values. NGR data were the only data to show long-term cyclicity, possibly related to cyclicity in terrigenous input. Unit I shows high variability in most measurements, likely from unconsolidation in the upper sediment. Unit II shows little MS variability, increasing density, decreasing porosity, and relatively steady NGR counts. Unit III is characterized by an increase in MS, increase in density, increase in NGR counts, decrease in porosity, and lower b* values, indicating more terrigenous material and clay relative to carbonate or siliceous fractions. Unit IV corresponds to lithostratigraphic Unit II. It has steady high MS values, steady high density, a continued decrease in porosity, variable NGR counts, and the lowest b* values that transition to a smaller Unit V, where MS values decrease, density decreases, porosity increases, NGR counts decrease, and b* begins to increase. The physical properties of Unit V likely indicate an increase in abundance of more biosilica-rich clays. All physical property measurements showed a very dramatic change at 379.1 m CSF-A, which was determined to mark an approximately 7 My hiatus.

Stratigraphic correlation

A composite scale (CCSF-A) and a splice were constructed for Site U1448 using Holes U1448A, U1448B, and U1448C using MS, NGR, and RGB data. Splicing among these holes enabled us to construct a continuous stratigraphic sequence to ~203 m CCSF-D. Following a set gap, a floating composite scale was constructed between ~205 and ~260 m CCSF-A using Holes U1448A and U1448B. Because of data quality and time availability issues, correlation should be viewed with caution deeper than ~115 m CCSF-A.

Highlights

In contrast to the sedimentation at Site U1447, where the lower Pleistocene and middle–upper Pliocene was partly affected by sediment gravity deposition (turbidites or fine-grained grain flows/debris flows), the lower Pleistocene and Pliocene of Site U1448 exhibit a complete hemipelagic succession with all calcareous biostratigraphic markers represented. The intermediate to high sedimentation rates of this succession (5–6 cm/ky) will allow high-resolution paleoclimatic reconstructions using calcareous and organic proxy indicators of paleotemperature and salinity in a continuous succession reaching into the late Miocene (6.91 Ma). Hole U1448C recovered an excellent mudline, with common fragile epifaunal tubular agglutinated foraminifers.

The high-resolution sedimentary succession of Site U1448 also allowed recognition of a suite of volcanic tephra layers that appear partly correlative to the tephra succession of Site U1443. In particular, the tephra of the Late Pleistocene Toba eruption (0.0738 Ma) could be recognized in all three holes of Site U1448 and provides an excellent marker bed for stratigraphic correlation.

The main highlight at Site U1448 was the recovery of pelagic middle Miocene sediment below the distinct seismic reflector at 1.865 s TWT on seismic Line AN01-26A. The reflector represents a major unconformity between late Miocene (oldest biostratigraphic datum just above the unconformity is 6.91 Ma, LO of *Reticulofenestra rotaria*) and middle Miocene (14.53 Ma, LO of *Praeorbulina sicana* just below the unconformity). The middle Miocene pelagic succession below the unconformity comprises a carbonate-rich biosiliceous sedimentary succession that was fully recovered in very high quality XCB cores and will provide the first insight in monsoonal influenced biogenic sedimentation during the middle Miocene climatic optimum.

Expedition 353 synthesis

Six sites were drilled during Expedition 353 in the Bay of Bengal, recovering a total of 4280 m of sediment section during 32.9 days of on-site operations. One hole was logged. This is substantially less than the initially planned campaign targeting 6256 m of section, including downhole logging at three sites (Clemens et al., 2014). This

difference amounts to approximately 15 days of lost operational time. Weather accounted for 1.6 days of lost operations. Mechanical breakdowns and broken coring equipment accounted for 1.98 days of lost operations. The remainder of the lost operational time was due to delays in attaining the necessary permissions to operate in Indian exclusive economic zone (EEZ) waters, scheduling and conducting the necessary vessel inspections required to operate in Indian EEZ waters, and negotiations over the concern that the *JOIDES Resolution* would incur excessive fees/duties upon entering port for inspection.

Operations at Site U1443 (NER) were scheduled to be three holes to 350 mbsf with logging. This was largely accomplished with the exception of logging because of loss of operational time as noted above. Recovery was excellent, and triple-coring produced the first complete spliced record of Neogene deepwater sediments in the Indian Ocean and a paleomagnetic reversal record spanning the lower Miocene and upper Oligocene. This will provide for the opportunity for high-resolution climate reconstructions with solid chronostratigraphic control.

Bengal Fan Site U1444 was not intended to be drilled during Expedition 353. Drilling this site was necessary because it was in international waters and occupied a portion of the time during which negotiations over fees, duties, and inspection matters were ongoing. Nevertheless, this site will promote the scientific goals of Expedition 354. We successfully dated the Unconformities Uc (Middle to Late Pleistocene) and Ud (middle Pliocene) defined in Schwenk and Spieß (2009). Preliminary results indicate that Unconformity Uc, within the error of dating, is the same age as found at Site 218, whereas Unconformity Ud may be considerably younger than the Site 218 unconformity hypothesized to be of the same age.

Operations at Site U1445, as planned, included two holes to 680 mbsf with logging. This was abbreviated to two holes spanning 672 and 305 m because of loss of operational time noted above. This site, located on the upper continental rise in the southern Mahanadi basin, although susceptible to turbidite and other gravity flow deposits, allowed recovery of lower Pleistocene to upper Miocene sediments; this portion of the Indian margin record is not available at the other Mahanadi site (U1446). Recovery was a remarkable 99% at this site, including 447 m of XCB coring. Loss of sediment because of gas expansion was minimized by using 8 m XCB advances, allowing accommodation space within the core barrel. This site was the only site at which centimeter-scale cold spots were detected by infrared scanning of the core on the catwalk prior to sectioning. These intervals were documented to be related to gas hydrates by Rhizon pore water sampling, which revealed reduced chlorinity driven by gas hydrate disassociation.

Site U1446 is located on the continental slope within the Mahanadi basin on a northwest-southeast–trending ridge, effectively isolated from turbidite deposition. Operations here called for three holes to 184 mbsf. Loss of operational time discussed above resulted in an abbreviated plan, including two holes to the target depth. Both holes were accomplished with APC coring with over 100% recovery and excellent core quality. Recovered sediments spanned the past 1.2 My, including the initiation of high-amplitude Northern Hemisphere glaciation. Combined with sediments from Site U1445, reconstruction of monsoon climate change from the latest Miocene through recent is now possible for the first time in this important region.

Andaman Sea Sites U1447 and U1448 are ~10 nmi apart but within different depositional settings. Site U1447 is located within a basin on the flank of a rise, susceptible to turbidite deposition but reaching back to the middle Miocene, whereas Site U1448 is on the top of the ridge, sheltered from turbidite deposition but reaching only into the late Miocene, where a hiatus transitions abruptly from ~7 to ~14 Ma. Operations at Site U1447 initially targeted two deep holes to 738 m with downhole logging at one site. Restrictions on operational time reduced this site to one deep hole (738 m) and one shallow hole (160 m) with no logging. Similarly, operations at Site U1448 called for three holes to 422 m. This plan was truncated to two holes, one to target depth and the other to 356 m. These Andaman Sea sites allow for the first time reconstruction of monsoonal climates from late Miocene to present in this region.

Expedition 353 science assessment

Drilling operations—core handling

Drilling operations and core handling were performed absolutely professionally and with outstanding commitment. Results were accordingly extraordinary (i.e., full-recovery APC coring to more than 350 mbsf in two holes and complete APC records to the early Oligocene at Site U1443, where previous APC coring terminated within the Pleistocene). In the cases of technical issues or sediment issues such as intense degassing within the core barrel, appropriate drilling and core handling adjustments were implemented rapidly, preserving the scientific value of the cored sections. Overall, the outstanding skills of the drillers and core technicians were the main reason why, despite initial setbacks, the scientific goals of Expedition 353 were able to be accomplished.

Critical aspects

Physical property data quality and stratigraphic correlation

Relatively poor data quality of MS (Section Half Multisensor Logger [SHMSL]), NGR, and color reflectance measurements (SHMSL) made it impossible to create reliable splices at sea for crucial parts of the records recovered during Expedition 353. In particular, sections that were cored using the HLAPC, which were of outstanding quality, could not be correlated with sufficient precision because of the lack of detail in the physical property data. This stemmed from two factors, the primary being the extremely noisy SHMSL data associated with the inability of the instrument to land the MS and spectral sensors flush on the core surface; it is possible that these measurements may simply have to be done by hand. The other contributing factor is specific to the sediments recovered. In many cases, the MS signal of the sediment was low because diagenetic factors and color variation within sediments was relatively low. Even so, the only data set that proved of reliable quality and sufficient resolution was the line scan RGB data. These data, however, cannot stand alone as the only data available for creating reliable splices at sea. A possible solution to this dilemma in the future would be to install a shipboard X-ray fluorescence (XRF) scanning facility. This would reliably compensate for low MS and color variability and greatly enhance the lithologic description available at sea.

To overcome significant problems with high-resolution sampling plans for Expedition 353, which are now jeopardized by the lack of a splice in many Pliocene and late Miocene intervals, IODP should facilitate rapid distribution of U-channels and archive sections for XRF scanning at shore-based facilities at Woods Hole, Bordeaux, Bremen, Kiel, and Canberra. These facilities are made available to shipboard scientists. With this effort, the generation of splices within a time window close to the sampling party will be possible.

Administrative preparation for operations within Indian EEZ waters

During Expedition 353, 4280 m of sediment section was recovered during 32.9 days of on-site operations. One hole was logged. As initially planned, the expedition targeted 6256 m of recovery and three logged holes (Clemens et al., 2014). The lost logging holes and nearly 2000 m of unrecovered sediment section are accounted for by close to 15 days of lost operational time. Weather accounted for 1.6 days of lost operations. Mechanical breakdowns, four broken core barrels, rusted winch wire, and parting of the winch wire (twice, once necessitating fishing the core barrel) accounted for 1.98 days of lost operations. This lost time can be largely attributed to the hazards of working in difficult environments.

The large majority of the lost operational time was due to delays in attaining the necessary permissions to operate in Indian EEZ waters, scheduling and conducting the vessel inspections required to operate in Indian EEZ waters, and protracted negotiations over concern that the *JOIDES Resolution* would incur excessive fees/duties upon entering port for inspection. These issues are typically addressed and resolved prior to an expedition and would not normally impact operational time. In this case, Expedition 353 had to compensate by cutting two of the three planned logging operations, canceling one primary site in the Mahanadi basin entirely, and canceling or shortening additional holes required to ensure complete spliced records to full target depths in the Mahanadi basin and Andaman Sea. Fortunately, formation characteristics and sea state worked strongly in our favor to produce excellent (near 100%) recovery, even in XCB cored intervals. This will serve to reduce the negative impact of lost operational time.

Operations

During Expedition 353 we conducted operations in 18 holes at 6 sites. A total of 4484.3 m was drilled, 4431.8 m was cored, and 4280.12 m of core was recovered (Table **T1**). Downhole logs were conducted in Hole U1445A. Here, we describe the coring and logging operations at each of the sites. The overall time distribution included 6.9 days in port, 15.8 days in transit, and 32.9 days on site.

Singapore port call

The *JOIDES Resolution*'s first line ashore in Singapore was at 0936 h on 29 November 2014. The vessel was berthed at Loyang Jetty 2A for the duration of the port call. The *JOIDES Resolution* Science Operator staff plus the Co-Chief Scientists boarded the ship on 29 November. The science party boarded the ship the next day, 30 November. The Siem Offshore and subcontractor crews changed on 30 November.

Fuel was loaded by barge along with three tanks of lube oil. All outbound surface freight and airfreight were offloaded. The vessel was secured for sea with final maintenance checks performed prior to departure. The pilot arrived on aboard at 0948 h, and the last line was released at 1010 h on 4 December. The vessel began the 966 nmi passage to Site U1443 (primary Site N90E-2C).

Transit to Site U1443

After a 966 nm transit from Singapore averaging 11.7 kt, the vessel arrived at Site U1443 at 2037 h (UTC + 8 h) on 7 December 2014. The thrusters were lowered, and dynamic positioning (DP) assumed control at 2105 h. The positioning beacon was deployed and the vessel positioned to the site coordinates.

Site U1443

Site U1443 consisted of four holes, ranging in depth from 8.2 to 344.0 m DSF. Overall, 118 cores were recorded for the site. A total of 444.06 m of core over a 471.7 m interval was recovered using the APC system (94% recovery). The HLAPC system was used to core a 156.4 m interval and 161.25 m of core was recovered (103%). The cored interval with the XCB system was 258.4 m with a core recovery of 220.35 m (85%). The overall recovery percentage for Site U1443 was 93%. The total time spent on Site U1443 was 7.1 days.

Hole U1443A

Hole U1443A was spudded at 1735 h on 8 December 2014. The seafloor was calculated to be 2940.2 m DRF (2929.4 mbsl) based on the recovery of Core 353-U1443A-1H. However, this depth calculation is ~5 m greater than the other three holes drilled at Site U1443 and at Site 758; therefore, this depth calculation is likely incorrect because of loss of core out of the core barrel. Nonmagnetic core barrels were used for APC coring of Core 2H and Cores 4H through 15H. The FlexIT tool was used for core orientation on Cores 2H to 13H. Temperature measurements were taken with the third-generation advanced piston corer temperature tool (APCT-3) shoe on Cores 4H, 7H, 10H, and 13H with good results. The HLAPC system, using nonmagnetic core barrels, was deployed for Cores 14F to 29F. Cores 30X to 48X were cored using the XCB system. The total depth of Hole U1443A is 344.0 m DSF. The drill string was pulled out of the hole and cleared the seafloor at 0225 h on 11 December, ending Hole U1443A.

A total of 15 APC cores were taken over a 134.8 m interval with a total recovery of 137.43 m of core (102% core recovery). Fourteen HLAPC cores were retrieved over a 67.2 m interval with 69.64 m recovered (104%). The XCB system was used for 19 cores over a drilled interval of 142.0 m with 119.73 m recovered (84%). Total core recovery for Hole U1443A was 95%.

Hole U1443B

After clearing the seafloor, the vessel was offset 20 m north of Hole U1443A. Hole U1443B was spudded at 0530 h on 11 December. The seafloor was calculated at 2935.5 m DRF (2924.8 mbsl). Non-magnetic core barrels were used for APC coring from Core 353-U1443B-1H to 18H. The FlexIT orientation tool was used for Cores 2H to 16H. The HLAPC coring system was deployed for Cores 19F to 28F. The XCB coring system was then used to take Cores 29X to 40X. The total depth of Hole U1443B is 326.4 m DSF. The drill string was pulled from the hole and cleared the seafloor at 2310 h on 12 December, ending Hole U1443B.

A total of 20 APC cores were taken over a 162.0 m interval with a total recovery of 158.35 m of core (98% core recovery). The HLAPC system was used for 10 cores over a 48 m interval with 49.54 m recovered (103%). The XCB system was used for 12 cores over a drilled interval of 116.4 m with 100.62 m recovered (86%). Total core recovery for Hole U1443B was 95%.

Hole U1443C

The vessel was offset 20 m west of Hole U1443B to initiate Hole U1443C. An APC core barrel was shot into the mudline and the core barrel broke. The vessel was offset 15 m to the north and a second steel core barrel was shot. This core barrel was also broken, with part of it remaining in the bottom-hole assembly (BHA); it was successfully fished out on the second attempt. The vessel was again offset 15 m to the north, and a third APC core barrel was broken

during the shot. An XCB assembly was deployed to check the BHA components. After confirming that the BHA was clear, it was decided to use the HLAPC to spud Hole U1443C. The vessel was offset 50 m south (20 m west of Hole U1443A).

Hole U1443C was spudded at 1040 h on 13 December 2014 and Cores 353-U1443C-1F and 2F were retrieved. Coring continued with nonmagnetic full-length APC core barrels from Cores 3H to 24H. Two drilled intervals (353-U1443C-141 and 171; 1.0 and 0.5 m, respectively) were necessary to offset cores for stratigraphic correlation. The IceField tool was used for orientation on Cores 3H to 5H, and the FlexIT orientation tool was used for Cores 6H to 19H. The HLAPC was again deployed for Cores 25F to 30F. The total depth of Hole U1443C is 209.4 m DSF. The drill string was pulled from the hole and cleared the seafloor at 1325 h on 14 December, ending Hole U1443C.

A total of 20 APC cores were taken over a 174.9 m interval with a total core recovery of 148.28 m (85% core recovery). The HLAPC system was used for 8 cores over a 33 m interval with 34.59 m recovered (105%). Total core recovery for Hole U1443C was 88%.

Hole U1443D

The vessel was offset 20 m to the south of Hole U1443C. Hole U1443D was spudded at 1455 h on 14 December 2044, and two HLAPC cores (353-U1443D-1F and 2F) were taken to recover a complete mudline section. Hole U1443D was drilled to a total depth of 8.4 m DSF.

A total of two HLAPC cores were recovered over an 8.2 m interval with 7.48 m recovered (91% core recovery).

Following Hole U1443D, the drill pipe was tripped and the bit cleared the drill floor at 0300 h on 15 December. The ship was then prepared for transit to Visakhapatnam, India.

Transit to Site U1444

Following end of Site U1443, the vessel had an 826 nmi transit to Visakhapatnam, India, to have a Naval Inspection of the ship. This inspection is mandatory for receiving clearance to operate within the Indian EEZ. At 1048 h on 18 December 2014, the ship arrived ~36 nmi outside of the port. The port agent alerted the ship not to come into port until all of the necessary permits and exemptions were in place. After 5 days of waiting on standby at the operator's request, the decision was made to begin coring operations at alternative sites on the Bengal Fan. After learning that Indian customs would not allow any additional passengers, including Indian scientists, to board until the ship docked and port formalities were conducted, the vessel began the transit to Site U1444 (proposed alternate Site BoB-11A).

The vessel arrived at Site U1444 at 0715 h on 24 December, after a 191 nmi transit. A beacon was deployed, an APC/XCB BHA was made up, and the drill string was assembled.

Site U1444

Site U1444 consisted of two holes, ranging in depth from 128.6 to 330.6 m DSF. Overall, 46 cores were recorded for the site. A total of 156.21 m of core over a 160.0 m cored interval was recovered using the APC system (98% recovery). The HLAPC system was used to core a 4.8 m interval and 3.94 m of core was recovered (82%). The cored interval with the XCB system was 246.9 m with a core recovery of 140.06 m (57%). The overall recovery percentage for Site U1444 was 73%. The total time spent on Site U1444 was 3.9 days.

Hole U1444A

The first attempt at a mudline core resulted in a broken and bent core barrel. The vessel was offset 10 m north to avoid core barrel debris and a second mudline core was attempted. Hole U1444A was spudded at 2035 h on 24 December. The water depth was estimated to be 3143.4 meters below rig floor (mbrf) based on the precision depth recorder. APC coring continued to 112.5 mbsf. The XCB system was then deployed. Core recovery dropped significantly between Cores 353-U1444A-20X and 30X (15%). The HLAPC was deployed for Core 24F in an attempt to recover more sediment. This core returned 3.94 m of watery, unconsolidated sand. When Core 37X was retrieved from 330.9 mbsf, it was noted that the cutting shoe had failed and part of it was left in the hole. Coring was terminated in Hole U1444A. The drill string was pulled out of the hole and cleared the seafloor at 0600 h on 27 December, ending Hole U1444A.

Nonmagnetic core barrels were used on Cores 353-U1444A-2H to 13H and 24F. Core orientation using the IceField tool was performed on Cores 2H to 13H. Temperature measurements were taken on Cores 4H, 7H, 10H, and 13H using the APCT-3; however, the temperature measurement for Core 13H appears to be erroneous, potentially because of the difficulties extracting the core barrel from the sediment.

A total of 13 APC cores were taken over a 112.5 m interval with a total core recovery of 112.93 m (100% core recovery). One HLAPC core was retrieved over a 4.8 m interval with 3.94 m recovered (82%). The XCB system was used for 23 cores over a cored interval of 213.3 m with 109.18 m recovered (51%). Total core recovery for Hole U1443A was 68%.

Hole U1444B

The vessel was offset 20 m to the south and Hole U1444B was spudded from 3142.5 mbrf. A full core was retrieved and the seafloor was estimated at 3142.5 mbrf. The APC system was deployed for Cores 353-U1444B-1H to 5H, which reached a depth of 47.5 mbsf. Nonmagnetic core barrels were used for Cores 2H to 5H. The hole was then drilled to 95 mbsf and the XCB system was deployed for Cores 7X to 10X. Hole U1444B was terminated at a total depth of 128.6 mbsf. The drill string was recovered and the bit cleared the seafloor at 2220 h on 27 December. The bit cleared the rotary table at 0445 h on 28 December and the beacon was recovered at 0600 h. The thrusters were raised at 0630 h and the sea voyage back to Visakhapatnam began at 0645 h.

A total of five APC cores were taken over a 47.5 m interval with a total core recovery of 43.28 m (91% core recovery). The XCB system was used for four cores over an interval of 33.6 m with 30.88 m recovered (92%). A drilled interval was recorded in Hole U1444B of 47.5 m. Total core recovery for Hole U1443B was 91%.

Port Visakhapatnam

The *JOIDES Resolution* transited 235 nmi from Site U1444 to Visakhapatnam, India, for an inspection by the Indian Navy and to gain permission to core the remaining primary sites for Expedition 353. The vessel was tied up at the Fertilizer Pier in Port Visakhapatnam with the first line ashore at 0720 h on 29 December 2014. The naval inspection took place on 30 December and was completed by 1630 h. Three scientists from Indian institutions boarded the vessel at 2130 h on 30 December. A diplomatic note from the Indian Ministry of External Affairs granting clearance to operate within the Indian EEZ was received at 2145 h.

Transit to Site U1445

The vessel departed Visakhapatnam for Site U1445 (proposed primary Site BB-5) on 31 December with the last line ashore at 0306 h. After an 87 nmi transit, the ship arrived at Site U1445. The thrusters were lowered and DP assumed control of the vessel at 1942 h.

Site U1445

Site U1445 consisted of three holes, ranging in depth from 33.0 to 672.6 m DSF. Overall, 117 cores were recorded for the site. A total of 487.34 m of core over a 476.3 m cored interval was recovered using the APC system (102% recovery). The cored interval with the XCB system was 534.5 m with a core recovery of 518.02 m (97%). The overall recovery percentage for Site U1445 was 99%. The total time spent on Site U1445 was 9.3 days.

Hole U1445A

Winds of 35 kt and heave up to 4.5 m forced operations to wait on weather until 0245 h on 1 January 2015. At that time, an APC/XCB BHA was made and deployed to the seafloor by 1015 h. High heave conditions caused spudding of Hole U1445A to be delayed.

Hole U1445A was spudded at 1900 h on 1 January. The seafloor was estimated at 2502 mbsl. Cores 353-U1445A-1H to 24H (0–225.1 m DSF) were retrieved using the APC system. Temperature measurements were taken on Cores 4H, 7H, 10H, and 13H. Core orientation data were obtained from Cores 3H to 24H using the IceField tool. The XCB system was deployed for Cores 25X to 77X (225.1–672.6 m DSF). Coring advances of 8 m were utilized for Cores 33X, 34X, and 38X to 66X to allow for core expansion within the core liner.

After completion of coring operations in Hole U1445A, the hole was swept with 50 barrels of high-viscosity mud and then displaced with heavy weight (10.6 lb/gallon) mud in preparation for downhole logging operations. The hole was then logged using the triple combo tool string, including the magnetic susceptibility sonde (MSS), and the FMS-sonic tool. Each tool string was run twice from 85 to 444 m DSF. Neither tool string was able to pass below a bridge at 444 m DSF. Downhole logging operations were completed at 0630 h on 7 January. The drill string was pulled from the hole with the bit clearing the seafloor at 0711 h, ending Hole U1445A.

A total of 24 APC cores were taken over a 225.1 m interval with a total core recovery of 234.31 m (104% core recovery). The XCB system was used for 53 cores over a cored interval of 447.5 m with 432.09 m recovered (97%). Total core recovery for Hole U1445A was 99%.

Hole U1445B

The vessel was offset 20 m south and Hole U1445B was spudded at 1010 h on 7 January 2015. Hole U1445B was dedicated for high-resolution pore water sampling. Cores 353-U1445B-1H to 4H were retrieved with 101% recovery. The bit cleared the seafloor at 1320 h, ending Hole U1445B.

A total of four APC cores were taken over a 33.0 m interval with a total core recovery of 33.36 m (101% core recovery).

Hole U1445C

The vessel was offset 20 m west, and Hole U1445C was spudded at 1415 h on 7 January 2015. Cores 353-U1445C-1H to 24H were retrieved using the APC system. The APCT-3 was used on Cores 20H and 22H. Cores 3H to 24H were oriented using the IceField tool. The XCB system was deployed for Cores 25X to 36X (218.2–305.2 m DSF). After coring operations were completed, the hole was displaced with heavy mud. The pipe trip out of the hole was delayed for 3 h while a hydraulic dump valve was replaced on the iron roughneck power unit. The bit cleared the rig floor at 0430 h on 10 January. The rig was secured for transit, and the sea voyage to Site U1446 (proposed Site BB-7) began at 0548 h on 10 January.

A total of 24 APC cores were taken over a 218.2 m interval with a total core recovery of 219.67 m (101% core recovery). The XCB system was used for 12 cores over a cored interval of 87.0 m with 85.93 m recovered (99%). Total core recovery for Hole U1445C was 100%.

Transit to Site U1446

After a 97 nm transit from Site U1445, the vessel arrived at Site U1446 at 1515 h on 10 January 2015. As the thrusters were lowered, a fishing line was spotted. The ship maneuvered around the line and DP assumed control at 1614 h.

Site U1446

Site U1446 consisted of three holes ranging in depth from 27.1 to 182.0 m DSF. Overall, 47 cores were recorded for the site. A total of 344.95 m of core over a 342.3 m cored interval was recovered using the APC system (101% recovery). The cored interval with the HLAPC system was 46.8 m with a core recovery of 49.43 m (106%). The overall recovery percentage for Site U1446 was 101%. The total time spent on Site U1446 was 2.3 days.

Hole U1446A

An APC/XCB BHA was made up and Hole U1446A was spudded at 2225 h on 10 January 2015. The water depth for Hole U1446A is 1430.2 mbsl. Cores 353-U1446A-1H to 18H were retrieved using the APC system. Downhole temperature measurements using the APCT-3 tool were taken on Cores 4H, 7H, 10H, and 15H. Orientation using the IceField tool was performed on Cores 2H to 18H. The HLAPC was deployed for Cores 19F to 21F. After reaching a total depth of 180.0 m DSF, the drill string was pulled from the hole and the bit cleared the seafloor at 2105 h on 11 January.

A total of 18 APC cores were taken over a 165.8 m interval with a total core recovery of 171.88 m (104% core recovery). The HLAPC system was used for 3 cores over a cored interval of 14.2 m with 14.75 m recovered (104%). Total core recovery for Hole U1446A was 104%.

Hole U1446B

The vessel was offset 20 m west and Hole U1446B was spudded at 2150 h on 11 January 2015. The seafloor depth for Hole U1446B is 1429.6 mbsl. Hole U1446B was dedicated for high-resolution pore water sampling. Cores 353-U1446B-1H to 3H were retrieved with 100% recovery. The pipe was pulled from the hole and the bit cleared the seafloor at 2325 h, ending Hole U1446B.

A total of three APC cores were taken over a 27.1 m interval with a total recovery of 27.2 m of core (100% core recovery).

Hole U1446C

The vessel was offset 20 m north, and Hole U1446C was spudded at 0005 h on 12 January 2015. The water depth for Hole U1446C is 1430.0 mbsl. Cores 353-U1446C-1H to 16H were retrieved using the APC system. Cores 13H and 15H had no recovery despite evidence that sediment had been in the core liner. Core 15H was reshot

from the same depth and a full core was recovered. Orientation using the IceField tool was used on Cores 2H to 16H. The HLAPC was deployed for Cores 17F to 23F. After reaching a total depth of 182.0 m, the drill pipe was pulled from the hole and cleared the seafloor at 1930 h on 12 January. The vessel began the transit to Site U1447 at 2400 h on 12 January.

A total of 16 APC cores were taken over a 149.4 m interval with a total core recovery of 145.87 m (98% core recovery). The HLAPC system was used for 7 cores over a cored interval of 32.6 m with 34.68 m recovered (106%). Total core recovery for Hole U1446C was 99%.

Transit to Site U1447

After a 709 nm transit from Site U1446, the vessel arrived at Site U1447. The thrusters were lowered and DP assumed control at 1430 h on 15 January 2015.

Site U1447

Site U1447 consisted of three holes ranging in depth from 24.4 to 738.0 m DSF. Overall, 108 cores were recorded for the site. A total of 451.27 m of core over a 444.3 m cored interval was recovered using the APC system (102% recovery). The cored interval with the HLAPC system was 67.8 m with a core recovery of 69.12 m (102%). The cored interval with the XCB system was 409.2 m with 395.15 m of core recovered (97%). The overall recovery percentage for Site U1446 was 99%. The total time spent on Site U1447 was 6.1 days.

Hole U1447A

Hole U1447A was spudded at 2320 h on 15 January 2015. Core 353-U1447A-1H was used to estimate the seafloor depth at 1390.9 mbsl. The APC system was used for Cores 1H to 29H. The HLAPC was deployed for Cores 30F to 44F. Cores 45X to 88X were cut with the XCB system. Downhole temperature measurements using the APCT-3 tool were taken on Cores 4H, 7H, 10H, and 15H. The IceField tool was used to obtain orientation data for Cores 3H to 29H. After coring operations, the hole was displaced with heavy mud and the pipe was pulled from the hole. The pipe cleared the seafloor at 1705 h on 20 January.

A total of 29 APC cores were taken over a 261.0 m interval with a total core recovery of 268.69 m (103% core recovery). The HLAPC system was used for 15 cores over a cored interval of 67.8 m with 69.12 m recovered (102%). A total of 44 XCB cores were cut over a 409.2 m interval with 395.15 m of core recovered (97%). Total core recovery for Hole U1447A was 99%.

Hole U1447B

The vessel was offset 20 m south of Hole U1447A, and Hole U1447B was spudded at 2045 h on 20 January 2015. Cores 353-U1447B-1H to 3H were recovered and sampled for high-resolution pore water chemistry. The pipe was pulled from the hole and cleared the seafloor at 2220 h.

A total of three APC cores were taken over a 24.4 m interval with a total core recovery of 24.26 m (99% core recovery).

Hole U1447C

The vessel was offset 20 m east of Hole U1447B, and Hole U1447C was spudded at 2300 h on 20 January 2015. Cores 353-U1447C-1H to 18H were cored with the APC system to a total depth of 160.9 m. A 2 m drilled interval (353-U1447C-31) extended from 16.4 to 18.4 m DSF. Cores 3H to 16H were oriented using the IceField tool. At the end of coring operations, the pipe was pulled from the hole and cleared the seafloor at 1405 h on 21 January. The remaining drill pipe was tripped during the 9.4 nmi transit to Site U1448.

A total of 17 APC cores were taken over a 158.9 m cored interval with a total core recovery of 158.32 m (100% core recovery).

Transit to Site U1448

The 9.4 nmi transit from Site U1447 to U1448 was completed in DP mode with much of the transit being completed while the drill pipe was being pulled. The vessel arrived at Site U1448 at 1845 h on 21 January 2015. A positioning beacon was deployed at 1916 h and the vessel settled over the site coordinates.

Site U1448

Site U1448 consisted of three holes ranging in depth from 34.3 to 421.0 m DSF. Overall, 121 cores were recorded for the site. A total of 427.52 m of core over a 416.2 m cored interval was recovered using the APC system (103% recovery). The cored interval with the HLAPC system was 318.6 m with a core recovery of 333.24 m (105%). The cored interval with the XCB system was 77.6 m with 78.21 m of core recovered (101%). The overall recovery percentage for Site U1448 was 103%. The total time spent on Site U1448 was 3.9 days.

Hole U1448A

Hole U1448A was spudded at 0010 h on 22 January 2015. Core 353-U1448A-1H was used to estimate the seafloor depth at 1098.3 mbsl. The APC system was used for Cores 1H to 23H. Core 23H had no core recovery and was reshot from the same depth. The HLAPC was deployed for Cores 24F to 52F. Cores 53X to 60X were cut with the XCB system. Downhole temperature measurements were attempted using the APCT-3, but when it was deployed for Core 4H, the reading was bad. The IceField tool was used to obtain orientation data for Cores 3H to 23H. At the end of coring operations, the drill pipe was pulled from the hole and cleared the seafloor at 1830 h on 23 January.

A total of 23 APC cores were taken over a 204.2 m interval with a total core recovery of 210.99 m (103% core recovery). The HLAPC system was used for 29 cores over a cored interval of 139.2 m with 145.62 m recovered (105%). A total of 8 XCB cores were cut over a 77.6 m interval with 78.21 m of core recovered (101%). Total core recovery for Hole U1448A was 103%.

Hole U1448B

The vessel was offset 20 m south of Hole U1448A, and Hole U1448B was spudded at 2010 h on 23 January 2015. Cores 353-U1448B-1H to 19H were recovered using the APC system. Before switching to the HLAPC system, the hole was advanced 1.5 m without coring. The HLAPC was used for Cores 21F to 58F. Temperature measurements using the APCT-3 were taken on Cores 4H, 7H, 10H, and 15H. Cores 3H to 19H were oriented using the IceField tool. The drill string was then pulled from the hole and the bit cleared seafloor at 0630 h on 25 January, ending Hole U1448B.

A total of 19 APC cores were taken over a 177.7 m interval with a total core recovery of 181.76 m (102% core recovery). The HLAPC system was used for 38 cores that were taken over a 179.4 m interval and had 187.62 m of core recovered (105%). One drilled interval of 1.5 m (353-U1448B-201) was recorded for the hole. Total core recovery for Hole U1448B was 103%.

Hole U1448C

The vessel was offset 20 m west of Hole U1448B, and Hole U1448C was spudded at 0750 h on 25 January 2015. Cores 353-U1448C-1H to 4H were cored with the APC system to a total depth of 34.3 m DSF. The drill string was then pulled from the hole with the bit clearing the seafloor at 1000 h. The rig was secured for transit to Singapore.

A total of four APC cores were taken over a 34.3 m cored interval with a total core recovery of 34.77 m (101% core recovery).

References

Achyuthan, H., Deshpande, R.D., Rao, M.S., Kumar, B., Nallathambi, T., Shashi Kumar, K., Ramesh, R., Ramachandran, P., Maurya, A.S., and Gupta, S.K., 2013. Stable isotopes and salinity in the surface waters of the Bay of Bengal: implications for water dynamics and palaeoclimate. *Marine Chemistry,* 149:51–62. **http://dx.doi.org/10.1016/j.marchem.2012.12.006**

Akhil, V.P., Durand, F., Lengaigne, M., Vialard, J., Keerthi, M.G., Gopalakrishna, V.V., Deltel, C., Papa, F., and de Boyer Montégut, C., 2014. A modeling study of the processes of surface salinity seasonal cycle in the Bay of Bengal. *Journal of Geophysical Research: Oceans,* 119(6):3926–3947. **http://dx.doi.org/10.1002/2013JC009632**

Ali, S., Hathorne, E.C., Frank, M., Gebregiorgis, D., Stattegger, K., Stumpf, R., Kutterolf, S., Johnson, J.E., Giosan, L., in press. South Asian monsoon history over the past 60 kyr recorded by radiogenic isotopes and clay mineral assemblages in the Andaman Sea. *Geochemistry, Geophysics, Geosystems*. **http://dx.doi.org/10.1002/2014GC005586**

Altabet, M.A., Higginson, M.J., and Murray, D.W., 2002. The effect of millennial-scale changes in Arabian Sea denitrification on atmospheric CO_2. *Nature,* 415(6868):159–162. **http://dx.doi.org/10.1038/415159a**

An, Z., Clemens, S.C., Shen, J., Qiang, X., Jin, Z., Sun, Y., Prell, W.L., Luo, J., Wang, S., Xu, H., Cai, Y., Zhou, W., Liu, X., Liu, W., Shi, Z., Yan, L., Xiao, X., Chang, H., Wu, F., Ai, L., and Lu, F., 2011. Glacial–interglacial Indian summer monsoon dynamics. *Science,* 333(6043):719–723. **http://dx.doi.org/10.1126/science.1203752**

Anand, P., Kroon, D., Singh, A.D., Ganeshram, R.S., Ganssen, G., and Elderfield, H., 2008. Coupled sea surface temperature–seawater $\delta^{18}O$ reconstructions in the Arabian Sea at the millennial scale for the last 35 ka. *Paleoceanography,* 23(4):PA4207. **http://dx.doi.org/10.1029/2007PA001564**

Antonov, J.I., Seidov, D., Boyer, T.P., Locarnini, R.A., Mishonov, A.V., Garcia, H.E., Baranova, O.K., Zweng, M.M., and Johnson, D.R., 2010. World Ocean Atlas 2009 (Vol. 2): Salinity. *In* Levitus, S. (Ed.), *NOAA Atlas NESDIS 69:* Washington D.C. (U.S. Government Printing Office). **ftp://ftp.nodc.noaa.gov/pub/WOA09/DOC/woa09_vol2_text_figures.pdf**

Balmaseda, M.A., Mogensen, K., and Weaver, A.T., 2012. Evaluation of the ECMWF ocean reanalysis system ORAS4. *Quarterly Journal of the Royal Meteorological Society,* 139(674):1132–1161. **http://dx.doi.org/10.1002/qj.2063**

Bemis, B.E., Spero, H.J., Bijma, J., and Lea, D.W., 1998. Reevaluation of the oxygen isotopic composition of planktonic foraminifera: experimental results and revised paleotemperature equations. *Paleoceanography,* 13(2):150–160. **http://dx.doi.org/10.1029/98PA00070**

Bolton, C.T., Chang, L., Clemens, S.C., Kodama, K., Ikehara, M., Medina-Elizalde, M., Paterson, G.A., Roberts, A.P., Rohling, E.J., Yamamoto, Y., and Zhao, X., 2013. A 500,000 year record of Indian summer monsoon dynamics recorded by eastern equatorial Indian Ocean upper water-column structure. *Quaternary Science Reviews,* 77:167–180. **http://dx.doi.org/10.1016/j.quascirev.2013.07.031**

Bosilovich, M.G., and Schubert, S.D., 2002. Water vapor tracers as diagnostics of the regional hydrologic cycle. *Journal of Hydrometeorology,* 3(2):149–165. **http://dx.doi.org/10.1175/1525-7541(2002)003<0149:WVTADO>2.0.CO;2**

Burton, K.W., and Vance, D., 2000. Glacial–interglacial variations in the neodymium isotope composition of seawater in the Bay of Bengal recorded by planktonic foraminifera. *Earth and Planetary Science Letters,* 176(3–4):425–441. **http://dx.doi.org/10.1016/S0012-821X(00)00011-X**

Burton, K.W., Gannoun, A., and Parkinson, I.J., 2010. Climate driven glacial–interglacial variations in the osmium isotope composition of seawater recorded by planktic foraminifera. *Earth and Planetary Science Letters,* 295(1–2):58–68. **http://dx.doi.org/10.1016/j.epsl.2010.03.026**

Caballero-Gill, R.P., Clemens, S.C., and Prell, W.L., 2012. Direct correlation of Chinese speleothem $\delta^{18}O$ and South China Sea planktonic $\delta^{18}O$: transferring a speleothem chronology to the benthic marine chronology. *Paleoceanography,* 27(2):PA2203. **http://dx.doi.org/10.1029/2011PA002268**

Cai, Y., An, Z., Cheng, H., Edwards, R.L., Kelly, M.J., Liu, W., Wang, X., and Shen, C.-C., 2006. High-resolution absolute-dated Indian Monsoon record between 53 and 36 ka from Xiaobailong Cave, southwestern China. *Geology,* 34(8):621–624. **http://dx.doi.org/10.1130/G22567.1**

Caley, T., Malaizé, B., Bassinot, F., Clemens, S.C., Caillon, N., Linda, R., Charlier, K., and Rebaubier, H., 2011a. The monsoon imprint during the "atypical" MIS 13 as seen through north and equatorial Indian Ocean records. *Quaternary Research,* 76(2):285–293. **http://dx.doi.org/10.1016/j.yqres.2011.07.001**

Caley, T., Malaizé, B., Revel, M., Ducassou, E., Wainer, K., Ibrahim, M., Shoeaib, D., Migeon, S., and Marieu, V., 2011b. Orbital timing of the Indian, East Asian and African boreal monsoons and the concept of a "global monsoon." *Quaternary Science Reviews,* 30(25–26):3705–3715. **http://dx.doi.org/10.1016/j.quascirev.2011.09.015**

Caley, T., Malaizé, B., Zaragosi, S., Rossignol, L., Bourget, J., Eynaud, F., Martinez, P., Giraudeau, J., Charlier, K., and Ellouz-Zimmermann, N., 2011c. New Arabian Sea records help decipher orbital timing of Indo-Asian monsoon. *Earth and Planetary Science Letters,* 308(3–4):433–444. **http://dx.doi.org/10.1016/j.epsl.2011.06.019**

Cane, M.A., and Molnar, P., 2001. Closing of the Indonesian Seaway as a precursor to East African aridification around 3–4 million years ago. *Nature,* 411(6834):157–162. **http://dx.doi.org/10.1038/35075500**

Cawthern, T., Johnson, J.E., Giosan, L., Flores, J.A., Rose, K., and Solomon, E., 2014. A late Miocene–early Pliocene biogenic silica crash in the Andaman Sea and Bay of Bengal. *Marine and Petroleum Geology,* 58(Part A):490–501. **http://dx.doi.org/10.1016/j.marpetgeo.2014.07.026**

Cerling, T.E., Harris, J.M., MacFadden, B.J., Leakey, M.G., Quade, J., Eisenmann, V., and Ehleringer, J.R., 1997. Global vegetation change through the Miocene/Pliocene boundary. *Nature,* 389(6647):153–158. **http://dx.doi.org/10.1038/38229**

Cheng, H., Edwards, R.L., Broecker, W.S., Denton, G.H., Kong, X., Wang, Y., Zhang, R., and Wang, X., 2009. Ice age terminations. *Science,* 326(5950):248–252. **http://dx.doi.org/10.1126/science.1177840**

Chesner, C.A., and Rose, W.I., 1991. Stratigraphy of the Toba tuffs and the evolution of the Toba caldera complex, Sumatra, Indonesia. *Bulletin of Volcanology,* 53(5):343–356. **http://dx.doi.org/10.1007/BF00280226**

Clemens, S.C., 2005. Millennial-band climate spectrum resolved and linked to centennial-scale solar cycles. *Quaternary Science Reviews,* 24(5–6):521–531. **http://dx.doi.org/10.1016/j.quascirev.2004.10.015**

Clemens, S.C., Kuhnt, W., and LeVay, L.J., 2014. iMonsoon: Indian monsoon rainfall in the core convective region. *International Ocean Discovery Program Scientific Prospectus,* 353. **http://dx.doi.org/10.14379/iodp.sp.353.2014**

Clemens, S.C., Murray, D.W., and Prell, W.L., 1996. Nonstationary phase of the Plio-Pleistocene Asian monsoon. *Science,* 274(5289):943–948. **http://dx.doi.org/10.1126/science.274.5289.943**

Clemens, S.C., Prell, W., Murray, D., Shimmield, G., and Weedon, G., 1991. Forcing mechanisms of the Indian Ocean monsoon. *Nature,* 353(6346):720–725. **http://dx.doi.org/10.1038/353720a0**

Clemens, S.C., and Prell, W.L., 2003. A 350,000 year summer-monsoon multi-proxy stack from the Owen Ridge, northern Arabian Sea. *Marine Geology,* 201(1–3):35–51. **http://dx.doi.org/10.1016/S0025-3227(03)00207-X**

Clemens, S.C., and Prell, W.L., 2007. The timing of orbital-scale Indian monsoon changes. *Quaternary Science Reviews,* 26(3–4):275–278. **http://dx.doi.org/10.1016/j.quascirev.2006.11.010**

Clemens, S.C., Prell, W.L., and Sun, Y., 2010. Orbital-scale timing and mechanisms driving late Pleistocene Indo-Asian summer monsoons: reinterpreting cave speleothem $\delta^{18}O$. *Paleoceanography,* 25(4):PA4207. **http://dx.doi.org/10.1029/2010PA001926**

Clemens, S.C., Prell, W.L., Sun, Y., Liu, Z., and Chen, G., 2008. Southern Hemisphere forcing of Pliocene $\delta^{18}O$ and the evolution of Indo-Asian monsoons. *Paleoceanography,* 23(4):PA4210. **http://dx.doi.org/10.1029/2008PA001638**

Clift, P.D., 2006. Controls on the erosion of Cenozoic Asia and the flux of clastic sediment to the ocean. *Earth and Planetary Science Letters,* 241(3–4):571–580. **http://dx.doi.org/10.1016/j.epsl.2005.11.028**

Clift, P.D., Hodges, K.V., Heslop, D., Hannigan, R., Long, H.V., and Calves, G., 2008. Correlation of Himalayan exhumation rates and Asian monsoon intensity. *Nature Geoscience,* 1(12):875–880. **http://dx.doi.org/10.1038/ngeo351**

Clift, P.D., and Plumb, R.A., 2008. *The Asian Monsoon: Causes, History and Effects:* Cambridge, UK (Cambridge University Press). **http://dx.doi.org/10.1017/CBO9780511535833**

Colin, C., Kissel, C., Blamart, D., and Turpin, L., 1998. Magnetic properties of sediments in the Bay of Bengal and the Andaman Sea: impact of rapid North Atlantic Ocean climatic events on the strength of the Indian monsoon. *Earth and Planetary Science Letters,* 160(3–4):623–635. **http://dx.doi.org/10.1016/S0012-821X(98)00116-2**

Collett, T.S., Riedel, M., Cochran, J., Boswell, R., Presley, J., Kumar, P., Sathe, A.V., Sethi, A., Lall, M., Sibal, V., and the NGHP Expedition 01 Scientists, 2008. *Indian National Gas Hydrate Program (NGHP) Expedition 01, Initial Report:* Noida, India (DGH, Ministry of Petroleum and Natural Gas).

Cullen, J.L., and Prell, W.L., 1984. Planktonic foraminifera of the northern Indian Ocean: distribution and preservation in surface sediments. *Marine Micropaleontology,* 9(1):1–52. **http://dx.doi.org/10.1016/0377-8398(84)90022-7**

Curray, J.R., 1991. Possible greenschist metamorphism at the base of a 22-km sedimentary section, Bay of Bengal. *Geology,* 19(11):1097–1100. **http://dx.doi.org/10.1130/0091-7613(1991)019<1097:PGMATB>2.3.CO;2**

Dehn, J., Farrell, J.W., and Schmincke, H.-U., 1991. Neogene tephrochronology from Site 758 on northern Ninetyeast Ridge: Indonesian arc volcanism of the past 5 Ma. *In* Weissel, J., Peirce, J., Taylor, E., Alt, J., et al., *Proceedings of the Ocean Drilling Program, Scientific Results,* 121: College Station, TX (Ocean Drilling Program), 273–295. **http://dx.doi.org/10.2973/odp.proc.sr.121.123.1991**

Dettman, D.L., Kohn, M.J., Quade, J., Ryerson, F.J., Ojha, T.P., and Hamidullah, S., 2001. Seasonal stable isotope evidence for a strong Asian monsoon throughout the past 10.7 m.y. *Geology,* 29(1):31–34. **http://dx.doi.org/10.1130/0091-7613(2001)029<0031:SSIEFA>2.0.CO;2**

Dickens, G.R., and Owen, R.M., 1999. The latest Miocene–early Pliocene biogenic bloom: a revised Indian Ocean perspective. *Marine Geology,* 161(1):75–91. **http://dx.doi.org/10.1016/S0025-3227(99)00057-2**

Ding, Y., and Chan, J.C.L., 2005. The East Asian summer monsoon: an overview. *Meteorology and Atmospheric Physics,* 89(1–4):117–142. **http://dx.doi.org/10.1007/s00703-005-0125-z**

Ding, Y., Li, C., and Liu, Y., 2004. Overview of the South China Sea monsoon experiment. *Advances in Atmospheric Sciences,* 21(3):343–360. **http://dx.doi.org/10.1007/BF02915563**

Emile-Geay, J., Cane, M.A., Naik, N., Seager, R., Clement, A.C., and van Geen, A., 2003. Warren revisited: atmospheric freshwater fluxes and "why is no deep water formed in the North Pacific?" *Journal of Geophysical Research: Oceans,* 108(C6):3178. **http://dx.doi.org/10.1029/2001JC001058**

Emmel, F.J., and Curray, J.R., 1984. Bengal Fan, Indian Ocean. *In* Bouma, A.H., Normark, W.P., and Barnes, N.E. (Eds.), *Submarine Fans and Related Systems:* New York (Springer Verlag), 248–275.

Farrell, J.W., and Janecek, T.R., 1991. Late Neogene paleoceanography and paleoclimatology of the northeast Indian Ocean (Site 758). *In* Weissel, J., Peirce, J., Taylor, E., Alt, J., et al., *Proceedings of the Ocean Drilling Program, Scientific Results,* 121: College Station, TX (Ocean Drilling Program), 297–355. **http://dx.doi.org/10.2973/odp.proc.sr.121.124.1991**

Farrell, J.W., Raffi, I., Janecek, T.R., Murray, D.W., Levitan, M., Dadey, K.A., Emeis, K.-C., Lyle, M., Flores, J.-A., and Hovan, S., 1995. Late Neogene sedimentation patterns in the eastern equatorial Pacific Ocean. *In* Pisias, N.G., Mayer, L.A., Janecek, T.R., Palmer-Julson, A., and van Andel, T.H. (Eds.), *Proceedings of the Ocean Drilling Program, Scientific Results,* 138: College Station, TX (Ocean Drilling Program), 717–756. **http://dx.doi.org/10.2973/odp.proc.sr.138.143.1995**

Federov, L.V., Ravich, M.G., and Hofmann, J., 1982. Geologic comparison of southeastern peninsular India and Sri Lanka with a part of East Antarctica (Enderby Land, MacRobertson Land, and Princess Elizabeth Land). *In* Craddock, C. (Ed.), *Antarctic Geoscience:* Madison, Wisconsin (University of Wisconsin Press), 73–78.

Flores, J.A., Johnson, J.E., Mejía-Molina, A.E., Álverez, M.C., Sierro, F.J., Singh, S.D., Mahanti, S., and Giosan, L., 2014. Sedimentation rates from calcareous nannofossil and planktonic foraminifera biostratigraphy in the Andaman Sea, northern Bay of Bengal, and eastern Arabian Sea. *Marine and Petroleum Geology,* 58(Part A):425–437. **http://dx.doi.org/10.1016/j.marpetgeo.2014.08.011**

France-Lanord, C., Schwenk, T., and Klaus, A., 2014. Bengal Fan: Neogene and late Paleogene record of Himalayan orogeny and climate: a transect across the Middle Bengal Fan. *International Ocean Discovery Program Scientific Prospectus,* 354. **http://dx.doi.org/10.14379/iodp.sp.354.2014**

Frank, M., Whiteley, N., van de Flierdt, T., Reynolds, B.C., and O'Nions, K., 2006. Nd and Pb isotope evolution of deep water masses in the eastern Indian Ocean during the past 33 Myr. *Chemical Geology,* 226(3–4):264–279. **http://dx.doi.org/10.1016/j.chemgeo.2005.09.024**

Frerichs, W.E., 1971. Planktonic foraminifera in the sediments of the Andaman Sea. *Journal of Foraminiferal Research,* 1(1):1–14. **http://dx.doi.org/10.2113/gsjfr.1.1.1**

Gourlan, A.T., Meynadier, L., and Allègre, C.J., 2008. Tectonically driven changes in the Indian Ocean circulation over the last 25 Ma: neodymium isotope evidence. *Earth and Planetary Science Letters,* 267(1–2):353–364. **http://dx.doi.org/10.1016/j.epsl.2007.11.054**

Gourlan, A.T., Meynadier, L., Allègre, C.J., Tapponnier, P., Birck, J.-L., and Joron, J.-L., 2010. Northern hemisphere climate control of the Bengali rivers discharge during the past 4 Ma. *Quaternary Science Reviews,* 29(19–20):2484–2498. **http://dx.doi.org/10.1016/j.quascirev.2010.05.003**

Guo, Z.T., Ruddiman, W.F., Hao, Q.Z., Wu, H.B., Qiao, Y.S., Zhu, R.X., Peng, S.Z., Wei, J.J., Yuan, B.Y., and Liu, T.S., 2002. Onset of Asian desertification by 22 Myr ago inferred from loess deposits in China. *Nature,* 416(6877):159–163. **http://dx.doi.org/10.1038/416159a**

Gupta, A.K., Singh, R.K., Joseph, S., and Thomas, E., 2004. Indian Ocean high-productivity event (10–8 Ma): linked to global cooling or to the initiation of the Indian monsoons? *Geology,* 32(9):753–756. **http://dx.doi.org/10.1130/G20662.1**

Gupta, A.K., Singh, R.K., and Verma, S., 2013. Deep-sea palaeoceanographic evolution of the eastern Indian Ocean during the late Oligocene–Pleistocene: species diversity trends in benthic foraminifera. *Current Science,* 104(7):904–910. **http://www.currentscience.ac.in/Volumes/104/07/0904.pdf**

Gupta, A.K., and Thomas, E., 2003. Initiation of Northern Hemisphere glaciation and strengthening of the northeast Indian monsoon: Ocean Drilling Program Site 758, eastern equatorial Indian Ocean. *Geology,* 31(1):47–50. **http://dx.doi.org/10.1130/0091-7613(2003)031<0047:IONHGA>2.0.CO;2**

Guptha, M.V.S., Curry, W.B., Ittekkot, V., and Muralinath, A.S., 1997. Seasonal variation in the flux of planktonic foraminifera: sediment trap results

from the Bay of Bengal, northern Indian Ocean. *Journal of Foraminiferal Research,* 27(1):5–19. **http://dx.doi.org/10.2113/gsjfr.27.1.5**

Hall, C.M., and Farrell, J.W., 1993. Laser $^{40}Ar/^{39}Ar$ age from ash D of ODP Site 758: dating the Brunhes-Matuyama reversal and oxygen isotope Stage 19.1. *Eos, Transactions American Geophysical Union,* 74 (Suppl.):110.

Hall, C.M., and Farrell, J.W., 1995. Laser $^{40}Ar/^{39}Ar$ ages of tephra from Indian Ocean deep-sea sediments: tie points for the astronomical and geomagnetic polarity time scales. *Earth and Planetary Science Letters,* 133(3–4):327–338. **http://dx.doi.org/10.1016/0012-821X(95)00087-S**

Hall, R., 2002. Cenozoic geological and plate tectonic evolution of SE Asia and the SW Pacific: computer-based reconstructions, model and animations. *Journal of Asian Earth Sciences,* 20(4):353–431. **http://dx.doi.org/10.1016/S1367-9120(01)00069-4**

Hall, R., Cottam, M.A., and Wilson, M.E.J., 2011. The SE Asian gateway: history and tectonics of the Australia–Asia collision. *Special Publication—Geological Society of London,* 355(1):1–6. **http://dx.doi.org/10.1144/SP355.1**

Hastenrath, S., and Greischar, L., 1993. The monsoonal heat budget of the hydrosphere atmosphere system in the Indian Ocean sector. *Journal of Geophysical Research: Oceans,* 98(C4):6869–6881. **http://dx.doi.org/10.1029/92JC02956**

Hermoyian, C.S., and Owen, R.M., 2001. Late Miocene–early Pliocene biogenic bloom: evidence from low-productivity regions of the Indian and Atlantic Oceans. *Paleoceanography,* 16(1):95–100. **http://dx.doi.org/y10.1029/2000PA000501**

Holbourn, A., Kuhnt, W., Clemens, S., Prell, W., and Andersen, N., 2013. Middle to late Miocene stepwise climate cooling: evidence from a high-resolution deep water isotope curve spanning 8 million years. *Paleoceanography,* 28(4):688–699. **http://dx.doi.org/10.1002/2013PA002538**

Holbourn, A., Kuhnt, W., Lyle, M., Schneider, L., Romero, O., and Anderson, N., 2014. Middle Miocene climate cooling linked to intensification of eastern equatorial Pacific upwelling. *Geology,* 42(1):19–22. **http://dx.doi.org/10.1130/G34890.1**

Holbourn, A., Kuhnt, W., Schulz, M., Flores, J.-A., and Andersen, N., 2007. Orbitally-paced climate evolution during the middle Miocene "Monterey" carbon-isotope excursion. *Earth and Planetary Science Letters,* 261(3–4):534–550. **http://dx.doi.org/10.1016/j.epsl.2007.07.026**

Hoogakker, B.A.A., Rohling, E.J., Palmer, M.R., Tyrrell, T., and Rothwell, R.G., 2006. Underlying causes for long-term global ocean $\delta^{13}C$ fluctuations over the last 1.20 Myr. *Earth and Planetary Science Letters,* 248(1–2):15–29. **http://dx.doi.org/10.1016/j.epsl.2006.05.007**

Hovan, S., and Rea, D.K., 1992. The Cenozoic record of continental mineral deposition on Broken and Ninetyeast Ridges, Indian Ocean: southern African aridity and sediment delivery from the Himalayas. *Paleoceanography,* 7(6):833–860. **http://dx.doi.org/10.1029/92PA02176**

Huang, Y., Clemens, S.C., Liu, W., Wang, Y., and Prell, W.L., 2007. Large-scale hydrological change drove the late Miocene C_4 plant expansion in the Himalayan foreland and Arabian Peninsula. *Geology,* 35(6):531–534. **http://dx.doi.org/10.1130/G23666A.1**

Jensen, T.G., 2001. Arabian Sea and Bay of Bengal exchange of salt and tracers in an ocean model. *Geophysical Research Letters,* 28(20):3967–3970. **http://dx.doi.org/10.1029/2001GL013422**

Jensen, T.G., 2003. Cross-equatorial pathways of salt and tracers from the northern Indian Ocean: modeling results. *Deep Sea Research, Part II,* 50(12–13):2111–2127. **http://dx.doi.org/10.1016/S0967-0645(03)00048-1**

Johnson, J.E., Phillips, S.C., Torres, M.E., Piñero, E., Rose, K.K., and Giosan, L., 2014. Influence of total organic carbon deposition on the inventory of gas hydrate in the Indian continental margins. *Marine and Petroleum Geology,* 58(Part A):406–424. **http://dx.doi.org/10.1016/j.marpetgeo.2014.08.021**

Kroon, D., Steens, T., and Troelstra, S.R., 1991. Onset of monsoonal related upwelling in the western Arabian Sea as revealed by planktonic foraminifers. *In* Prell, W.L., Niitsuma, N., et al., *Proceedings of the Ocean Drilling Program, Scientific Results,* 117: College Station, TX (Ocean Drilling Program), 257–263. **http://dx.doi.org/10.2973/odp.proc.sr.117.126.1991**

Kuhnt, W., Holbourn, A., Hall, R., Zuvela, M., and Käse, R., 2004. Neogene history of the Indonesian Throughflow. *In* Clift, P., Wang, P., Kuhnt, W., and Hayes, D. (Eds.), *Continent-Ocean Interactions within East Asian Marginal Seas.* Geophysical Monograph, 149:299–320. **http://dx.doi.org/10.1029/149GM16**

Kumar, S.P., Muraleedharan, P.M., Prasad, T.G., Gauns, M., Ramaiah, N., de Souza, S.N., Sardesai, S., and Madhupratap, M., 2002. Why is the Bay of Bengal less productive during summer monsoon compared to the Arabian Sea? *Geophysical Research Letters,* 29(24):2235. **http://dx.doi.org/10.1029/2002GL016013**

Le Houedec, S., Meynadier, L., Cogné, J.-P., Allègre, C.J., and Gourlan, A.T., 2012. Oceanwide imprint of large tectonic and oceanic events on seawater Nd isotope composition in the Indian Ocean from 90 to 40 Ma. *Geochemistry, Geophysics, Geosystems,* 13(6):Q06008. **http://dx.doi.org/10.1029/2011GC003963**

Licht, A., van Cappelle, M., Abels, H.A., Ladant, J.-B., Trabucho-Alexandre, J., France-Lanord, C., Donnadieu, Y., Vandenberghe, J., Rigaudier, T., Lécuyer, C., Terry, D., Jr., Adriaens, R., Boura, A., Guo, Z., Soe, A.N., Quade, J., Dupont-Nivet, G., and Jaeger, J.-J., 2014. Asian monsoons in a late Eocene greenhouse world. *Nature,* 513(7519):501–506. **http://dx.doi.org/10.1038/nature13704**

Lisiecki, L.E., and Raymo, M.E., 2005. A Pliocene–Pleistocene stack of 57 globally distributed benthic $\delta^{18}O$ records. *Paleoceanography,* 20(1):PA1003. **http://dx.doi.org/10.1029/2004PA001071**

Lisiecki, L.E., and Raymo, M.E., 2007. Plio–Pleistocene climate evolution: trends and transitions in glacial cycle dynamics. *Quaternary Science Reviews,* 26(1–2):56–69. **http://dx.doi.org/10.1016/j.quascirev.2006.09.005**

Liu, W.T., and Tang, W., 2004. Oceanic influence on the precipitation in India and China as observed by TRMM and QuikSCAT [paper presented at 2nd TRMM International Science Conference, Nara, Japan, 6–10 September 2004]. **http://airsea-www.jpl.nasa.gov/publication/paper/Liu-Tang-2004-trmm.pdf**

Liu, W.T., and Tang, W., 2005. Estimating moisture transport over oceans using space-based observations. *Journal of Geophysical Research: Atmospheres,* 110(D10):D10101. **http://dx.doi.org/10.1029/2004JD005300**

Liu, W.T., Zhang, A., and Bishop, J.K.B., 1994. Evaporation and solar irradiance as regulators of sea surface temperature in annual and interannual changes. *Journal of Geophysical Research: Oceans,* 99(C6):12623–12637. **http://dx.doi.org/10.1029/94JC00604**

Liu, X., Liu, Z., Kutzbach, J.E., Clemens, S.C., and Prell, W.L., 2006. Hemispheric insolation forcing of the Indian Ocean and Asian monsoon: local versus remote impacts. *Journal of Climate,* 19(23):6195–6208. **http://dx.doi.org/10.1175/JCLI3965.1**

Locarnini, R.A., Mishonov, A.V., Antonov, J.I., Boyer, T.P., Garcia, H.E., Baranova, O.K., Zweng, M.M., and Johnson, D.R., 2010. World Ocean Atlas 2009 (Vol. 1): Temperature. *In* Levitus S. (Ed.), *NOAA Atlas NESDIS 68:* Washington D.C. (U.S. Government Printing Office). **ftp://ftp.nodc.noaa.gov/pub/WOA09/DOC/woa09_vol1_text_figures.pdf**

Loschnigg, J., and Webster, P.J., 2000. A coupled ocean–atmosphere system of SST modulation for the Indian Ocean. *Journal of Climate,* 13(19):3342–3360. **http://dx.doi.org/10.1175/1520-0442(2000)013<3342:ACOASO>2.0.CO;2**

Mantyla, A.W., and Reid, J.L., 1995. On the origins of deep and bottom waters of the Indian Ocean. *Journal of Geophysical Research: Oceans,* 100(C2):2417–2439. **http://dx.doi.org/10.1029/94JC02564**

Misra, S., and Froelich, P.N., 2012. Lithium isotope history of Cenozoic seawater: changes in silicate weathering and reverse weathering. *Science,* 335(6070):818–823. **http://dx.doi.org/10.1126/science.1214697**

Molnar, P., 2005. Mio–Pliocene growth of the Tibetan Plateau and evolution of East Asian climate. *Palaeontologia Electronica,* 8(1):1–23. **http://palaeo-electronica.org/2005_1/molnar2/molnar2.pdf**

Molnar, P., Boos, W.R., and Battisti, D.S., 2010. Orographic controls on climate and paleoclimate of Asia: thermal and mechanical roles for the Tibetan Plateau. *Annual Review of Earth and Planetary Sciences,* 38(1):77–102. **http://dx.doi.org/10.1146/annurev-earth-040809-152456**

Mudelsee, M., and Raymo, M.E., 2005. Slow dynamics of the Northern Hemisphere glaciation. *Paleoceanography,* 20(4):PA4022. **http://dx.doi.org/10.1029/2005PA001153**

Nicholls, R.J., Wong, P.P., Burkett, V., Codignotto, J., Hay, J., McLean, R., Ragoonaden, S., and Woodroffe, C.D., 2007. Coastal systems and low-lying areas. *In* Parry, M.L., Canziani, O.F., Palutikof, J.P., van der Linden, P.J., and Hanson, C.E. (Eds.), *Climate Change 2007: Impacts, Adaptation and Vulnerability. Contribution of Working Group II to the Fourth Assessment Report of the Intergovernmental Panel on Climate Change:* Cambridge, UK (Cambridge University Press), 315–356. **https://www.ipcc.ch/pdf/assessment-report/ar4/wg2/ar4-wg2-chapter6.pdf**

Ninkovich, D., 1979. Distribution, age and chemical composition of tephra layers in deep-sea sediments off western Indonesia. *Journal of Volcanology and Geothermal Research,* 5(1–2):67–86. **http://dx.doi.org/10.1016/0377-0273(79)90033-7**

Ninkovich, D., Shackelton, N.J., Abdel-Monem, A.A., Obradovich, J.D., and Izett, G., 1978. K-Ar age of the late Pleistocene eruption of Toba, north Sumatra. *Nature,* 276(5688):574–577. **http://dx.doi.org/10.1038/276574a0**

Park, S.-C., Sohn, B.-J., and Wang, B., 2007. Satellite assessment of divergent water vapor transport from NCEP, ERA40, and JRA25 reanalyses over the Asian summer monsoon region. *Journal of the Meteorological Society of Japan,* 85(5):615–632. **http://dx.doi.org/10.2151/jmsj.85.615**

Peirce, J., Weissel, J., et al., 1989. *Proceedings of the Ocean Drilling Program, Initial Reports,* 121: College Station, TX (Ocean Drilling Program). **http://dx.doi.org/10.2973/odp.proc.ir.121.1989**

Phillips, S.C., Johnson, J.E., Giosan, L., and Rose, K., 2014a. Monsoon-influenced variation in productivity and lithogenic sediment flux since 110 ka in the offshore Mahanadi Basin, northern Bay of Bengal. *Marine and Petroleum Geology,* 58(Part A):502–525. **http://dx.doi.org/10.1016/j.marpetgeo.2014.05.007**

Phillips, S.C., Johnson, J.E., Underwood, M.B., Guo, J., Giosan, L., and Rose, K., 2014b. Long-timescale variation in bulk and clay mineral composition of Indian continental margin sediments in the Bay of Bengal, Arabian Sea, and Andaman Sea. *Marine and Petroleum Geology,* 58(Part A):117–138. **http://dx.doi.org/10.1016/j.marpetgeo.2014.06.018**

Ponton, C., Giosan, L., Eglinton, T.I., Fuller, D.Q., Johnson, J.E., Kumar, P., and Collett, T.S., 2012. Holocene aridification of India. *Geophysical Research Letters,* 39(3):L3407. **http://dx.doi.org/10.1029/2011GL050722**

Powell, C.McA., Roots, S.R., and Veevers, J.J., 1988. Pre-breakup continental extension in East Gondwanaland and the early opening of the eastern Indian Ocean. *Tectonophysics,* 155(1–4):261–283. **http://dx.doi.org/10.1016/0040-1951(88)90269-7**

Prell, W.L., Murray, D.W., Clemens, S.C., and Anderson, D.M., 1992. Evolution and variability of the Indian Ocean summer monsoon: evidence from the western Arabian Sea drilling program. *In* Duncan, R.A., Rea, D.K., Kidd, R.B., von Rad, U., and Weissel, J.K. (Eds.), *Synthesis of Results from Scientific Drilling in the Indian Ocean.* Geophysical Monograph, 70:447–469. **http://dx.doi.org/10.1029/GM070p0447**

Quade, J., and Cerling, T.E., 1995. Expansion of C_4 grasses in the late Miocene of northern Pakistan: evidence from stable isotopes in paleosols. *Palaeogeography, Palaeoclimatology, Palaeoecology,* 115(1–4):91–116. **http://dx.doi.org/10.1016/0031-0182(94)00108-K**

Ramana, M.V., Ramprasad, T., Collett, T.S., Kumar, P., Boswell, R.M., Riedel, M., Sathe, A.V., Lall, M., Vishwanath, K., Muzumdar, A., Sain, K., and Cochran, J. (Eds.), 2014. *Geologic Implications of Gas Hydrates in the Offshore of India: Results of the National Gas Hydrate Program Expedition 01,* Marine and Petroleum Geology, 58(Part A). **http://www.sciencedirect.com/science/journal/02648172/58/supp/PA**

Randall, D.A., Wood, R.A., Bony, S., Colman, R., Fichefet, T., Fyfe, J., Kattsov, V., Pitman, A., Shukla, J., Srinivasan, J., Stouffer, R.J., Sumi, A., and Taylor, K.E., 2007. Climate models and their evaluation. *In* Solomon, S., Qin, D., Manning, M., Chen, Z., Marquis, M., Averyt, K.B., Tingor, M., and Miller, H.L. (Eds.), *Climate Change 2007: The Physical Science Basis. Contribution of Working Group I to the Fourth Assessment Report of the Intergovernmental Panel on Climate Change:* Cambridge, UK (Cambridge University Press), 589–662. **http://www.ipcc.ch/pdf/assessment-report/ar4/wg1/ar4-wg1-chapter8.pdf**

Rayner, N.A., Parker, D.E., Horton, E.B., Folland, C.K., Alexander, L.V., Rowell, D.P., Kent, E.C., and Kaplan, A., 2003. Global analyses of sea surface temperature, sea ice, and night marine air temperature since the late nineteenth century. *Journal of Geophysical Research: Atmospheres,* 108(D14):4407. **http://dx.doi.org/10.1029/2002JD002670**

Rodriguez, M., Chamot-Rooke, N., Huchon, P., Fournier, M., and Delescluse, M., 2014. The Owen Ridge uplift in the Arabian Sea: implications for the sedimentary record of Indian monsoon in late Miocene. *Earth and Planetary Science Letters,* 394:1–12. **http://dx.doi.org/10.1016/j.epsl.2014.03.011**

Royer, J.-Y., Peirce, J.W., and Weissel, J.K., 1991. Tectonic constraints on the hotspot formation of the Ninetyeast Ridge. *In* Weissel, J., Peirce, J., Taylor, E., Alt, J., et al., *Proceedings of the Ocean Drilling Program, Scientific Results,* 121: College Station, TX (Ocean Drilling Program), 763–776. **http://dx.doi.org/10.2973/odp.proc.sr.121.122.1991**

Ruddiman, W.F., 2006. What is the timing of orbital-scale monsoon changes? *Quaternary Science Reviews,* 25(7–8):657–658. **http://dx.doi.org/10.1016/j.quascirev.2006.02.004**

Ryan, W.B.F., Carbotte, S.M., Coplan, J.O., O'Hara, S., Melkonian, A., Arko, R., Weissel, R.A., Ferrini, V., Goodwillie, A., Nitsche, F., Bonczkowski, J., and Zemsky, R., 2009. Global multi-resolution topography synthesis. *Geochemistry, Geophysics, Geosystems,* 10(3):Q03014. **http://dx.doi.org/10.1029/2008GC002332**

Sager, W.W., Paul, C.F., Krishna, K.S., Pringle, M., Eisin, A.E., Frey, F.A., Gopala Rao, D., and Levchenko, O., 2010. Large fault fabric of the Ninetyeast Ridge implies near-spreading ridge formation. *Geophysical Research Letters,* 37(17):L17304. **http://dx.doi.org/10.1029/2010GL044347**

Schlitzer, R., 2000. Electronic atlas of WOCE hydrographic and tracer data now available. *Eos, Transactions American Geophysical Union,* 81(5):45. **http://dx.doi.org/10.1029/00EO00028**

Schmittner, A., Galbraith, E.D., Hostetler, S.W., Pedersen, T.F., and Zhang, R., 2007. Large fluctuations of dissolved oxygen in the Indian and Pacific Oceans during Dansgaard–Oeschger oscillations caused by variations of North Atlantic Deep Water subduction. *Paleoceanography,* 22(3):PA3207. **http://dx.doi.org/10.1029/2006PA001384**

Schott, F.A., and McCreary, J.P., Jr., 2001. The monsoon circulation of the Indian Ocean. *Progress in Oceanography,* 51(1):1–123. **http://dx.doi.org/10.1016/S0079-6611(01)00083-0**

Schott, F.A., Xie, S.-P., and McCreary, J.P., Jr., 2009. Indian Ocean circulation and climate variability. *Reviews of Geophysics,* 47(1):RG1002. **http://dx.doi.org/10.1029/2007RG000245**

Schulz, H., von Rad, U., and Erlenkeuser, H., 1998. Correlation between Arabian Sea and Greenland climate oscillations of the past 110,000 years. *Nature,* 393(6680):54–57. **http://dx.doi.org/10.1038/31750**

Schwenk, T., and Spieß, V., 2009. Architecture and stratigraphy of the Bengal Fan as response to tectonic and climate revealed from high-resolution seismic data. *In* Kneller, B.C., Martinsen, O.J., and McCaffrey, B. (Eds.), *External Controls on Deep-Water Depositional Systems.* Special Publication - SEPM (Society of Sedimentary Geologists), 92:107–131.

Scotese, C.R., Gahagan, L.M., and Larson, R.L., 1988. Plate tectonic reconstructions of the Cretaceous and Cenozoic ocean basins. *Tectonophysics,* 155(1–4):27–48. **http://dx.doi.org/10.1016/0040-1951(88)90259-4**

Sharmila, S., Joseph, S., Sahai, A.K., Abhilash, S., and Chattopadhyay, R., 2015. Future projection of Indian summer monsoon variability under climate change scenario: an assessment from CMIP5 climate models. *Global and Planetary Change,* 124:62–78. **http://dx.doi.org/10.1016/j.gloplacha.2014.11.004**

Shipboard Scientific Party, 1989. Site 758. *In* Peirce, J., Weissel, J., et al., *Proceedings of the Ocean Drilling Program, Initial Reports,* 121: College Station, TX (Ocean Drilling Program), 359–453. **http://dx.doi.org/10.2973/odp.proc.ir.121.112.1989**

Simmonds, I., Bi, D., and Hope, P., 1999. Atmospheric water vapor flux and its association with rainfall over China in summer. *Journal of Climate,* 12(5):1353–1367. **http://dx.doi.org/10.1175/1520-0442(1999)012<1353:AWVFAI>2.0.CO;2**

Singh, A., Jani, R.A., and Ramesh, R., 2010. Spatiotemporal variations of the $\delta^{18}O$–salinity relation in the northern Indian Ocean. *Deep Sea Research, Part I,* 57(11):1422–1431. **http://dx.doi.org/10.1016/j.dsr.2010.08.002**

Singh, A.D., Jung, S.J.A., Darling, K., Ganeshram, R., Ivanochko, T., and Kroon, D., 2011. Productivity collapses in the Arabian Sea during glacial cold phases. *Paleoceanography*, 26(3):PA3210. **http://dx.doi.org/10.1029/2009PA001923**

Singh, R.K., and Gupta, A.K., 2005. Systematic decline in benthic foraminiferal species diversity linked to productivity increases over the last 26 Ma in the Indian Ocean. *Journal of Foraminiferal Research,* 35(3):219–227. **http://dx.doi.org/10.2113/35.3.219**

Singh, S.C., Moeremans, R., McArdle, J., and Johansen, K., 2013. Seismic images of the sliver strike-slip fault and back thrust in the Andaman-Nicobar region. *Journal of Geophysical Research: Solid Earth,* 118(10):5208–5224. **http://dx.doi.org/10.1002/jgrb.50378**

Stöckli, R., Vermote, E., Saleous, N., Simmon, R., and Herring, D., 2005. *The Blue Marble Next Generation—A true color Earth dataset including seasonal dynamics from MODIS.* NASA Earth Observatory. **http://earthobservatory.nasa.gov/Features/BlueMarble/bmng.pdf**

Stoll, H.M., Vance, D., and Arevalos, A., 2007. Records of the Nd isotope composition of seawater from the Bay of Bengal: implications for the impact of Northern Hemisphere cooling on ITCZ movement. *Earth and Planetary Science Letters,* 255(1–2):213–228. **http://dx.doi.org/10.1016/j.epsl.2006.12.016**

Subrahmanyam, V., Subrahmanyam, A.S., Murty, G.P.S., and Murthy, K.S.R., 2008. Morphology and tectonics of Mahanadi Basin, northeastern continental margin of India from geophysical studies. *Marine Geology,* 253(1–2):63–72. **http://dx.doi.org/10.1016/j.margeo.2008.04.007**

Sun, X., and Wang, P., 2005. How old is the Asian monsoon system?—Palaeobotanical records from China. *Palaeogeography, Palaeoclimatology, Palaeoecology,* 222(3–4):181–222. **http://dx.doi.org/10.1016/j.palaeo.2005.03.005**

Sun, Y., Clemens, S.C., Morrill, C., Lin, X., Wang, X., and An, Z., 2011. Influence of Atlantic meridional overturning circulation on the East Asian winter monsoon. *Nature Geoscience,* 5(1):46–49. **http://dx.doi.org/10.1038/ngeo1326**

Thomas, D.J., Bralower, T.J., and Jones, C.E., 2003. Neodymium isotopic reconstruction of late Paleocene–early Eocene thermohaline circulation. *Earth and Planetary Science Letters,* 209(3–4):309–322. **http://dx.doi.org/10.1016/S0012-821X(03)00096-7**

Tomczak, M., and Godfrey, J.S., 2003. *Regional Oceanography: An Introduction* (2nd ed.): Delhi (Daya Publishing House).

Varkey, M.J., Murty, V.S.N., and Suryanarayana, A., 1996. Physical oceanography of the Bay of Bengal and Andaman Sea. *Oceanography and Marine Biology,* 34:1–70. **http://drs.nio.org/drs/handle/2264/2276**

von der Borch, C.C., Sclater, J.G., et al., 1974. *Initial Reports of the Deep Sea Drilling Project,* 22: Washington (U.S. Government Printing Office). **http://dx.doi.org/10.2973/dsdp.proc.22.1974**

Wajsowicz, R.C., and Schopf, P.S., 2001. Oceanic influences on the seasonal cycle in evaporation over the Indian Ocean. *Journal of Climate,* 14(6):1199–1226. **http://dx.doi.org/10.1175/1520-0442(2001)014<1199:OIOTSC>2.0.CO;2**

Wang, P., Clemens, S., Beaufort, L., Braconnot, P., Ganssen, G., Jian, Z., Kershaw, P., and Sarnthein, M., 2005. Evolution and variability of the Asian monsoon system: state of the art and outstanding issues. *Quaternary Science Review,* 24(5–6):595–629. **http://dx.doi.org/10.1016/j.quascirev.2004.10.002**

Wang, Y., Cheng, H., Edwards, R.L., Kong, X., Shao, X., Chen, S., Wu, J., Jiang, X., Wang, X., and An, Z., 2008. Millennial- and orbital-scale changes in the East Asian monsoon over the past 224,000 years. *Nature,* 451(7182):1090–1093. **http://dx.doi.org/10.1038/nature06692**

Wang, Y.J., Cheng, H., Edwards, R.L., An, Z.S., Wu, J.Y., Shen, C.-C., and Dorale, J.A., 2001. A high-resolution absolute-dated late Pleistocene monsoon record from Hulu Cave, China. *Science,* 294(5580):2345–2348. **http://dx.doi.org/10.1126/science.1064618**

Webster, P.J., 1987a. The elementary monsoon. *In* Fein, J.S., and Stephens, P.L. (Eds.), *Monsoons:* New York (Wiley), 3–32.

Webster, P.J., 1987b. The variable and interactive monsoon. *In* Fein, J.S., and Stephens, P.L. (Eds.), *Monsoons:* New York (Wiley), 269–330.

Webster, P.J., 1994. The role of hydrological processes in ocean-atmosphere interactions. *Reviews of Geophysics,* 32(4):427–476. **http://dx.doi.org/10.1029/94RG01873**

Webster, P.J., Magaña, V.O., Palmer, T.N., Shukla, J., Tomas, R.A., Yanai, M., and Yasunari, T., 1998. Monsoons: processes, predictability, and the prospects for prediction. *Journal of Geophysical Research: Oceans,* 103(C7):14451–14510. **http://dx.doi.org/10.1029/97JC02719**

Wyrtki, K., 1971. *Oceanographic Atlas of the International Ocean Expedition.* National Science Foundation.

Xie, P., and Arkin, P.A., 1997. Global precipitation: a 17-year monthly analysis based on gauge observations, satellite estimates, and numerical model outputs. *Bulletin of the American Meteorological Society,* 78(11):2539–2558. **http://dx.doi.org/10.1175/1520-0477(1997)078<2539:GPAYMA>2.0.CO;2**

Xu, J., Kuhnt, W., Holbourn, A., Andersen, N., and Bartoli, G., 2006. Changes in the vertical profile of the Indonesian Throughflow during Termination II: evidence from the Timor Sea. *Paleoceanography,* 21(4):PA4202. **http://dx.doi.org/10.1029/2006PA001278**

Yancheva, G., Nowaczyk, N.R., Mingram, J., Dulski, P., Schettler, G., Negendank, J.F.W., Liu, J., Sigman, D.M., Peterson, L.C., and Haug, G.H., 2007. Influence of the intertropical convergence zone on the East Asian monsoon. *Nature,* 445(7123):74–77. **http://dx.doi.org/10.1038/nature05431**

You, Y., and Tomczak, M., 1993. Thermocline circulation and ventilation in the Indian Ocean derived from water mass analysis. *Deep Sea Research, Part I,* 40(1):13–56. **http://dx.doi.org/10.1016/0967-0637(93)90052-5**

Zachos, J., Pagani, M., Sloan, L., Thomas, E., and Billups, K., 2001. Trends, rhythms, and aberrations in global climate 65 Ma to present. *Science,* 292(5517):686–693. **http://dx.doi.org/10.1126/science.1059412**

Zachos, J.C., Flower, B.P., and Paul, H., 1997. Orbitally paced climate oscillations across the Oligocene/Miocene boundary. *Nature,* 388(6642):567–570. **http://dx.doi.org/10.1038/41528**

Zhu, Y., and Newell, R.E., 1998. A proposed algorithm for moisture fluxes from atmospheric rivers. *Monthly Weather Review,* 126(3):725–735. **http://dx.doi.org/10.1175/1520-0493(1998)126<0725:APAFMF>2.0.CO;2**

Ziegler, M., Lourens, L.J., Tuenter, E., Hilgen, F., Reichart, G.-J., and Weber, N., 2010. Precession phasing offset between Indian summer monsoon and Arabian Sea productivity linked to changes in Atlantic overturning circulation. *Paleoceanography,* 25(3):PA3213. **http://dx.doi.org/10.1029/2009PA001884**

Table T1. Summary of Expedition 353 drilling operations.

Site	Hole	Latitude	Longitude	Seafloor depth (mbrf)	Cores (*N*)	Cored (m)	Recovered (m)	Recovery (%)	Drilled (m)	Total penetration (m)	Total depth (mbrf)	Time on hole (h)	Time on site (days)
U1443	A	5°23.0098′N	90°21.7100′E	2940.2	48	344.00	326.80	95	0.0	344.0	3284.2	77.50	
U1443	B	5°23.0190′N	90°21.7091′E	2935.5	40	326.40	308.51	95	0.0	326.4	3261.9	44.75	
U1443	C	5°23.0078′N	90°21.6984′E	2935.4	28	207.90	182.87	88	1.5	209.4	3144.8	38.00	
U1443	D	5°22.9991′N	90°21.6992′E	2935.3	2	8.20	7.48	91	0.0	8.2	2943.5	12.25	
			Site U1443 totals:		118	886.50	825.66	93	1.5	888.0			7.12
U1444	A	14°00.0057′N	84°49.7405′E	3143.4	37	330.60	226.05	68	0.0	330.6	3474.0	70.75	
U1444	B	13°59.9940′N	84°49.7412′E	3142.5	9	81.10	74.16	91	47.5	128.6	3271.1	24.75	
			Site U1444 totals:		46	411.70	300.21	73	47.5	459.2			4.00
U1445	A	17°44.7217′N	84°47.2518′E	2513.1	77	672.60	666.40	99	0.0	672.6	3185.7	155.50	
U1445	B	17°44.7098′N	84°47.2498′E	2514.5	4	33.00	33.36	101	0.0	33.0	2547.5	6.00	
U1445	C	17°44.7095′N	84°47.2387′E	2513.5	36	305.20	305.60	100	0.0	305.2	2818.7	64.50	
			Site U1445 totals:		117	1010.80	1005.36	99	0.0	1010.8			9.42
U1446	A	19°5.0090′N	85°44.0894′E	1441.2	21	180.00	186.63	104	0.0	180.0	1621.2	28.75	
U1446	B	19°5.0085′N	85°44.0786′E	1440.5	3	27.10	27.20	100	0.0	27.1	1467.6	2.50	
U1446	C	19°5.0215'N	85°44.0780′E	1441.1	23	182.00	180.55	99	0.0	182.0	1623.1	24.50	
			Site U1446 totals:		47	389.10	394.38	101	0.0	389.1			2.32
U1447	A	10°47.4061′N	92°59.9999′E	1402.2	88	738.00	732.96	99	0.0	738.0	2140.2	122.50	
U1447	B	10°47.3945′N	93°00.0028′E	1403.1	3	24.40	24.26	99	0.0	24.4	1427.5	5.25	
U1447	C	10°47.3952′N	93°00.0114′E	1403.6	17	158.90	158.32	100	2.0	160.9	1564.5	19.25	
			Site U1447 totals:		108	921.30	915.54	99	2.0	923.3			6.13
U1448	A	10°38.0315′N	93°00.0036′E	1109.7	60	421.00	434.82	103	0.0	421.0	1530.7	47.75	
U1448	B	10°38.0202′N	93°00.0032′E	1107.9	57	357.10	369.38	103	1.5	358.6	1466.5	36.00	
U1448	C	10°38.0830′N	93°00.0233′E	1108.2	4	34.30	34.77	101	0.0	34.3	1142.5	9.25	
			Site U1448 totals:		121	812.40	838.97	103	1.5	813.9			3.90
			Expedition 353 totals:		557	4431.8	4280.12	97	52.5	4484.3		789.75	32.90

Figure F1. ODP and IODP monsoon-related expeditions. Satellite image from Stöckli et al., 2005.

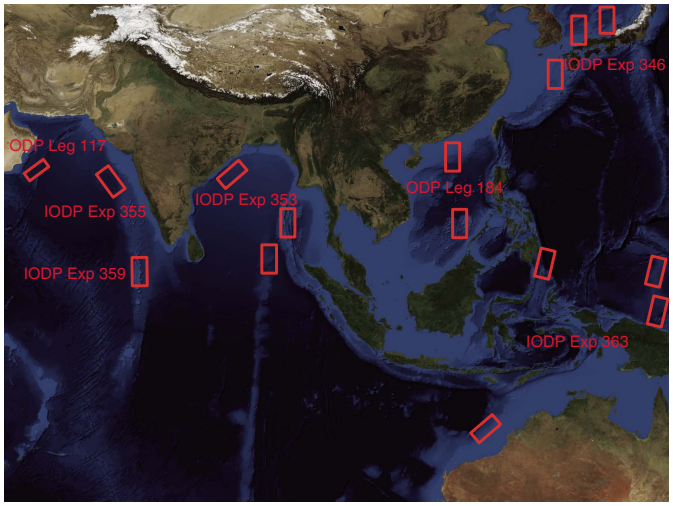

Figure F2. Location of Expedition 353 sites and seafloor depths. Map was generated using GeoMapApp (**www.geomapapp.org**), using topography and bathymetry from the Global Multi-Resolution Topography synthesis (Ryan et al., 2009).

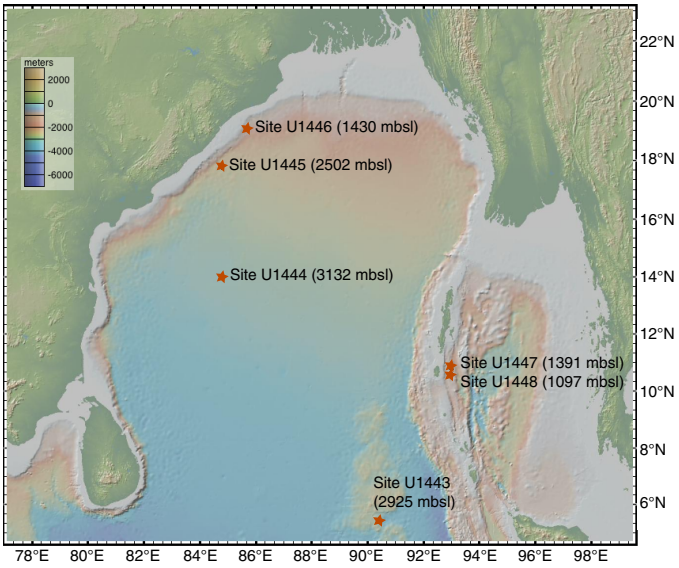

Figure F3. Climatological (A) July–August and (B) January–February mean precipitation rates (shading in mm/day) and 925 hPa wind vectors (arrows). Precipitation and wind climatology are derived from CMAP (Xie and Arkin, 1997) (1979–2000) and NCEP/NCAR reanalysis (1951–2000), respectively.

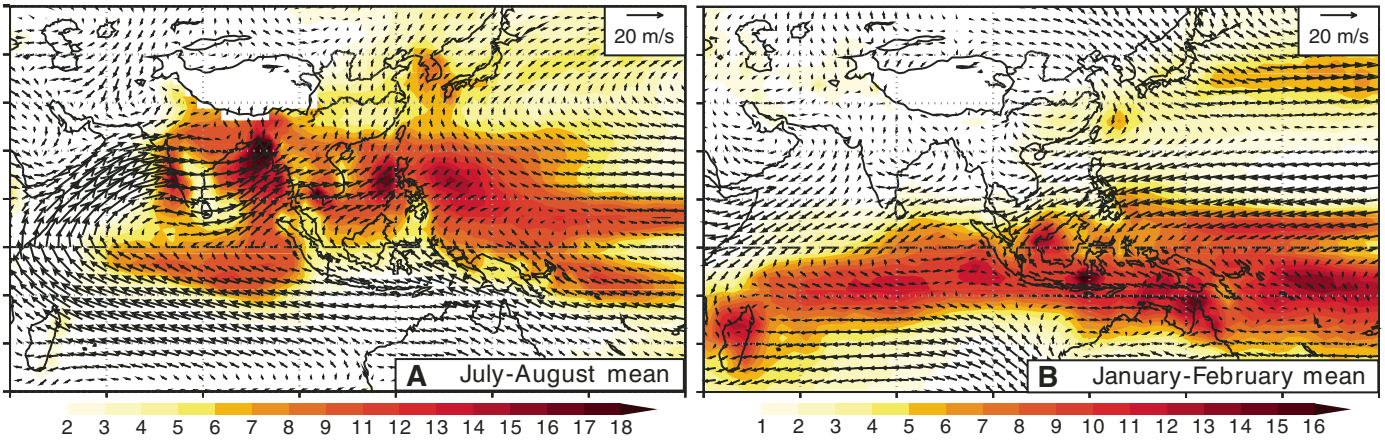

Figure F4. World Ocean Atlas Monthly Mean Salinity for 1955–2006 (Antonov et al., 2010). Areas drilled in the Andaman Sea (AA), Mahanadi basin, southern Bay of Bengal (BB), and Ninetyeast Ridge (ODP Site 758) are shown.

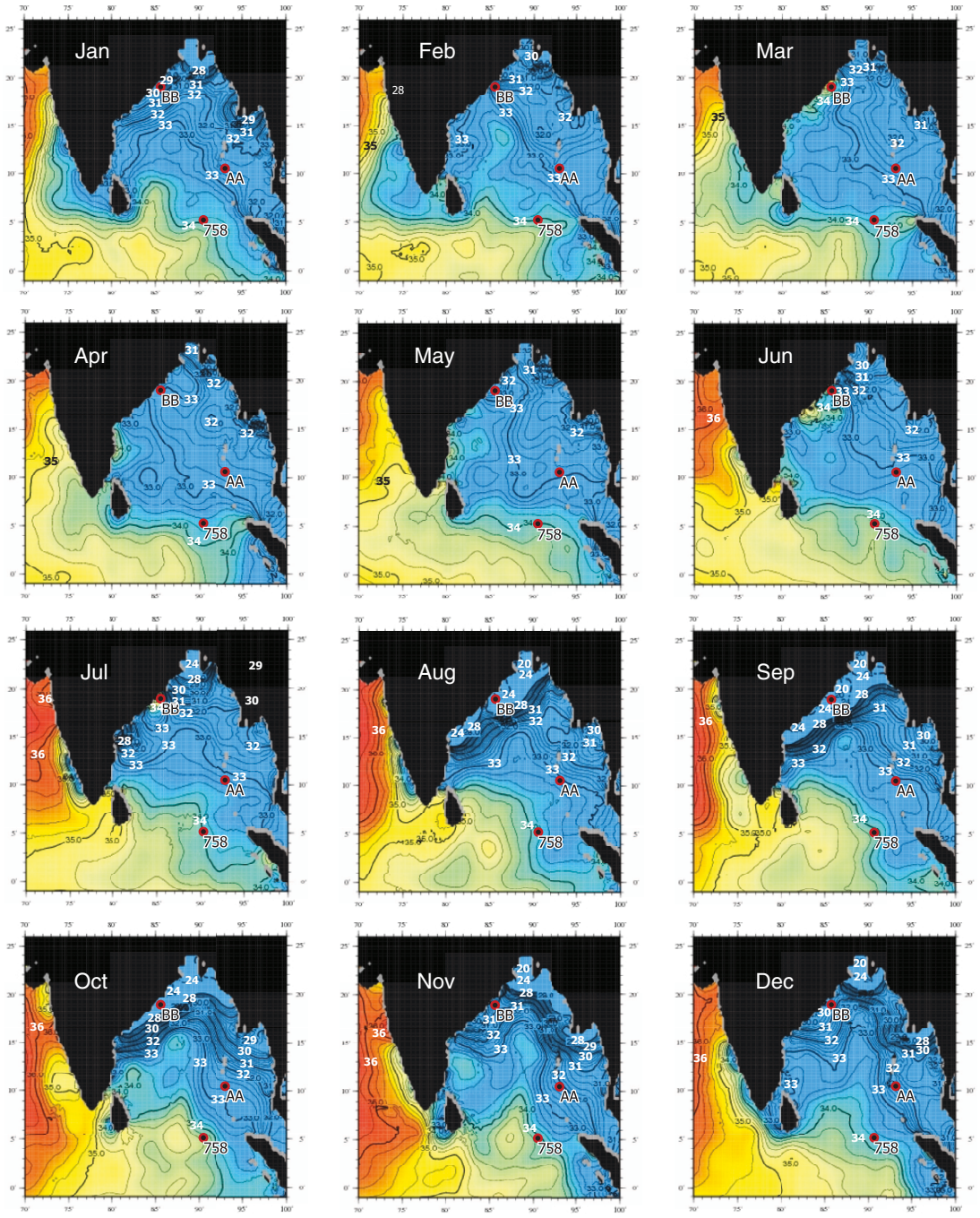

Figure F5. Ten-day National Oceanic and Atmospheric Administration HYSPLIT backtracks (2007–2011). Green indicates rain-bearing air trajectories. Rain-bearing trajectories over India are dominated by summer season (southwest) winds, whereas both winter (northerly) and summer (southerly) air masses carry precipitation to the monsoonal region of southeast China. This is consistent with World Meteorological Organization rainfall records indicating that June, July, and August rainfall accounts for 50% of the total annual rainfall in this region. The Bay of Bengal location better isolates the summer season dynamics.

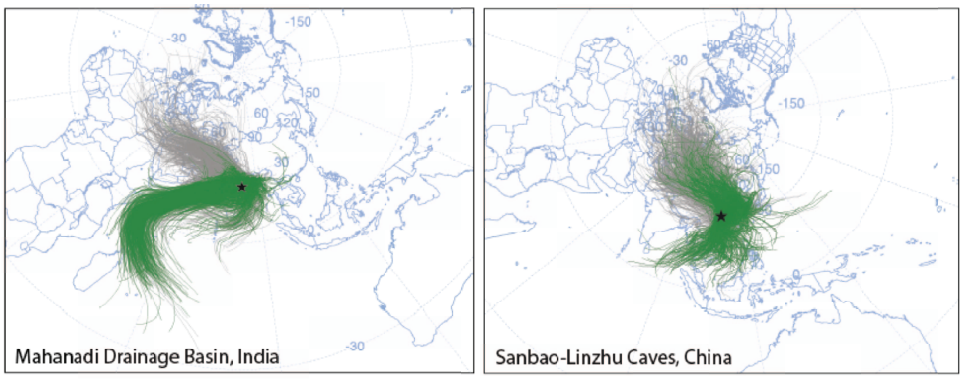

Figure F6. Main river basins draining into the Bay of Bengal and Andaman Sea. Map was generated using GeoMapApp (**www.geomapapp.org**), using topography and bathymetry from the Global Multi-Resolution Topography synthesis (Ryan et al., 2009).

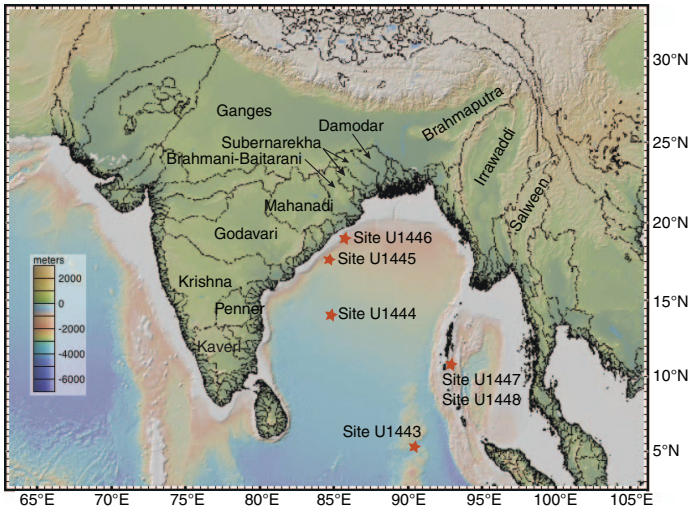

Figure F7. Summary sketch after Singh et al. (2013) showing the subduction zone through the back-arc basin to ~40 km depth. DF = Diligent fault, NAB = Nicobar Andaman Basin, ANF = Andaman-Nicobar fault.

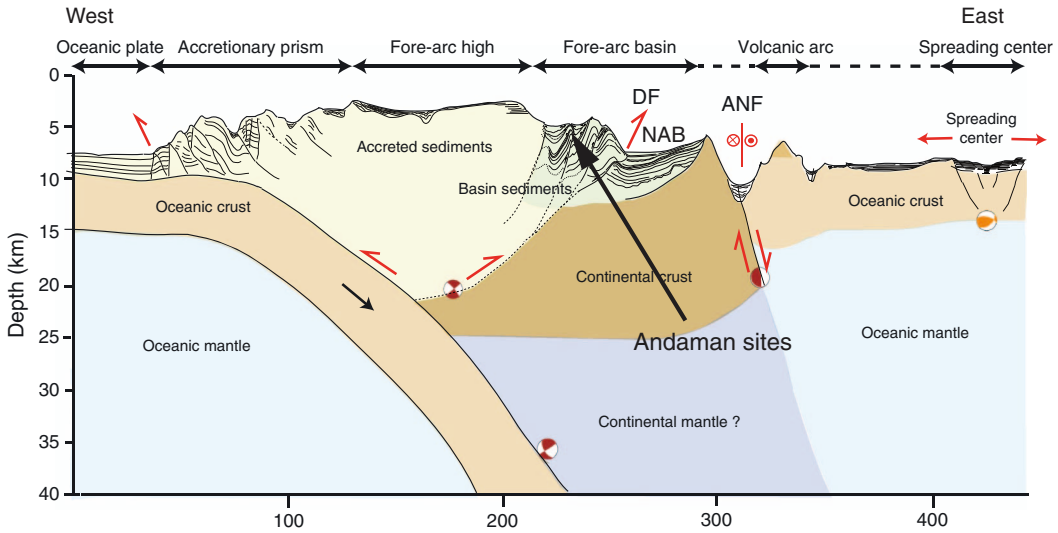

Figure F8. Summer monsoon moisture budget and transport path (inset) after Ding et al. (2004). Moisture budget averaged for 1990–1999 (June, July, and August; units are 10^6 kg/s). The southern Indian Ocean is the dominant moisture (latent heat) source. The Bay of Bengal, Indochina, the South China Sea, and China are all moisture sinks. No significant Pacific moisture source is indicated. Summer monsoon moisture transport patterns (inset) averaged for 1990–1999 (the 5th pentad of May through the 2nd pentad of July; units are kg/m/s).

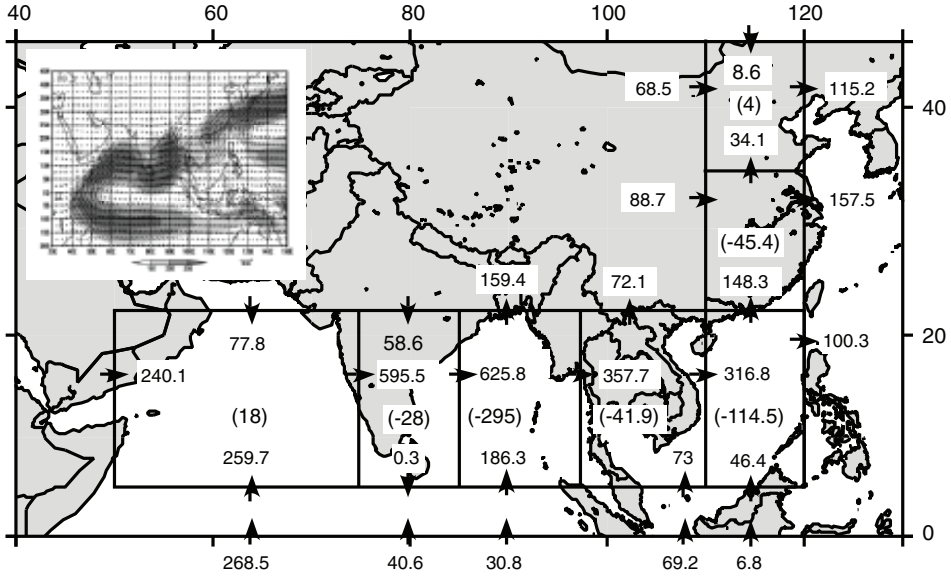

Figure F9. Monthly precipitation data for 1948–2011 (as available) for locations with drainage into the Bay of Bengal. Cherrapunji precipitation is scaled separately. Data from World Meteorological Organization (**climexp.knmi.nl**).

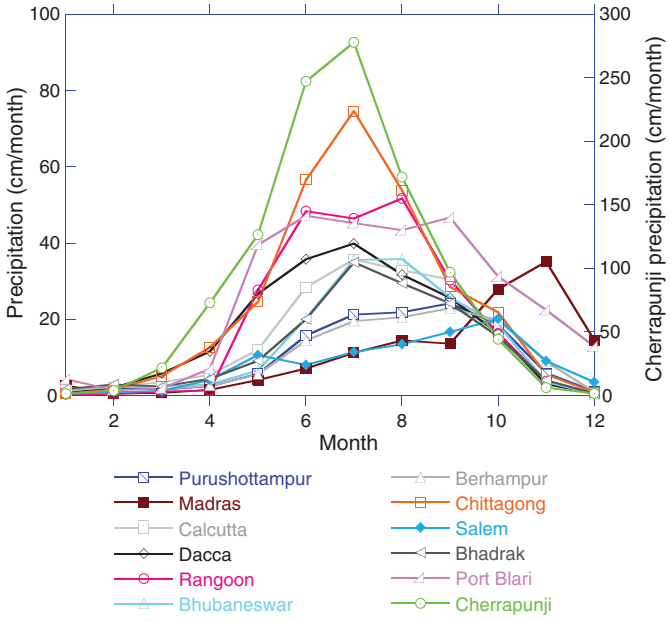

Figure F10. World Ocean Atlas Monthly Mean Temperature (°C) for 1955–2006 (Locarnini et al., 2010). Summer and winter monsoon current systems follow Schott and McCreary (2001). Proposed site locations in the Andaman Sea (AA), Mahanadi basin, Bay of Bengal (BB), and N90E-2C (redrill ODP Site 758) are shown. EICC = East Indian Coastal Current, WICC = West Indian Coastal Current, SMC = Southwest Monsoon Current, WMC = Winter Monsoon Current.

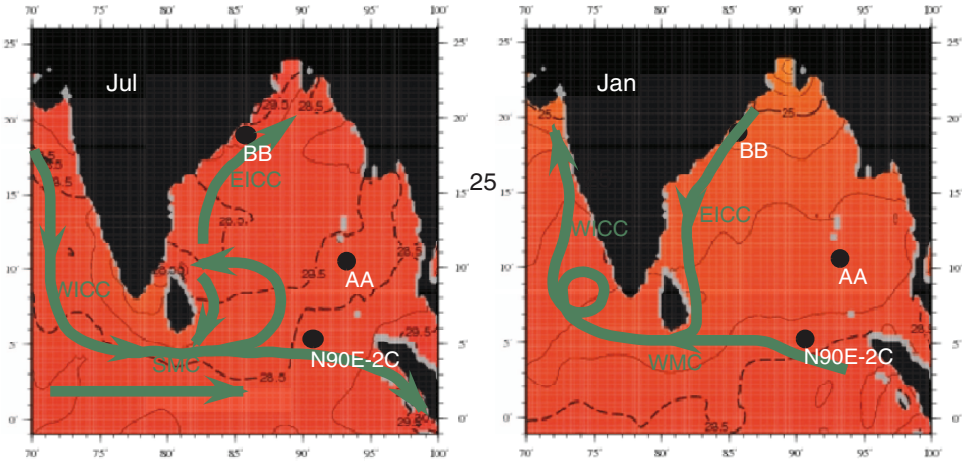

Figure F11. Estimated monthly *G. ruber* $\delta^{18}O$ derived from monthly salinity and temperature climatologies at (A) 5°N, 90°E and (B) 20°N, 86°E, Bay of Bengal. Monthly mean ±1σ over 1958–2013. Sea-surface temperature (SST) from HadISST data set (Rayner, 2003). Sea-surface salinity (SSS) from ORA-S4 data set (Balmaseda, 2012). Pseudo-$\delta^{18}O$ of *G. ruber* (white) constructed from SST and SSS data set using low-light equation of Bemis et al. (1998) and open-ocean Bay of Bengal $\delta^{18}O_{seawater}$-salinity relationship from Singh et al. (2010).

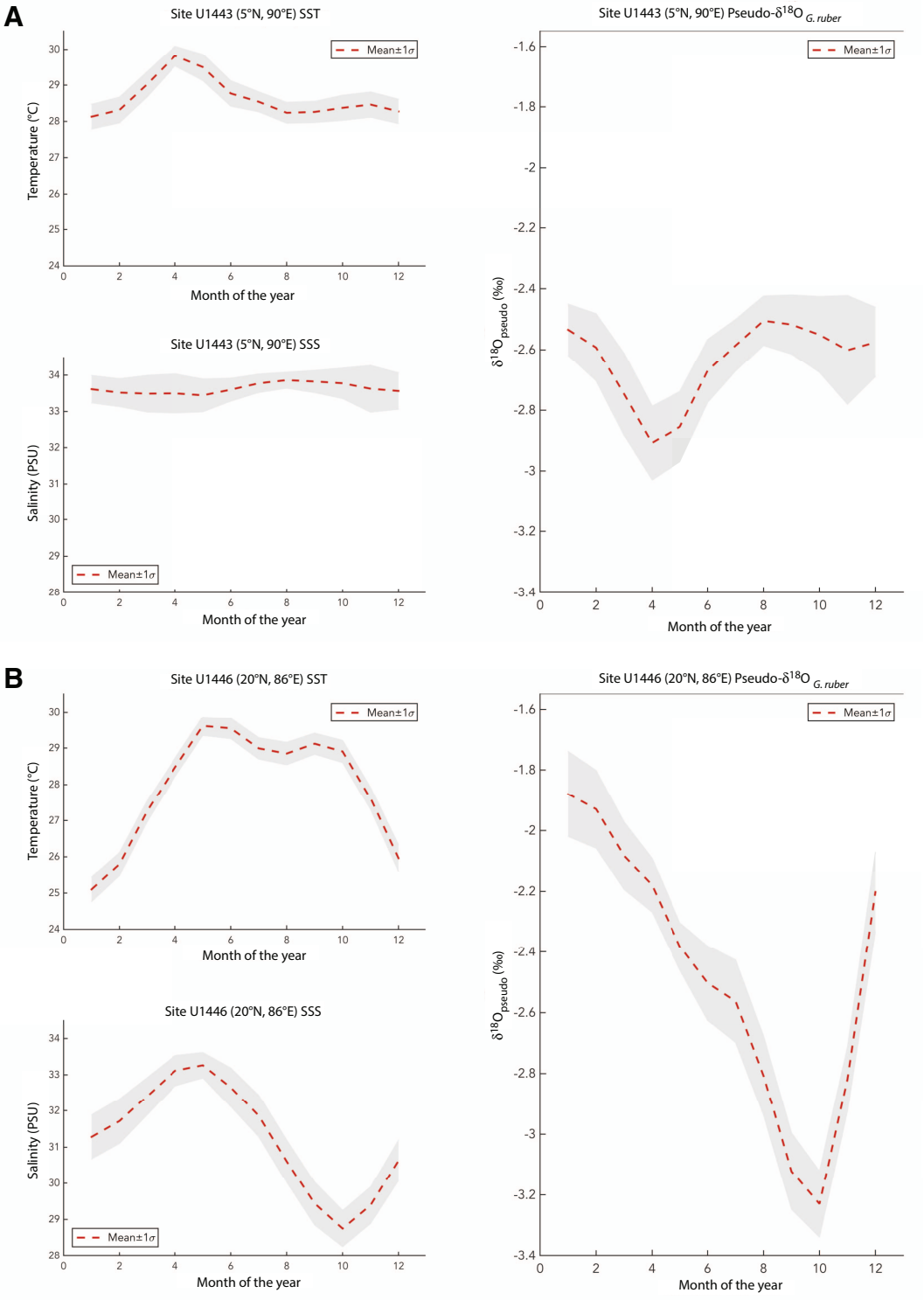

Figure F12. Indian Ocean deep and bottom water circulation (from Frank et al., 2006). Blue arrows represent the deep and bottom water flow patterns in the Indian Ocean. After Mantyla and Reid (1995).

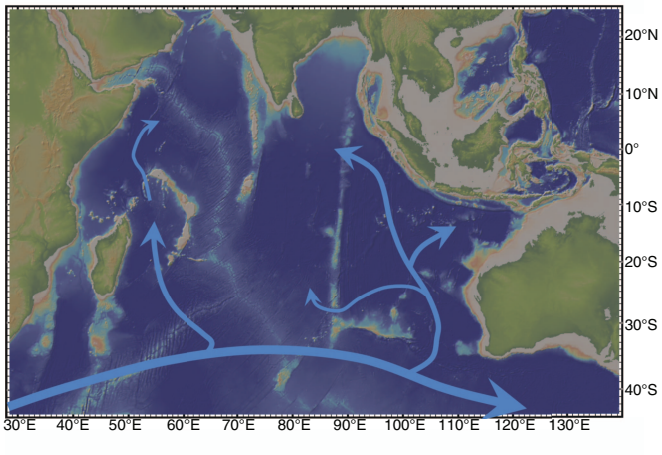

Figure F13. Salinity, silicate, and oxygen from eastern Indian Ocean WOCE meridional Transect I09, eastern Indian Ocean (from eWOCE Gallery, **www.ewoce.org/gallery** [Schlitzer, 2000]).

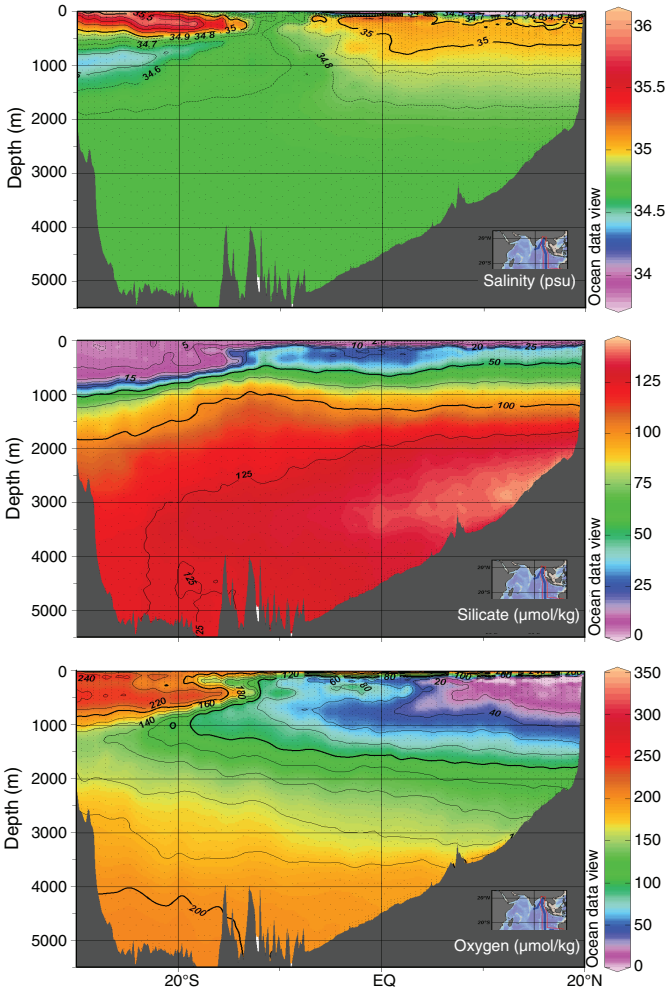

Figure F14. Mean (A) temperature and (B) salinity in the upper thermocline on isopycnal Surface 25.7, located in the depth range 150–200 m (after You and Tomczak, 1993). Arrows indicate movement of Indian Central Water (black) and Indonesian Throughflow Water (red). From Xu et al. (2006).

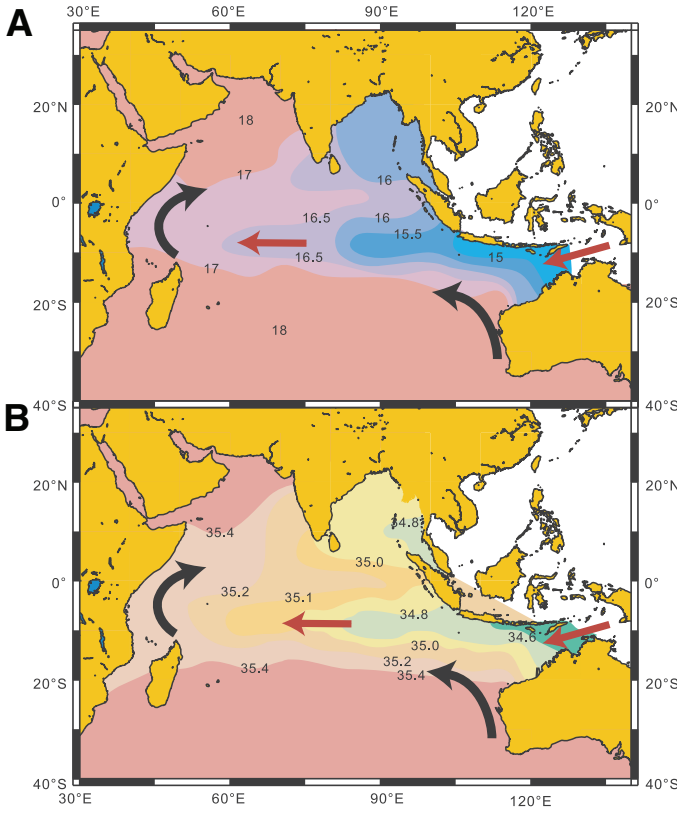

Figure F15. Site U1443 splice RGB, magnetic susceptibility (loop and spot), L*, a*, b*, and NGR data tuned to LR04 benthic isotope stack for the last 3.4 My.

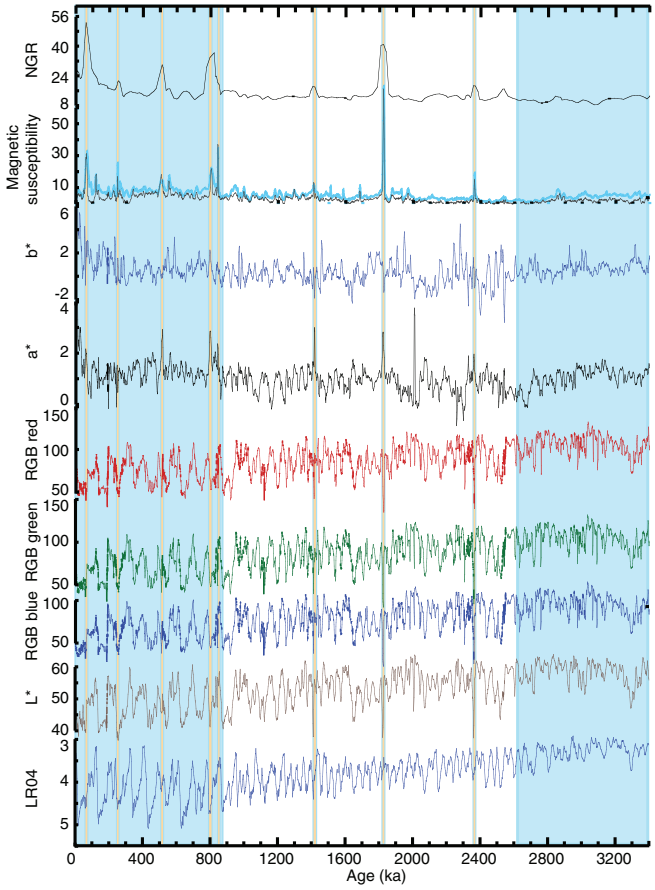

Figure F16. Toba Tephra layers D, d, and E in (A) Holes U1443A and (B) U1443B.

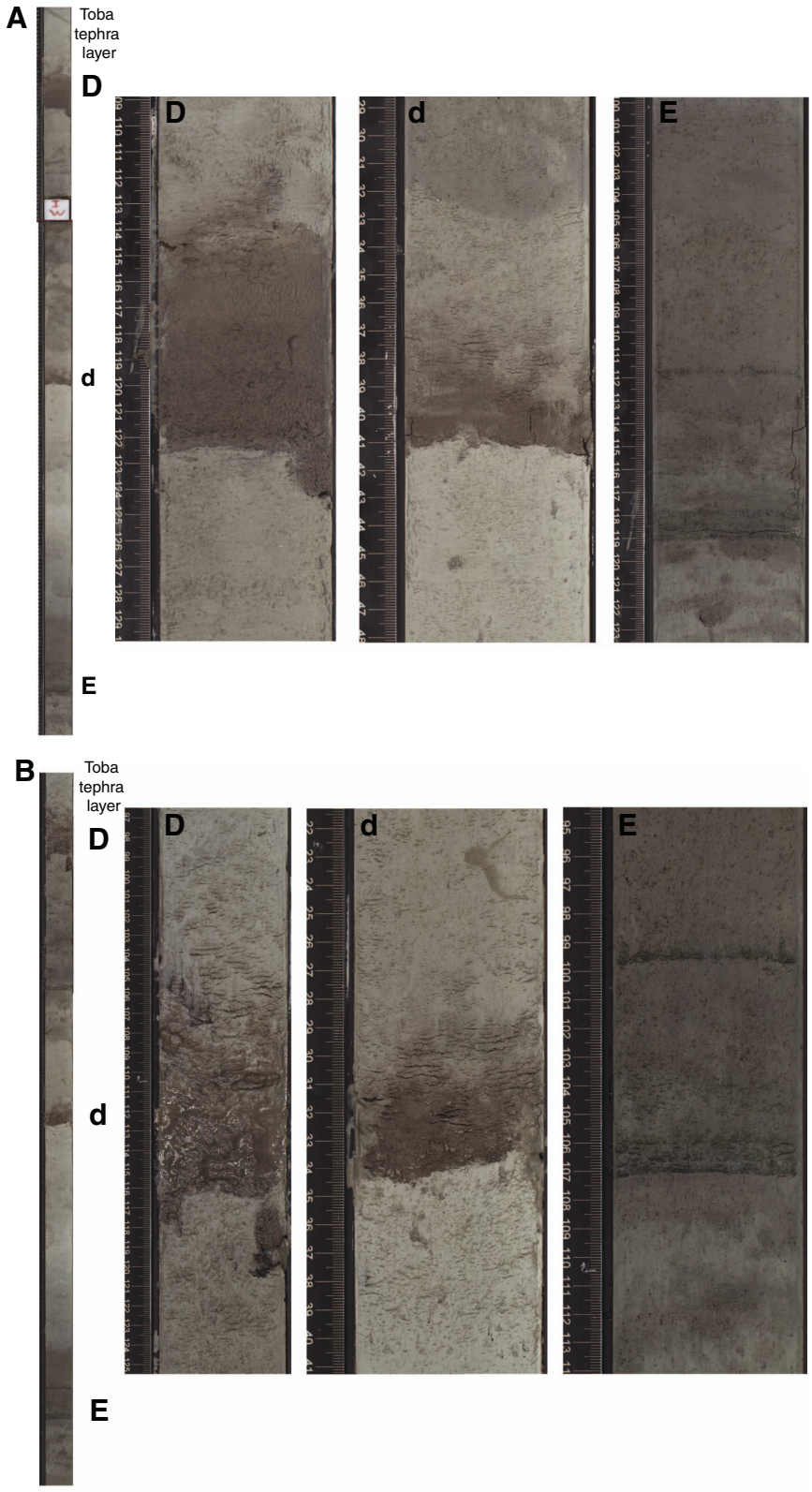

Figure F17. Correlation of mudline cores in Holes U1443A, U1443B, U1443C, and U1443D.

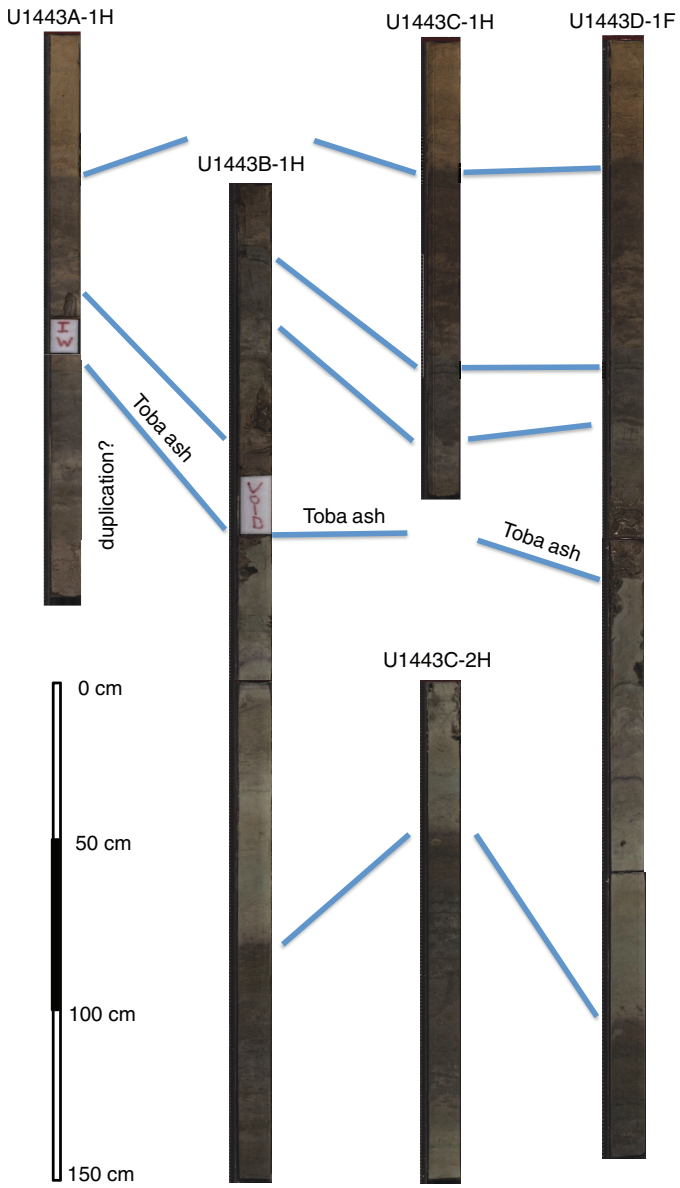

Figure F18. Site U1443 Cretaceous/Paleocene transitional boundary.

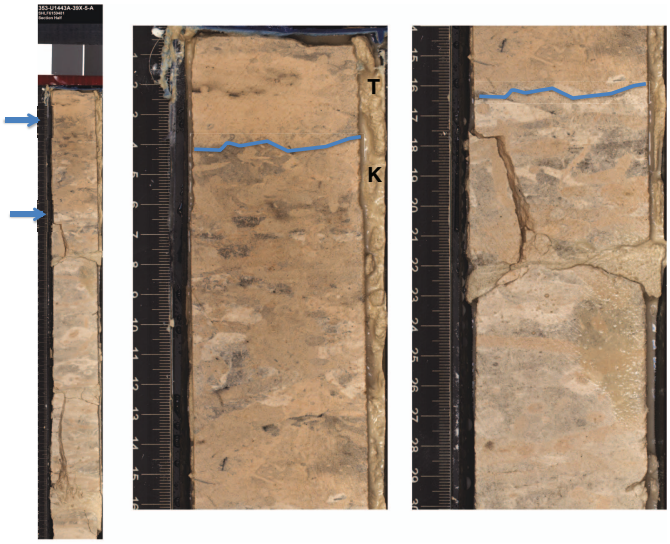

Figure F19. A. Transition from greenish glauconitic chalk to brownish-reddish nannofossil marls, Hole U1443A (42X-1). B. Glauconitic marl with inoceramid shell material (46X-1).

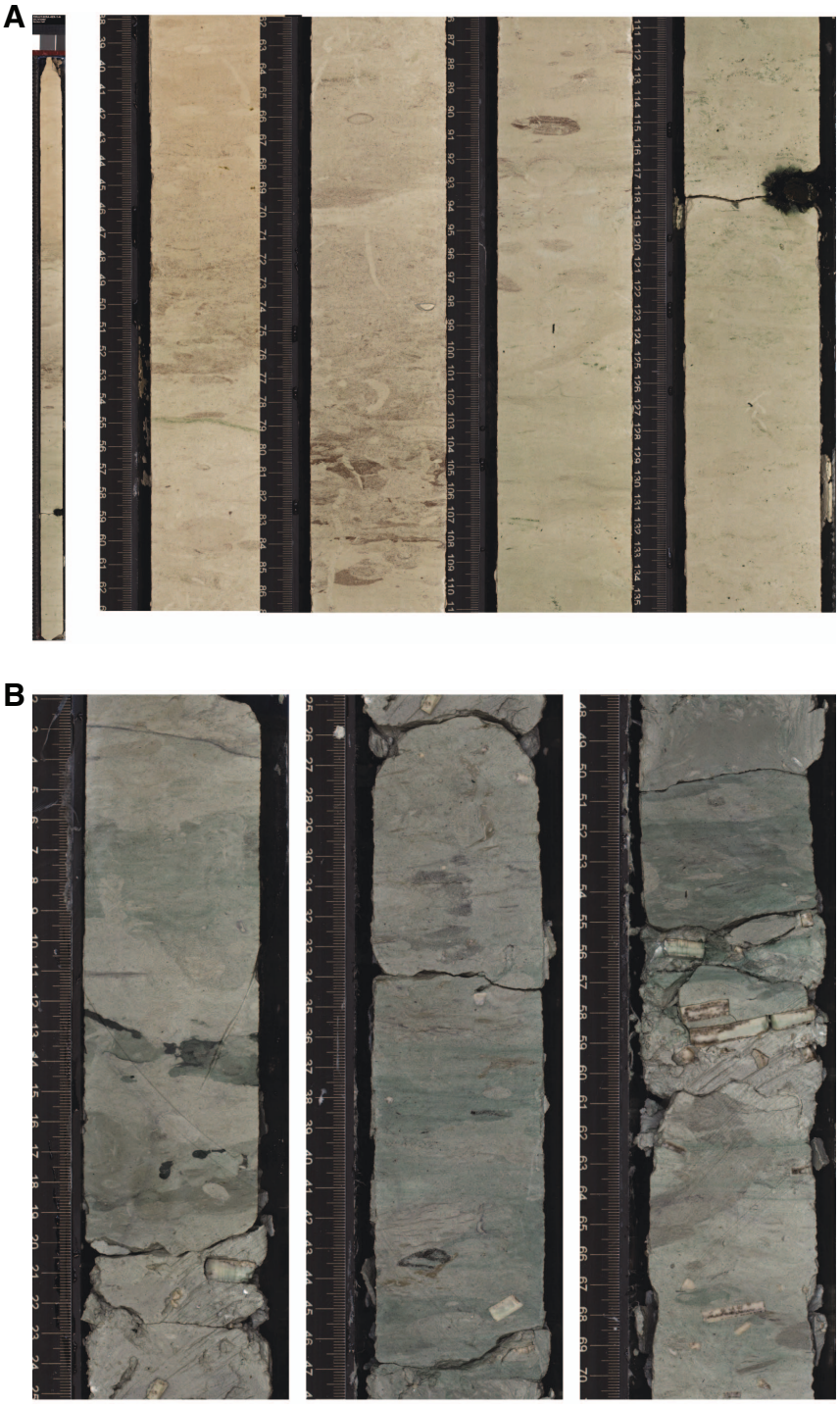

Figure F20. Hole U1443A/U1443B correlation of Cores 353-U1443A-1H to 2H and 353-U1443B-1H, indicating a 5.4 m gap at the base of Core 353-U1443A-1H.

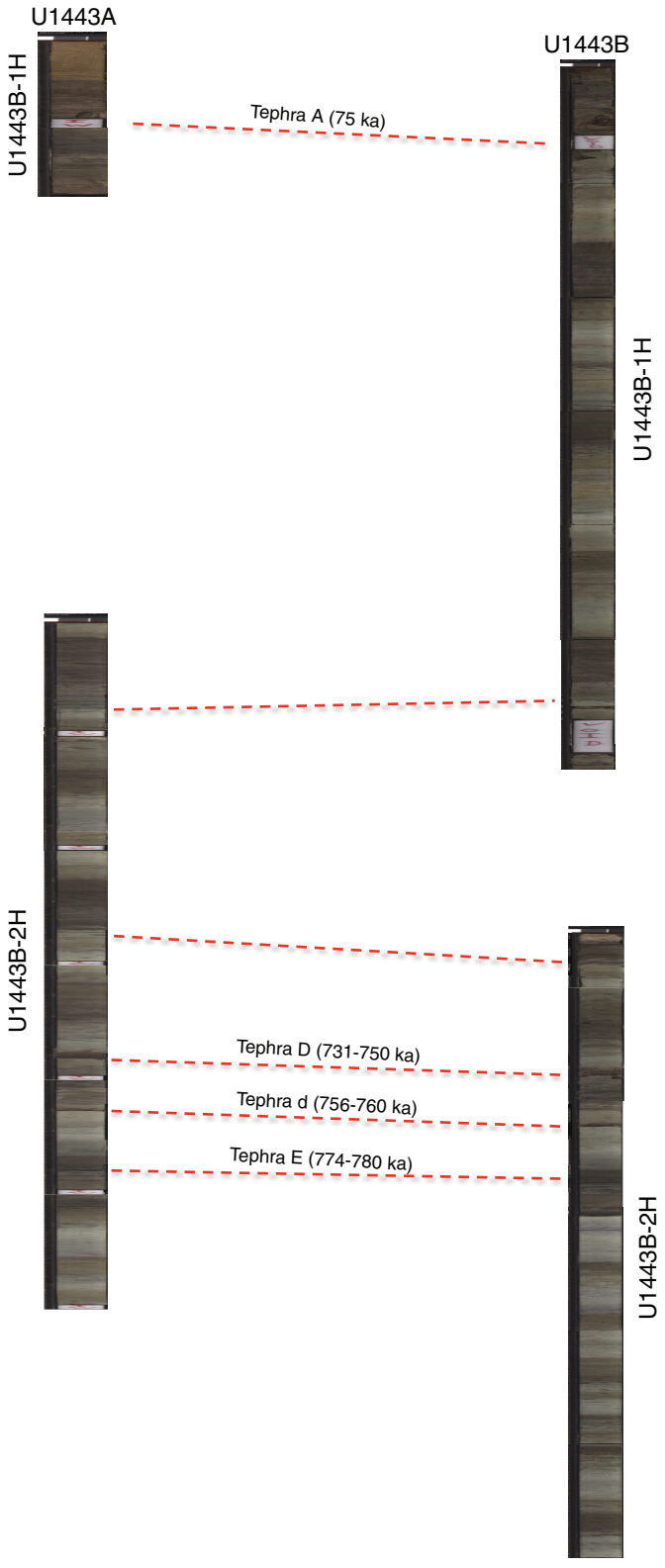

Figure F21. (A) Location of Site U1444 (after Emmel and Curray, 1984), (B) seismic line, and (C) line-drawing interpretation (after Schwenk and Spieß, 2009). In the line drawing, gray indicates buried channel-levee systems and bold black lines indicate seismic unconformities (Uc and Ud). (Continued on next page.)

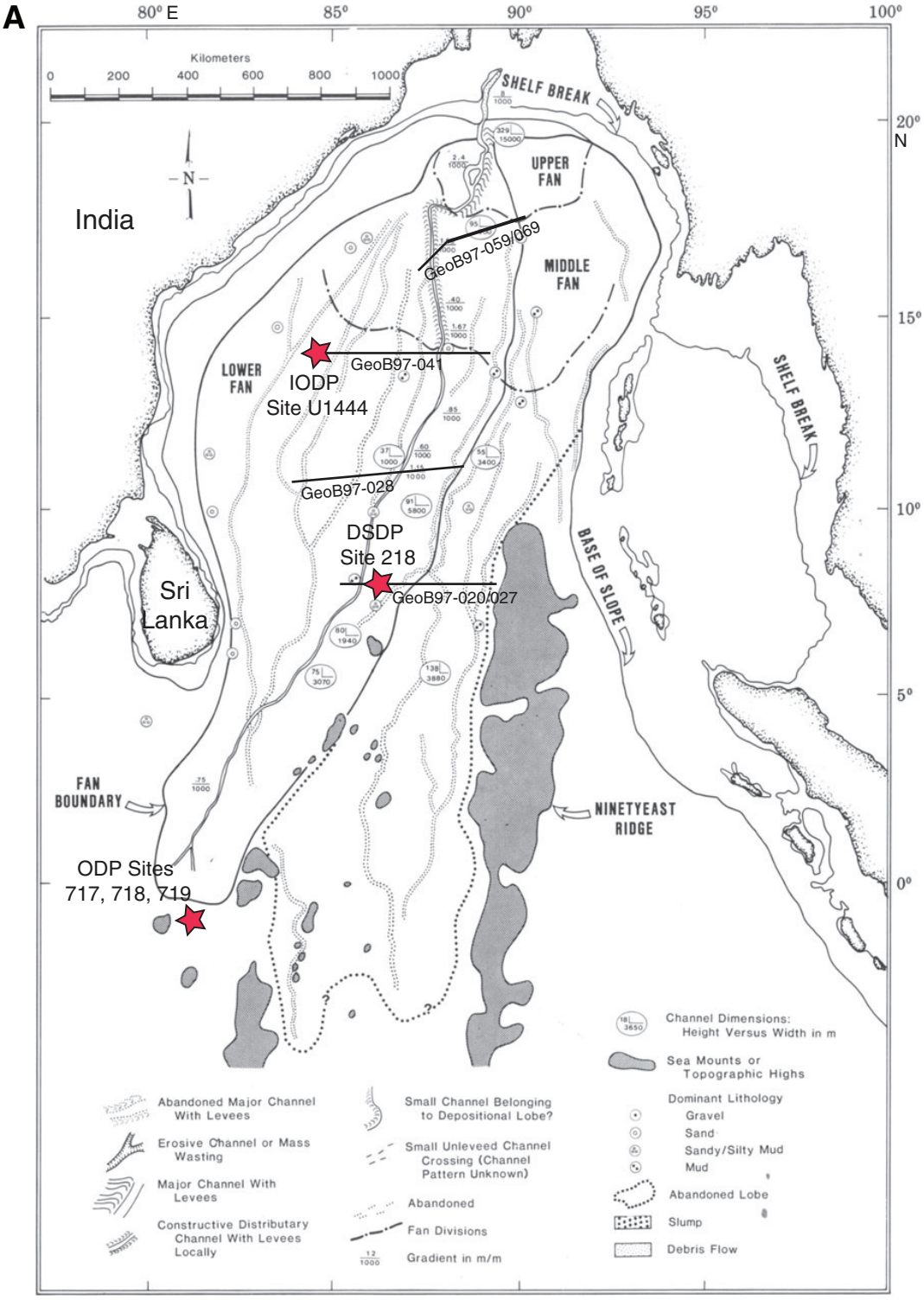

Figure 21 (continued).